UNIVERSIDADE FEDERAL DO RIO GRANDE DO SUL
INSTITUTO DE FÍSICA
DEPARTAMENTO DE ASTRONOMIA

Search, spectral classification and benchmarking of brown dwarfs

Marina Dal Ponte

Msc. dissertation taken under the supervision of Dr. Basílio Xavier Santiago submitted to the Graduate Program of Instituto de Física - Universidade Federal do Rio Grande do Sul (UFRGS) as part of the fulfilment to obtain the master's degree in physics with emphasis in astrophysics.

Porto Alegre, RS, Brasil
2019

⋆ This work has received financial support from Coordenação de Aperfeiçoamento de Pessoal de Nível Superior (CAPES)

UNIVERSIDADE FEDERAL DO RIO GRANDE DO SUL
INSTITUTO DE FÍSICA
DEPARTAMENTO DE ASTRONOMIA

Procura, classificação espectral e benchmarking de anãs marrons

Marina Dal Ponte

Porto Alegre, RS, Brasil
2019

⋆ Trabalho financiado pela Coordenação de Aperfeiçoamento de Pessoal de Nível Superior (CAPES)

"There's comfort in melancholy
When there's no need to explain
It's just as natural as the weather
In this moody sky today"
Joni Mitchell
(Hejira,1976.)

Acknowledgements

To my family, especially my mother Zenaide and father Santo, for all the support. Even though my life choice was the oddest for them, it was fundamental never being questioned for my decisions. I also appreciate all their curiosity related to my work and the pride in their voices when referring to me as the scientist of the family.

To my advisor, Basílio Xavier Santiago for all the patience, the sharing of knowledge, the teaching of how to question, for all the trust and support in difficult times and all the efforts that made me grow as a researcher.

To my astro friends Anna, Lari, Nicolas, Ale, Ingrid, Fernanda for all the support, for encouraging me in life and work and for all the beer nights. An extra special thanks for the astro girls, who always share their amazing power with me.

To the people of M207, especially Amanda and Vinicius, for providing lots of coffee every single day. Also thanks for the chocolate, cake, bread and caipirinha. Also an extra thanks to Vini, my bike partner, who taught me how to be nicer and gentle with car drivers even when they don't deserve.

To my friend Gabrielly, a true sister, and Nick for sharing so much so fast. We learn a lot together and I feel really privileged having you in my life.

To my boyfriend Fabio for being there in the most stressful and anxious moments of my life. Thanks a lot for helping me and for constantly trying to convince me that everything is going to be ok.

To Aurelio for the amazing brown dwarfs journey, for the patience, all the shared tasks and knowledge and for encouraging me to move forward.

All of my life I studied in public institutions and without them, I wouldn't be able to be where I am today. We must support quality public education to provide all kinds of opportunities to people who wouldn't have them otherwise.

Abstract

Brown dwarfs are a very common type of object in our Galaxy, but due to their very low luminosity they rank among the hardest sources to detect. The known samples are still largely restricted to a distance of few tens of parsecs. Our motivation is to make a first large scale census of L and T dwarfs in order to study structural Milky Way parameters and to constrain the properties and formation history of this population. In order to do so, we developed a color selection method for brown dwarfs and applied it to large survey data. Our color selection was based on DES+VHS+WISE photometry. We also used these data for spectral classification of MLT dwarfs, by developing and applying a code that compares their observed colours to expected template values, with the minimization of the χ^2. With the L and T dwarfs candidate sample in hand, we measured the scale height of disk L-type dwarfs. The L dwarf scale height was estimated with the aid of a brown dwarf simulation code, which we call `GalmodBD`, by comparing the observed and simulated number counts of such objects for a grid of models of varying spatial distributions. The initial estimate of scale height was $h_{z,thin} \sim 450$ parsec.

We also studied benchmark systems, specifically the wide binary systems made up of L or T dwarfs orbiting main sequence stars. These systems are useful to improve brown dwarf evolutionary models, since their chemical composition and age constraints may be taken from the primary star assuming that the pair formed from the same gas cloud and at the same time. Our approach was to use our sample of brown dwarfs candidates selected from DES+VHS+WISE data and then search for possible companions in the Gaia DR2 and DES DR1 stellar data. We also searched for L and T dwarfs binary systems among themselves. We found 197 new binary systems made up by an L or T dwarf orbiting a main sequence star or in a double LT system and we also found 2 multiple system candidates, triple and quadruple. All the systems with $< 10{,}000$ AU projected separation.

Key-words: Brown Dwarfs, Benchmarks, Dark Energy Survey

Resumo

Anãs marrons são um tipo comum de objeto na nossa Galáxia, mas devido à sua baixa luminosidade elas são fontes difícies de detectar. As amostras conhecidas ainda são em geral restritas a uma distância de poucas dezenas de parsecs. Nossa motivação é fazer um primeiro censo em grande escala de anãs L e T para então estudar parâmetros da Via Láctea e também restringir as propriedades e histórico da formação desta população. Para tal, nós desenvolvemos um método de seleção em cor para anãs marrons e o aplicamos a dados de grandes levantamentos. A seleção de cores foi feita usando a fotometria do DES+VHS+WISE. Usamos também os mesmos dados em um código de classificação espectral para anãs MLT, baseada na comparação das cores observadas e esperadas e minimização do χ^2. Com a amostra de candidatas a anãs L e T em mãos, nós medimos a escala de altura do disco para as anãs L. A escala de altura foi estimada com o auxílio de um código chamado `GalmodBD`, que simula anãs marrons, pela comparação entre a contagem observada e as simuladas para uma grade de modelos com diferentes distribuições espaciais. Nossa primeira estimativa da escala de altura do disco foi da ordem de $h_{z,fino} \sim 450$ pc.

Também estudamos sistemas *benchmark*, especificamente em sistemas binários formados por uma anã L ou T orbitando uma estrela de sequência principal. Esses sistemas são úteis para melhorar modelos evolutivos de anãs marrons, dado que a composição química e idade podem ser obtidas através da estrela primária, assumindo que o par se formou de uma mesma nuvem de gás e ao mesmo tempo. Nossa abordagem foi usar nossa amostra de candidatas a anãs marrons selecionadas nos dados do DES+VHS+WISE e então procurar por possíveis companheiros nos dados do Gaia DR2 e da amostra estelar do DES DR1. Também procuramos por sistemas binários entre as próprias anãs L e T. Encontramos 197 novos sistemas binários constituídos por uma anã L ou T orbitando uma estrela de sequência principal ou em um sistema contituído por duas anãs marrons e encontramos 2 candidatos a sistemas múltiplos, um triplo e quádruplo. Todos os sistemas possuem uma separação projetada $< 10{,}000$ UA.

Palavras-chaves: Anãs marrons, Benchmarks, Dark Energy Survey

Contents

Chapter 1

Introduction

1.1 Brief history of brown dwarfs

The existence of objects with a mass less that a certain limit that cannot burn hydrogen because of their temperature and density was demonstrated by Kumar (1963), based on theoretical calculations. Instead, the object contracts, becomes completely degenerate and the electron degeneracy pressure provides the hydrostatic equilibrium. The hydrogen burning minimum mass of $m_{HBMM} \sim 0.085 M_{\odot}$ was proposed by Grossman et al. (1974) based on detailed evolutionary calculations, however the term brown dwarf was given by Tarter (1975) to designate such objects.

The firsts discoveries of bona fide brown dwarfs were made only in the 1990s. Gliese 229B, shown in Figure 1.1, discovered by Oppenheimer et al. (1995), exhibited a strong methane (CH_4) absorption line which implied an object too cool to be a star. Also, in the Pleiades cluster, PP1 15 and Teide 1 (Stauffer et al., 1994, Rebolo et al., 1995) were identified as promising brown dwarfs candidates and were confirmed later by the detection of lithium (Li) (see Section 1.2), therefore becoming the first known free-floating brown dwarfs.

The early models for low mass stars and brown dwarfs suggested by Vandenberg et al. (1983), Dantona & Mazzitelli (1985), Nelson et al. (1986), Lunine et al. (1986), Burrows et al. (1989), Dorman et al. (1989) failed to reproduce the observations at the bottom of the Main Sequence (MS) and to provide a reliable determination of properties such as mass, age, effective temperature (T_{eff}) and luminosity. Only the subsequent models presented by Brett & Smith (1993), Saumon et al. (1994), Allard & Hauschildt (1995) allowed the computation of non-grey evolutionary models (Baraffe et al., 1995) and enabled a direct confrontation between theory and observation. We will return to the structure and evolutionary models of brown dwarfs in

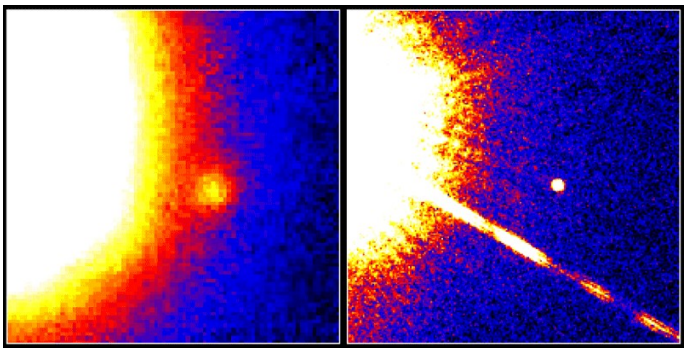

Figure 1.1: The left panel shows the image of Gliese 229B obtained in the Palomar Observatory and the right panel the Hubble Space Telescope image, both from 1995. Image taken from `http://hubblesite.org/image/372/news_release/1995-48`.

Section 1.3.

1.2 Brown dwarfs properties and characteristics

Brown dwarfs are considered substellar objects linking the lowest mass stars and giant planets, with masses ranging 0.085 down to 0.013 $M_{\odot}$. For solar composition and age, evolutionary models predict a central density (ρ_c) range from $\sim 10^3$ to 10 g/cm^3 and the T_{eff} range from $\sim$ 2,000 to $\sim$ 100 K, if we consider objects with mass from the m_{HBMM} to Saturn.

For brown dwarfs, the interior is essentially made by fully ionized plasma and degenerate electrons. The central density decreases with decreasing mass ($\rho_c \propto m^2$). The energy transport is essentially made by convection, but may also take place by conduction. As brown dwarfs undergo cooling throughout most of their lives, the interior of a brown dwarf eventually becomes degenerate enough so that the conductive flux becomes larger than the convective flux (Chabrier & Baraffe, 2000).

The evolutionary timescale is many orders of magnitude larger than the convective timescale (Bildsten et al., 1997). This means that the abundances in the interior and the atmosphere are the same. Rebolo et al. (1992) was the first to proposed the Li test to identify bona-fide brown dwarfs. The Li remaining in a fully mixed object older than 10^8 years means lack of H burning in its interior. The minimum mass for the occurrence of lithium burning is $\simeq 0.06\ M_{\odot}$ (Chabrier et al., 1996). However, it is important to mention that the Li test could lead to false positive cases. An example is young low mass stars (t $< 10^8$ years, and with specific masses), which will exhibit lithium in their photosphere because they did not yet have the time to burn it. Also, more massive brown dwarfs ($\simeq 0.06\ M_{\odot}$) older than 10^8 years will

have burned all the Li, thus escaping detection based on this element. Similar tests can be applied to deuterium (D). For D, the minimum mass for the burning to occur is $\simeq 0.013\ M_{\odot}$ (Shu et al., 1987).

The low temperature and high pressures in the photosphere of brown dwarfs are appropriate for formation of many molecular species, whose chemical features and opacities result in a complex spectral energy distribution (SEDs). For example, at a m $\sim 0.085\ M_{\odot}$ and $T_{eff} \sim$ 2,000 K broad molecular absorption bands as VO, FeH, CaH disappear from the spectral distribution, only with some TiO remaining. The decreasing of TiO led to the proposition of the new L spectral type, since the TiO band is often an indicator of M dwarfs. Also, as the temperature decreases the carbon will be mainly found in the form of CH_4, whose spectral features again claimed for another spectral type, known as T dwarfs. The Figure 1.2 shows the spectra for the M, L and T dwarfs, in special for the L type sequence, with an emphasis in the most prominent lines and bands. The L and T transition effective temperature is not precisely determined but it is in a narrow range of 1,400 to 1,200 K. Also, objects with $T_{eff} < 600$ K are the Y types.

For late M dwarfs and L types, there is a cloud formation very near to the photosphere. Figure 1.3 shows many interesting features about the characteristics of L and T dwarfs. It shows a natural extension from the M to the L dwarfs, suggesting that clouds play a continuous role from late M through the L. From L to T dwarfs, there is a change in color which its characterized by the lack of cloud opacity and also for the appearance of CH_4. This change in color is due to CH_4 absorption in the H and K bands, yielding relatively blue near infrared colors. In terms of model implications, the L/T transition requires a change in properties in a small range of T_{eff}, something that is challenging to achieve.

1.3 Evolutionary models

The evolutionary models for brown dwarfs are very sensitive to the chemical composition of the photosphere. Moreover, the spectra of brown dwarfs are composed by several types of molecules, as discussed in the previous section, and the line opacities for several of them still need improvement.

The evolutionary models connects the surface properties as T_{eff} and surface gravity (g) to the interior properties as mass, luminosity, radius and age. For the structure and evolution, the model needs the mass equation, the equation of hydrostatic equilibrium, the equation of conservation of energy and the equation of

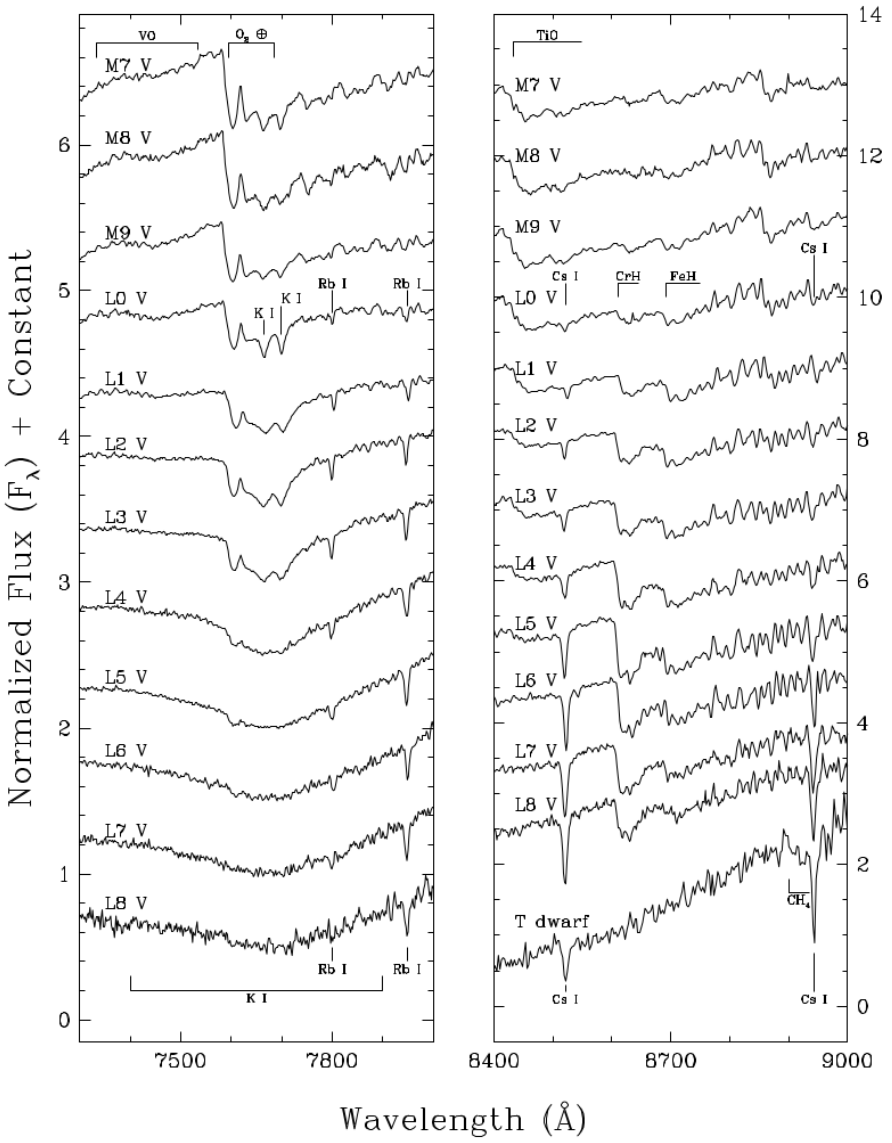

Figure 1.2: Spectra for the L-dwarf sequence, a T dwarf (Gliese 229B) and three late-M dwarfs. The late-M dwarfs and T dwarf spectra are shown for comparison to the L dwarfs. The prominent lines and bands are marked. Image taken from Kirkpatrick et al. (1999).

state (Saumon et al., 1995). The non-gray, realistic atmosphere models provide the surface boundary condition for the interior structure calculations and also the colors and magnitudes for a given star at a given age. The last evolutionary models was proposed by Saumon & Marley (2008), including two different atmospheres for the models: cloudy and cloudless. The cloudy atmospheres have larger opacity than clear models.

Figure 1.4 shows that the difference between the cloudy and cloudless models

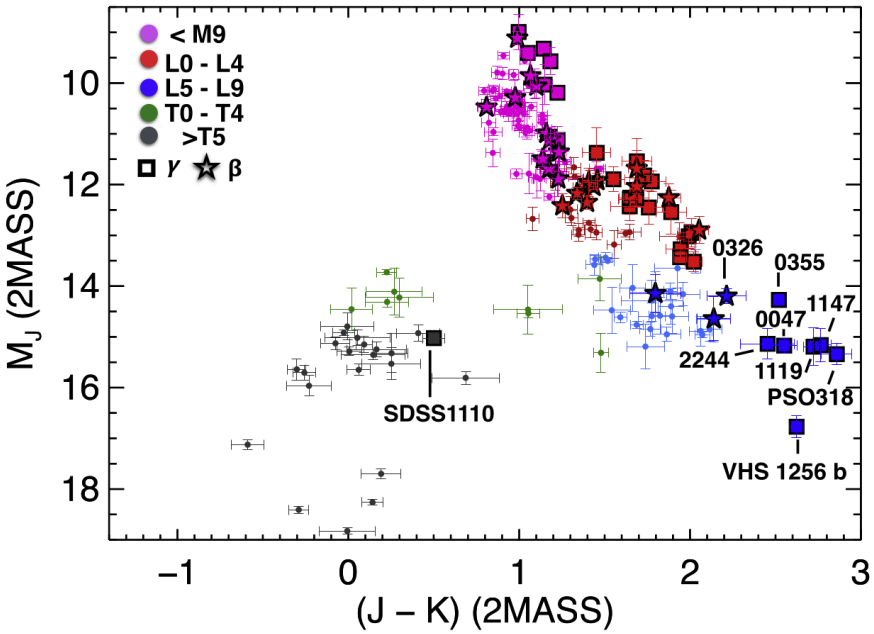

Figure 1.3: Near infrared color-magnitude diagram for brown dwarfs, where the objects have been color-coded according to the spectral subtype. Image taken from Faherty et al. (2016).

vanishes at low and high effective temperature. At intermediate temperature, the models are more discrepant. This figure also shows that a object with a known luminosity has a upper limit to its T_{eff}. For the cloudless evolutionary model the surface gravity has a limit of $logg = 5.465$ for 0.068 $M_{\odot}$ at $T_{eff} = 1160$ K. In the cloudy model, the $logg = 5.366$ at the same mass, with $T_{eff} = 1380$ K.

The cloudy model was compared with DUSTY00 (Chabrier et al., 2000, Baraffe et al., 2002) and the cloudless with the COND03 (Baraffe et al., 2003). Both models have the same interior, no significant difference in the nuclear reaction rates, but COND03 and DUSTY00 include the energy transportation by conduction. Comparing the models, the luminosities are slightly higher in COND03 and DUSTY00 models. However, for all masses and ages above a few Myr the models agreed very well. At young ages, there are more discrepancies, but it is a reflection of different choices for the initial conditions. Also, for objects with more than 10 Gyr, the effect of a non inclusion of electron conduction reflects in a larger luminosity difference between the models. Also, Saumon & Marley (2008) presented a single model, called hybrid, which is an approach to describe the L/T transition where the clouds vanish with decreasing T_{eff}. This hybrid model was proposed because neither cloud nor cloudless models alone can describe the observed or simulated populations.

Also, the binaries play an important role in evolutionary models (Chabrier, 2002,

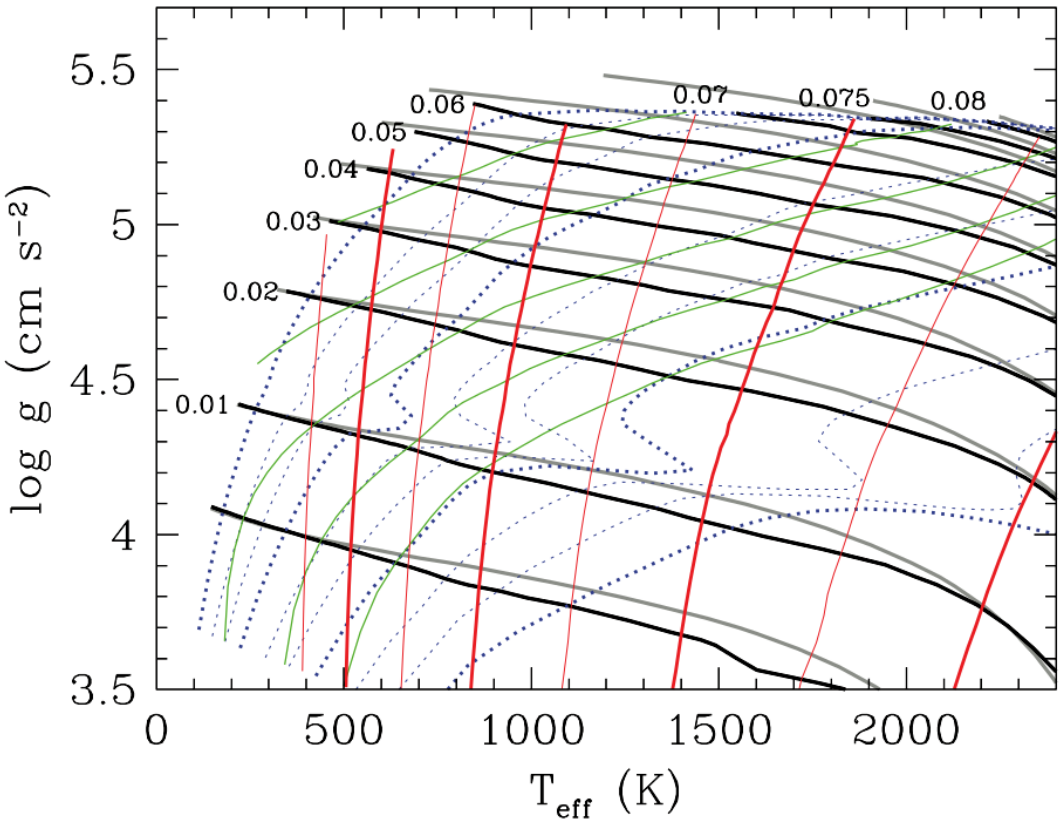

Figure 1.4: Surface gravity versus effective temperature for evolutionary models based on cloudless and cloudy atmospheres proposed by Saumon & Marley (2008). The black lines represents the cloudy atmospheres with masses ranging from 0.08 to 0.005 $M_{\odot}$ as indicated on the left of each line. The cloudless tracks are the gray lines. The isochrones are the blue dotted lines ranging from 0.01, 0.02, 0.04, 0.1, 0.2, 0.4, 1, 2, 4 to 10 Gyr (right to left). The red vertical lines are curves from constant luminosity from log $L/L_{\odot}$ = -3 to -6.5 (from right to left). The green curves represent constant radius from 0.08 to 0.13 $R_{\odot}$ (from top to bottom). The kink in the isochrones represents the deuterium burning phase. Image taken from Saumon & Marley (2008).

Burgasser, 2007). Almost 10-20 % of brown dwarfs are predicted to be in binaries systems, as we will discuss in more details in Section 1.6. Unresolved binaries also affect photometric measurements, with an upward shift by 0.75 magnitude for a secondary to primary mass ratio of $q = 1$, when the total flux is doubled with respect to a single object. Notice that the mass ratio distribution is in general peaked at or close to $q = 1$.

1.4 Luminosity and Mass Function

The problem in the determination of the luminosity and mass function is based on the limited number of objects, since the available samples are limited to the solar neighbourhood. Brown dwarf observations will be biased toward young and massive objects, since most of the sources formed at the early stages of the Galaxy will have dimmed to very low luminosities ($L \sim 1/t$).

In the stellar regime, the initial mass function (IMF) is often characterized by a power law $dN/dM \propto M^{-\alpha}$, with $\alpha = 2.35$ for Salpeter IMF (Salpeter, 1955). For brown dwarfs there is no unique mass-luminosity relationship that one can use to convert the luminosity function into the IMF. The luminosity function (LF) is influenced by the formation history, which is still lacking details and relies on many possible formation scenarios. Considering young clusters and associations, it is possible to break the age-mass-luminosity relations because their age and metallicities are known and, therefore, remove the dependency of the LF with the formation history. In the case of field brown dwarfs, the benchmarks systems play an important role in the determination of age and metallicity, since the primary star could constrain these parameters for the brown dwarf. However, the field populations require assumptions of the formation history. Also, an IMF measure requires a well known space density for LTY types and a precise determination of the binary fraction.

For brown dwarfs, the value of α changes with the sample, binary fraction and space density. For field surveys, the slope is $\alpha < 0$ (Burningham et al., 2010) and for young clusters and associations, as for Upper Sco is $\alpha = 0.6 \pm 0.1$ (Lodieu et al., 2007), for Pleaides is $\alpha = 0.6 \pm 0.1$ (Moraux et al., 2003) and for σ Orionis is $\alpha = 0.5 \pm 0.2$ (Lodieu et al., 2009). The variations on the slope arise from the different methods and quantities considered to derive it.

The shape of the IMF, binary fraction and multiplicity function of brown dwarfs are important discriminants to scenarios of brown dwarf formation. According to Luhman (2012), there are five basic such scenarios: i) formation in a proto stellar cluster, where tidal shears and high internal velocities negatively affect the mass accretion by small mass cores (Bonnell et al., 2008); ii) brown dwarfs are the least massive cores inside a proto cluster and are therefore ejected due to dynamical interaction with more massive ones, hence halting their mass growth (Boss, 2001, Bate & Bonnell, 2005); iii) massive OB stars form first and their ionizing flux removes the gas around least massive cores, again with a negative feedback to brown dwarf progenitors (Whitworth & Zinnecker, 2004); iv) brown dwarfs form in circumstellar disks around more massive proto stars and then are ejected into the field by inter-

action with other (proto)stars (Bate et al., 2002, Bate & Bonnell, 2005, Stamatellos et al., 2011); v) a proto cluster fragments into smaller cores spanning a wide range of masses, the smallest of which turn into brown dwarfs (Padoan & Nordlund, 2002, Elmegreen, 2011). Ruling out or even constraining these models, however, requires larger samples and more accurate estimates of the IMF, space densities, binary fractions and multiplicity functions than currently available.

1.5 Spectroscopic and photometric samples of L, T and Y dwarfs

With the advent of deep and wide field surveys, such as Deep Near Infrared Survey of the Southern Sky (DENIS; Epchtein et al., 1997), Sloan Digital Sky Survey (SDSS; York et al., 2000), Two-Micron All-Sky Survey (2MASS; Skrutskie et al., 2006), UKIRT Infrared Deep Sky Survey (UKIDSS; Lawrence et al., 2007), VISTA Hemisphere Survey (VHS; McMahon et al., 2013) and Wide-field Infrared Survey Explorer (WISE; Wright et al., 2010), ever larger samples of L,T and Y dwarfs were provided. This increase in the census of brown dwarfs brought an increase in statistical significance to constraints to current models for the structure and evolution of brown dwarfs. Up to now there are several samples selected in different ways, depending on the main photometric bands from each survey. Some of them are listed bellow.

Using the SDSS data, Chiu et al. (2006) presented the discovery and properties of 71 LT dwarfs using a $(i-z)_{SDSS} > 2.2$ color selection. 65 of these dwarfs have been classified spectroscopically and the spectral types range from L3 to T7. A similar method is presented in Schmidt et al. (2010), who identified a sample of 484 L dwarfs candidates applying $(i-z)_{SDSS} > 1.4$ color selection. In this candidate sample, 210 L dwarfs were new discoveries and the authors have not made the spectroscopic confirmation.

The Canada–France Brown Dwarfs Survey presented in Albert et al. (2011) was carried out with MegaCam at the Canada–France–Hawaii Telescope, and covers a surface area of 780 deg^2. This survey identified about 70 T dwarf candidates where 43 were spectroscopically confirmed and 6 were previously published and 37 were new discoveries, with spectral types ranging from T0 to T8.5.

Using WISE data, Kirkpatrick et al. (2011) were able to identify and classify 6 Y dwarfs, 89 T dwarfs and 8 L dwarfs. The selection was made by color cuts and the sample has spectrocopic confirmation. With this sample, it was able to extend the

optical T dwarf classification scheme from T8 to T9. Also, using WISE and VISTA, Lodieu et al. (2012) presented the results of a photometric search for brown dwarfs using $W1-W2 > 1.4$ and $J-W2 > 1.9$ color cuts. The search led to the discovery of 13 T dwarfs, including two previously published in the literature and 5 new ones confirmed spectroscopically, with spectral types between the T4.5 and T8 range.

Using UKIDSS and covering 495 deg^2 of the sky, Day-Jones et al. (2013) presented a new sample of mid-L to mid-T dwarfs, which were confirmed spectroscopically. This sample contains 63 L and T dwarfs, including the identification of 12 likely unresolved binaries. Also using UKIDSS, Burningham et al. (2013) discovered 76 new T dwarfs with spectroscopic confirmation.

Skrzypek et al. (2015) used the combination of SDSS, UKIDSS and WISE data to search for brown dwarfs using $Y - J > 0.8$ and $13.0 < J < 17.5$ as selection criteria. The final sample consists in 1,361 L and T dwarfs with a spectral types estimates based on photometry alone. Following the same approach, Sorahana et al. (2019) selected a sample of 3,665 L dwarfs using the Hyper Suprime-Cam Subaru Strategic Program, covering about 130 deg^2 at high galactic latitudes. Also, the number counts obtained differentially using the z magnitude were compared with predictions of an exponential disk model to estimate the thin-disk scale height. Our current investigation has a direct connection with these two previous works. For the search and spectral classification of L and T dwarfs, we follow a similar methodology as in Skrzypek et al. (2016), but using DES, VHS and WISE data (see Section 1.7) and different set of color cuts. We also made an estimate of the thin-disk scale height as Sorahana et al. (2019), using a simulations from a population synthesis model called `GALMODBD`. More details are provided in Chapter 2.

The J. Gagné compilation[1] contains most of the samples described earlier and other data sets of spectroscopically confirmed brown dwarfs up to 2014, covering spectral types from late M, L and T dwarfs. The compilation consists of 1,772 sources, covering most parts of the sky to distances less than 100 parsec. Also, the Gagné sample was adopted to define our color selection and to create the photometric templates that will be used during the spectral classification step and in the `GALMODBD` simulations. Again, we refer to Chapter 2 for more information.

[1] https://jgagneastro.wordpress.com/list-of-ultracool-dwarfs/

1.6 Benchmark brown dwarfs

Benchmark brown dwarfs are very useful because we can use them to break degeneracies in age, mass and metallicity, thus being very helpful for the characterisation of cool substellar objects. A common type of benchmark system are wide binaries, composed of resolved companions, where the primary is commonly a main sequence star and the secondary is a L or T dwarf. The metallicity and age constraints may be taken from the primary star since it is very difficult to measure these properties for the L and T dwarfs. For that purpose, one naturally has to rely on the assumption that the pair formed at the same time, from the same material, and evolved in the same environment.

One issue in finding benchmark systems involving L or T dwarfs is that the binary fraction seems to decrease from early to late primary's spectral types (Kraus & Hillenbrand, 2012). For solar type stars, the binary fraction ranges within 50-60% (Raghavan et al., 2010) and for M stars it is in the 30-40% range (Janson et al., 2012). For brown dwarfs in the field, the resolved binary frequency ranges around 10-20% (Burgasser et al., 2006, Gelino et al., 2011, Huélamo et al., 2015). Also, for binary systems with a solar type as a primary and a brown dwarfs as a secondary, we find a called *brown dwarf desert*, which corresponds to a very small binary fraction $(1-3\%)$ for small separations (few AU) (Grether & Lineweaver, 2006, Metchev & Hillenbrand, 2009). For brown dwarfs, the binary fraction, mass-ratio distribution or separation could provide constrains on star formation and dynamical evolution (Goodwin & Whitworth, 2007).

In the case of wide binary systems, for solar type stars Tokovinin & Lépine (2012) estimates 4.4 % are wider than 2,000 AU. More recently Dhital et al. (2011) and Dhital et al. (2015) presented the Sloan Low-mass Wide Pairs of Kinematically Equivalent Stars (SLoWPoKES), which is a catalog containing common proper motion and common distance of wide ($\sim$ 500-60,000 AU) candidate pairs. For the mid K and mid M type dwarfs presented in both catalogs, the wide binary frequency was $\sim 1.1\%$. For L and T dwarfs in wide systems this frequency still remains uncertain. Also, brown dwarfs in wide binary systems could impact the formation theories, especially the ejection model, since this type of system is not expected to survive ejection from their birth environments.

Since it is harder in practice to sample and measure resolved pairs with large primary to secondary mass ratios, for which the magnitude difference is large. Often either the primary may be saturated or the secondary be undetected. Our expectation is to find mostly pairs involving late type main-sequence dwarfs as primaries.

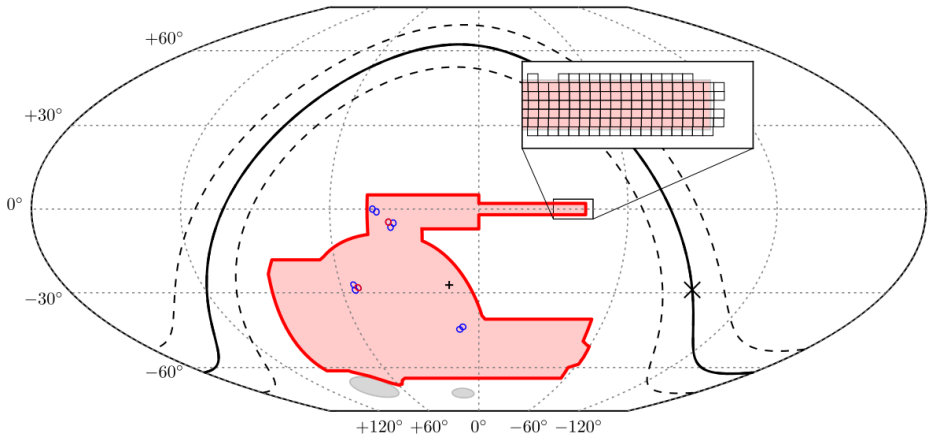

Figure 1.5: The DES footprint is shown in red. The eight shallow SN fields are shown as blue circles, and the two deep SN fields are shown as red circles. The Milky Way plane is shown as a solid line, with dashed lines at b = ±10 deg. The Galactic center are marked as a cross and south Galactic pole as a plus sign. The Large and Small Magellanic Clouds are indicated as gray ellipses. Image taken from Abbott et al. (2018).

Based on the discussion earlier in this section, binaries involving two brown dwarfs should be rare. Also L dwarfs should appear in fewer wide binary companions when compared to M dwarfs, and most of these systems should have an M as a primary.

1.7 L and T dwarfs and the Dark Energy Survey

The Dark Energy Survey (DES) is a wide field optical survey in the $grizY$ bands, covering 5,000 deg^2 in the south Galactic cap, using the Dark Energy Camera (DECam; Flaugher et al., 2015), which is installed at the prime focus of the 4 m Blanco telescope at Cerro Tololo Inter-American Observatory (CTIO) in northern Chile.

The DES wide-area footprint shape, shown in Figure 1.5, was selected to obtain an overlap with the South Pole Telescope survey (Carlstrom et al., 2011) and Stripe 82 from SDSS (Abazajian et al., 2009). The Galactic plane was avoided in order to maintain the main DES goals, which are cosmological and extragalactic in nature, by minimizing stellar foregrounds and extinction from interstellar dust.

DES Data Release 1 (DR1; Abbott et al., 2018) is composed by 345 distinct nights spread over the first 3 years of DES operations from 2013 August 15 to 2016 February 12. The DR1 uses exposure times are of 90s for $griz$ bands and 45s for Y band, yielding a typical single-epoch point-spread function (PSF) depth at signal-to-noise ratio (S/N) = 10 of $g = 23.57$, $r = 23.34$, $i = 22.78$, $z = 22.10$, and Y

= 20.69 (AB system). The DES DR1 co-add source extraction process detected and cataloged 399,263,026 distinct objects. The Figure 1.5 shows the DES DR1 footprint.

The DES filters izY were the most important to our project, since due to their very red nature, brown dwarfs could be detected using red optical bands. Also, we decided to match DES data with two other surveys: VISTA Hemisphere Survey (VHS) and Wide-field Infrared Survey Explorer (WISE). The main reason was to increase the number of bands, especially the infrared ones. This combination of optical bands with infrared is very helpful to identify red and late-type objects, as has been demonstrated in the literature and mentioned in the earlier sections.

Chapter 2

DES L and T dwarfs sample

In this section we describe our L and T candidates sample selected using DES, VHS and WISE data. The candidate L and T dwarfs were initially selected based on color criteria in optical and near-infrared bands. For that purpose we used available catalogs containing MLT dwarfs with spectroscopic confirmation and located inside the common footprint between DES and VHS. The colours of these objects, and also of a high redshift quasar sample, were used to find cuts in colour-space that best isolate L and T dwarfs from M stars and quasars.

We also performed spectral classification using only the available photometry, based on the approach presented in Skrzypek et al. (2015) and Skrzypek et al. (2016), which relies a minimization of the χ^2 relative to empirical templates. The templates were created using the samples of confirmed MLT dwarfs inside the footprint. Spectral types were obtained for all sources that passed the colour cuts, and led to an additional cleaning of the L and T candidates. The final catalog contains 11,745 L and T dwarfs candidates and is the biggest to date.

We also used a simulation code called `GalmodBD` to estimate the completeness and purity of our photometric brown dwarfs catalogue as well as to constrain the thin disk scale height for the early L population. `GalmodBD` creates synthetic samples of brown dwarfs based on the expected number counts for a given footprint and down to a given magnitude limit, using empirically determined space densities of objects, absolute magnitudes and colors as a function of spectral type. Using the synthetic samples, we compared the number counts between simulation and data and find a scale height of the order of $h_{z,thin} \sim 450$ pc. However, T dwarfs are less than 2% of the sample and are limited to 100 pc. This implies that we are estimating the scale height for the early L dwarfs.

The rest of this chapter is presented as submitted paper (Carnero Rosell et al.,

2019) to the Monthly Notices of the Royal Astronomical Society. It is important to mention that this paper has passed through an extensive internal review by DES members.

DES 2017-0293
FERMILAB-PUB-19-104-AE

MNRAS **000**, 000–000 (2019) Preprint 14 May 2019 Compiled using MNRAS LATEX style file v3.0

Brown dwarf census with the Dark Energy Survey year 3 data and the thin disk scale height of early L types

A. Carnero Rosell,[1,2,3] B. Santiago,[4,2] M. dal Ponte,[4] B. Burningham,[5] L. N. da Costa,[2,3] D. J. James,[6,7] J. L. Marshall,[8] R. G. McMahon,[9,10] K. Bechtol,[11,12] L. De Paris,[4] T. Li,[13,23] A. Pieres,[2,3] T. M. C. Abbott,[14] J. Annis,[13] S. Avila,[15] G. M. Bernstein,[16] D. Brooks,[17] D. L. Burke,[18,19] M. Carrasco Kind,[20,21] J. Carretero,[22] J. De Vicente,[1] A. Drlica-Wagner,[14,23] P. Fosalba,[24,25] J. Frieman,[13,23] J. García-Bellido,[15] E. Gaztanaga,[24,25] R. A. Gruendl,[20,21] J. Gschwend,[2,3] G. Gutierrez,[13] D. L. Hollowood,[26] M. A. G. Maia,[2,3] F. Menanteau,[20,21] R. Miquel,[27,22] A. A. Plazas,[28] A. Roodman,[18,19] E. Sanchez,[1] V. Scarpine,[13] R. Schindler,[19] S. Serrano,[24,25] I. Sevilla-Noarbe,[1] M. Smith,[29] F. Sobreira,[30,2] E. Suchyta,[31] M. E. C. Swanson,[21] G. Tarle,[32] V. Vikram,[33] and A. R. Walker[14]

(DES Collaboration)

Affiliations are listed at the end of the paper.

Accepted XXX. Received YYY; in original form ZZZ

ABSTRACT

In this paper we present a catalogue of 11,745 brown dwarfs with spectral types ranging from L0 to T9, photometrically classified using data from the Dark Energy Survey (DES) year 3 release matched to the Vista Hemisphere Survey (VHS) DR3 and Wide-field Infrared Survey Explorer (WISE) data, covering $\approx 2,400\ deg^2$ up to $i_{AB} = 22$. The classification method follows the same photo-type method previously applied to SDSS-UKIDSS-WISE data. The most significant difference comes from the use of DES data instead of SDSS, which allow us to classify almost an order of magnitude more brown dwarfs than any previous search and reaching distances beyond 400 parsecs for the earliest types. Next, we also present and validate the *GalmodBD* simulation, which produces brown dwarf number counts as a function of structural parameters with realistic photometric properties of a given survey. We use this simulation to estimate the completeness and purity of our photometric LT catalogue down to $i_{AB} = 22$, as well as to compare to the observed number of LT types. We put constraints on the thin disk scale height for the early L population to be around 450 parsecs, in agreement with previous findings. For completeness, we also publish in a separate table a catalogue of 20,863 M dwarfs that passed our colour cut with spectral types greater than M6. Both the LT and the late M catalogues are found at https://des.ncsa.illinois.edu/releases/other/y3-mlt.

Key words: Catalogues, Surveys, brown dwarfs, infrared: stars, techniques: photometric

1 INTRODUCTION

Ultra-cool dwarfs are mostly sub-stellar objects (brown dwarfs, BDs) with very cool ($T_{\rm eff} < 2,300\ K$) atmospheres with spectral types later than M7, including the L, T and Y sequences. Their spectra are typified by the effects of clouds and deep molecular absorption bands. In L dwarfs ($2,200 \gtrsim T_{\rm eff} \gtrsim 1,400\ K$) clouds block radiation from emerging from deep in the atmosphere in the opacity windows between molecular absorption bands, narrowing the pressure range of the observed photosphere, and redistributing flux to longer wavelengths giving these objects red near-infrared colours. The transition to the T sequence (LT transition, $T_{\rm eff} \sim 1,200 - 1,400\ K$) is driven by the disappearance of clouds from the near-infrared photosphere, leading to relatively bluer colours. This is accompanied by the transition from CO (L dwarfs) to CH_4 (T dwarfs) dominated carbon chemistry. At cooler temperatures ($T_{\rm eff} < 500\ K$), the devel-

opment of the Y dwarf sequence is thought to be driven by the emergence of clouds due to sulphide and chloride condensates, as well as water ice (e.g. Leggett et al. 2013, 2015; Skemer et al. 2016).

BDs never achieve sufficient core temperatures to maintain main-sequence hydrogen fusion. Instead, they evolve from relatively warm temperatures at young ages to ever cooler temperatures with increasing age as they radiate the heat generated by their formation. As a result, the late-M and early-L dwarf regime includes both young, high-mass, brown dwarfs and the lowest mass stars. The latter can take several hundred million years to reach the main sequence. Objects with late-L, T and Y spectral types are exclusively substellar. In this work, we focus on L and T dwarfs, and for brevity refer to this group as BDs.

BDs have very low luminosity, especially the older or lower mass ones. Their mass function, star formation history (SFH) and spatial distribution are still poorly constrained, and the evolutionary models still lack details, especially the lowest-masses and old ages. They are supported at their cores by degenerate electron pressure and, because the degeneracy determines the core density (instead of the Coulomb repulsion), more massive BDs have smaller radii. BDs are actually partially-degenerate, in the sense that while in their atmospheres reign thermal pressure, somewhere in their interior there must be a transition from degenerate electron to thermal pressure.

The current census covers an age range from a few million years (Liu et al. 2013; Gagné et al. 2017) to > 10 Gyr halo members (Burgasser et al. 2003; Zhang et al. 2017), and spans the entire mass interval between planetary and stellar masses. The diverse range of properties that these objects display reflects the continual luminosity and temperature evolution of these partially-degenerate objects. As a numerous and very long-lived component of our Galaxy, these continually evolving objects could be used to infer structural components of the Milky Way, and tracing the low-mass extreme of star formation over cosmic timescales. However, studies of L dwarfs have typically been restricted to the nearest 100 pc, while T dwarfs are only known to distances of a few tens of parsecs.

The era of digital wide-field imaging surveys has allowed the study of brown dwarfs to blossom, with thousands now known in the solar neighbourhood. But this collection is heterogeneous and very shallow and therefore, not suitable for large-scale statistical analysis of their properties. The new generation of deep and wide surveys (DES (Dark Energy Survey Collaboration et al. 2016), VHS (McMahon et al. 2013), UKIDDS (Lawrence et al. 2007), LSST (Abell et al. 2009), HSC (Miyazaki et al. 2018)) offer the opportunity to place the brown dwarf population in their Galactic context, echoing the transition that occurred for M dwarfs with the advent of the Sloan Digital Sky Survey (SDSS; Bochanski et al. 2007; West et al. 2011). These surveys should be able to create homogeneous samples of BDs to sufficient distance to be suitable for various applications, such as kinematics studies (Faherty et al. 2009, 2012; Schmidt et al. 2010; Smith et al. 2014), the frequency of binary systems in the LT population (Burgasser et al. 2006a; Burgasser 2007; Luhman 2012), benchmark systems (Pinfield et al. 2006; Burningham et al. 2013; Marocco et al. 2017), the search for rare or unusual objects (Burgasser et al. 2003; Folkes et al. 2007; Looper et al. 2008; Skrzypek et al. 2016), and the study of Galactic parameters (Ryan et al. 2005; Jurić et al. 2008; Sorahana et al. 2018). In this latter case, we will also need simulations to confront observed samples. Realistic simulations will benefit from improved spectral type-luminosity and spectral type-local density relations in the solar neighbourhood.

The UKIRT Infrared Deep Sky Survey (UKIDSS; Lawrence et al. 2007) imaged 4000 deg^2 in the Y, J, H, K filter passbands, and provided discovery images for over 200 T dwarfs, making it one of the principal contributors to the current sample of LT dwarfs, particularly at fainter magnitudes (e.g. Burningham et al. 2010; Burningham et al. 2013; Burningham 2018). Experience gained through the exploitation of UKIDSS has demonstrated that significant amounts of 8m-class telescope time are required to spectroscopically classify samples of 10s to 100s of LT dwarfs within 100 pc. For example, total observation times of 40 - 60 minutes were needed to obtain low-resolution spectra of $J \sim 18.5$ targets at a signal-to-noise ratio (SNR) = 20, necessary for spectral classification (Burningham et al. 2013). Obtaining homogeneous samples to the full depth available in the new generation of surveys is thus only feasible today through photometric classification. Such an approach was demonstrated in Skrzypek et al. (2015) and Skrzypek et al. (2016), where they obtained a sample of more than 1000 LT dwarfs, independent of spectroscopic follow-up, using $i, z, Y, J, H, K_s, W1, W2$ from $SDSS \cap UKIDDS \cap WISE$.

A summary of surveys that attempted to select BDs candidates photometrically can be found in Table 1. We identify two approaches: one based on a colour selection in optical bands and another with colour selection in the near-infrared. In the first case, a common practice is to apply a cut on $(i - z)$. For example, Schmidt et al. (2010) apply a cut at $(i - z)_{SDSS} > 1.4$, while Chiu et al. (2006) cut at $(i - z)_{SDSS} > 2.2$ to select T types. This latter cut would be interesting to study the transition between L and T types, but not for a complete sample of L types. In any case, since the i, z bands in DES are not precisely the same as in SDSS, we expect changes in our nominal colour cuts.

When infrared bands are available, it is common to make the selection on J band. For example, Skrzypek et al. (2016) apply a cut on Vega magnitudes $(Y - J)_{UKIDSS,vega} > 0.8$, which, in our case, would translate into $(Y_{AB} - J_{vega})_{UKIDSS} > 1.4$. Burningham et al. (2013) search for T types, applying a cut at $z_{AB} - J_{Vega} > 2.5$. Again, the UKIDSS filters are not exactly the same as DES or VHS, so we expect these cuts to change when applied to our data.

In this paper, we follow the photo-type methodology of Skrzypek et al. (2015) to find and classify L and T dwarfs in the $DES \cap VHS \cap AllWISE$ system (The AllWISE program was built by combining data from the WISE cryogenic and NEOWISE post cryogenic phases). We can go to greater distances due to the increased depth in the DES optical bands i, z in comparison with SDSS while maintaining high completeness in the infrared bands, needed for a precise photometric classification. In fact, the optical bands can drive the selection of L dwarfs, as demonstrated here, improving upon previous photometric BDs searches. In the case of T dwarfs, the infrared bands are the limiting ones, and therefore, our

Table 1. Summary of the major photometric brown dwarf census so far. In the third column we show the colour selection in its original systems, according to the surveys used (indicated in the first column). For comparison, we also show the selection used in this paper, where we classify more than 10,000 BDs up to $z_{AB} = 22$.

Reference (Surveys)	Area (deg^2)	Selection	Spectral Types	Number
Chiu et al. (2006) (SDSS)	3,526	$(i-z)_{AB} > 2.2$, $z_{AB} < 20.4$	LT	73
Schmidt et al. (2010) (SDSS, 2MASS)	11,000	$(i-z)_{AB} > 1.4$	L	484
Albert et al. (2011) (CFHT)	780	$(i-z)_{AB} > 2.5$	T	37
Kirkpatrick et al. (2011) (WISE)	All sky	T5: $(W1-W2)_{Vega} > 1.5$, $(W2-W3)_{Vega} < 3.$ L: $(W1-W2)_{Vega} > 0.$	LT	103
Lodieu et al. (2012) (VHS, WISE)	675	$(W1-W2)_{Vega} > 1.4$, $(J-W2)_{Vega} > 1.9$	T	13
Day-Jones et al. (2013) (UKIDSS)	500	$J_{Vega} < 18.1$	LT	63
Burningham et al. (2013) (UKIDSS)	2,000	$(z_{AB}-J_{Vega}) > 2.5$, $J_{Vega} < 18.8$	T	76
Skrzypek et al. (2016) (SDSS, UKIDSS, WISE)	3,070	$(Y-J)_{Vega} > 0.8$, $J_{Vega} < 17.5$	LT	1,361
Sorahana et al. (2018) (HSC)	130	$1 < (i-z)_{AB} < 2.0$, $0.75 < (z-Y)_{AB} < 1.0$, $z_{AB} < 24$	L	3,665
This paper (2019) (DES, VHS, WISE)	2,400	$(i-z)_{AB} > 1.2$, $(z-Y)_{AB} > 0.15$, $(Y_{AB}-J_{Vega}) > 1.6$, $z_{AB} < 22$	LT	11,745

sample will have a similar efficiency in that spectral regime in comparison with previous surveys.

The methodology is based on three steps: first a photometric selection in colour space $(i-z)$, $(z-Y)$, $(Y-J)$ is done; second, a spectral classification is performed by comparing observed colours in $i, z, Y, J, H, K_s, W1, W2$ to a set of colour templates for various spectral types, ranging from M1 to T9. These templates are calibrated using a sample of spectroscopically confirmed ultra-cool dwarfs (MLT). Finally, we remove possible extragalactic contamination with the use of a galaxy template fitting code, in particular, we use `Lephare` photo-z code[1] (Arnouts et al. 1999; Ilbert et al. 2006).

After completion of a homogeneous sample of LT dwarfs, we proceed to measure the thin disk scale height ($h_{z,thin}$). Unfortunately, current simulations present many inconsistencies with observations and are not trustworthy. Therefore, we also introduce a new simulation which computes expected number counts of LT dwarfs and creates synthetic samples following the properties of a given survey. We have called it *GalmodBD*. Finally, we can compare the output of the simulation for different formation scenarios, to the number of BDs found in the sample footprint, placing constraints on $h_{z,thin}$ and other fundamental parameters.

In Section 2 we describe the data used in this paper ($DES \cap VHS \cap AllWISE$) and how these samples were matched and used through the analysis. In Section 3 we detail the samples we have used to define our colour selection as well as to create the colour templates that will feed the classification and the *GalmodBD* simulation.

In Section 4 we show the colour based target selection scheme we have defined and how it compares with the previous analysis, in particular to Skrzypek et al. (2015). In Section 5 we explain our classification methodology and how we apply it to the DES data in Section 6. In Section 7 we detail the public catalogue. In Sections 8 and 9 we introduce the *GalmodBD* simulation and how we tune it to our data in Section 10. In Section 11 we present results of running the simulation. In Section 12 we use the *GalmodBD* to study the completeness of our photometric selection and other systematics applying to the number of BDs detected. Finally, in Section 13 we compare results from the *GalmodBD* simulation to our data, placing constraints on the thin disk scale height of L types.

Through the paper, we will use the photometric bands i, z, Y from DES in AB magnitudes, J, H, K_s from VHS in Vega and $W1, W2$ from AllWISE in Vega. The use of Vega or AB normalisation is not important since it is only a constant factor when calculating colours.

2 THE DATA

In this section we present the three photometric data sets used in this analysis: the Dark Energy Survey (DES), with 5 filters covering from 0.38 to 1 μm (from which we use i, z, Y), VHS, with 3 filters covering from 1.2 to 2.2 μm and AllWISE

[1] http://www.cfht.hawaii.edu/~arnouts/LEPHARE/lephare.html

$W1$ and $W2$, at 3.4 and 4.6 μm. Finally, in Subsection 2.4 we detail the catalogue matching process and quality cuts.

2.1 The Dark Energy Survey (DES)

DES is a wide-field optical survey in the g, r, i, z, Y bands, covering from 3800 Å to ~ 1 μm. The footprint was designed to avoid extinction contamination from the Milky Way as much as possible, therefore pointing mostly towards intermediate and high Galactic latitudes. The observational campaign ended on the 9th of January 2019. The final DES data compromises 758 nights of observations over six years (from 2013 to 2019).

In this paper we use DES year 3 (Y3) data, an augmented version of the Data Release 1 (The DR1; Dark Energy Survey Collaboration et al. 2018)[2] which contains all the observations from 2013 to 2016. DES DR1 covers the nominal 5,000 deg^2 survey region. The median coadded catalogue depth for a 1.95″ diameter aperture at $S/N = 10$ is $i \sim 23.44$, $z \sim 22.69$, and $Y \sim 21.44$. DR1 catalogue is based on coaddition of multiple single epochs (Morganson et al. 2018) using `SExtractor` (Bertin & Arnouts 1996). The DES Data Management (DESDM) system also computes morphological and photometric quantities using the "Single Object Fitting" pipeline (SOF), based on the `ngmix`[3] code, which is a simplified version of the MOF pipeline as described in (Drlica-Wagner et al. 2018). The SOF catalogue was only calculated in g, r, i, z, but not in Y, therefore we use `SExtractor` Y measurement from DR1 data. All magnitudes have been corrected by new zeropoint values produced by the collaboration, improving over those currently published in the DR1 release.

Information about the mean wavelength of each passband and magnitude limit at 5σ (defined as the mode of the magnitude distribution, as cited above, for a catalogue with $S/N > 5\sigma$) is given in Table 2. In Fig. 1 we show the DES footprint with coverage in i, z, Y. It has an area = 5019 deg^2 and all coloured areas represent the DES footprint.

To ensure high completeness in the i band and infrared bands with sufficient quality, we impose a magnitude limit cut of $z < 22$ with a detection of 5σ at least in the z and Y magnitudes. To avoid corrupted values due to image artefacts or reduction problems, we also apply the following cuts: `SEXTRACTOR_FLAGS_z,Y = 0`: ensures no reduction problems in the z and Y bands. `IMAFLAGS_ISO_i,z,Y = 0`: ensures the object has not been affected by spurious events in the images in i, z, Y bands.

2.2 VISTA Hemisphere survey (VHS)

The VISTA Hemisphere Survey (VHS, McMahon et al. 2013) is an infrared photometric survey aiming to observe 18,000 deg^2 in the southern hemisphere, with full overlap with DES in two wavebands, J and K_s, to a depth $J_{AB} \sim 21.2$, $K_{s,AB} \sim 20.4$ at 5σ for point sources ($J_{Vega} \sim 20.3$, $K_{s,Vega} \sim 18.6$, respectively) and partial coverage in H band, with depth $H_{AB} \sim 19.85$ at 5σ ($H_{Vega} \sim 18.5$). The VHS uses the 4m VISTA telescope at ESO Cerro Paranal Observatory in Chile with the VIRCAM camera (Dalton et al. 2006). The data were downloaded by the DESDM system from the ESO Science Archive Facility (Cross et al. 2012) and the VISTA Science Archive[4].

The VHS DR3 covers 8,000 deg^2 in J, K_s of observations from the year 2009 to 2013, from which a smaller region overlaps with DES, as shown in brown in Fig. 1. The coverage area in common with DES is 2374 deg^2 for the J, K_s filters, whereas addition of the H band reduces this to 1331 deg^2 (shown as light brown in Fig. 1).

In this paper, we use only sources defined as primary in the VHS data. We also impose 5σ detection in J; whenever H, K_s are available, we use them for the spectral classification (see Section 5).

We use `apermag3` as the standard VHS magnitude, in the Vega system, defined as the magnitude for a fixed aperture of 2″. In Table 2 we show the summary of the filters and magnitude limits for VHS. VHS magnitude limits are in AB, even though we work in Vega throughout the paper. We use the transformation given by the VHS collaboration [5]: $J_{AB} = J_{Vega} + 0.916$, $H_{AB} = H_{Vega} + 1.366$, $K_{s,AB} = K_{s,Vega} + 1.827$.

2.3 AllWISE

We also use AllWISE[6] data, a full sky infrared survey in 3.4, 4.6, 12, and 22 μm, corresponding to $W1, W2, W3, W4$, respectively. AllWISE data products are generated using the imaging data collected and processed as part of the original WISE (Wright et al. 2010) and NEOWISE (Mainzer et al. 2011) programs.

Because LT colours tend to saturate for longer wavelengths, we will make use only of $W1$ and $W2$. The AllWISE catalogue is >95% complete for sources with $W1 < 17.1$ and $W2 < 15.7$ (Vega).

In Table 2 we also show the properties of the AllWISE filters and magnitude limits. Magnitudes are given in AB using the transformations given by the collaboration [7]: $W1_{AB} = W1_{Vega} + 2.699$, $W2_{AB} = W2_{Vega} + 3.339$.

Since our primary LT selection criteria do not use $W1$ and $W2$ magnitudes, we do not demand the availability of magnitudes in these bands when selecting our candidate sample. In other words, if a source has no data from AllWISE, we still keep it and flag their $W1$ and $W2$ magnitudes as unavailable in the classification.

2.4 Combining DES, VHS and AllWISE data

We first match DES to VHS with a matching radius of 2″, and with the resulting catalogue, we repeat the same process to match to the AllWISE catalogue, using DES coordinates. The astrometric offset between DES and VHS sources was estimated in Banerji et al. (2015), giving a standard deviation of 0.18″. For sources with significant proper motions, this matching radius may be too small. For instance, an

[2] https://des.ncsa.illinois.edu/releases/dr1
[3] https://github.com/esheldon/ngmix
[4] http://horus.roe.ac.uk/vsa/coverage-maps.html
[5] http://casu.ast.cam.ac.uk/surveys-projects/vista/technical/filter-set
[6] http://wise2.ipac.caltech.edu/docs/release/allwise/
[7] http://wise2.ipac.caltech.edu/docs/release/allsky/expsup/sec4_4h.html

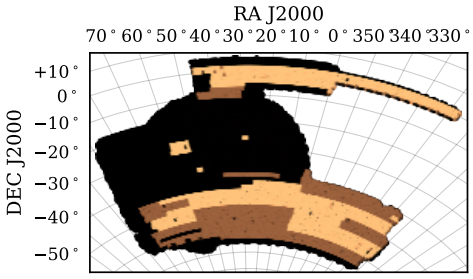

Figure 1. The footprint of DES Y3 data considering the intersection of i, z, Y bands. The effective area for this region is 5019 deg^2. In brown shaded regions, we show the overlap between DES and VHS, covering 2,374 deg^2 with J, K_s and 1331 deg^2 if the H band is included (in light brown).

object at 10 pc distance, moving at 30 km/s in tangential velocity, has a proper motion of $0.6''/yr$. So, a matching radius of $2''$ will work except for the very nearby ($<= 6pc$) or high-velocity ($> 50km/s$) cases, given a 2-year baseline difference in the astrometry. In fact, high velocity nearby BDs are interesting, since they may be halo BDs going through the solar neighbourhood. A small percentage of BDs will be missing from our catalogue due to this effect. In Section 12 we quantify this effect.

We use the $DES \cap VHS \cap AllWISE$ sample (called target sample) to find BDs. Matching the three catalogues and removing sources that do not pass the DES quality cuts, we find 42,046,583 sources. Applying the cut in signal-to-noise (SNR) greater than 5σ in z, Y, J and selecting sources with $z < 22$, we find 27,249,118 sources in our 2,374 deg^2 footprint.

We do not account for interstellar reddening. Our target sample is concentrated in the solar neighbourhood and therefore, applying any known extinction maps, like Schlegel et al. (1998) or Schlafly & Finkbeiner (2011) maps, we would overestimate the reddening.

3 CALIBRATION SAMPLES

In this section, we present and characterise the calibration samples used to define our colour selection (Section 4) and to create the photometric templates (see Section 3.4) that will be used during the spectral classification step (Section 5) and to feed the *GalmodBD* simulation (Section 8). Quasars are only used as a reference in the first stage, while the M dwarfs and BDs are used both to select the colour space and to create the colour templates that will be used during the analysis.

The calibration samples are: J. Gagné's compilation of brown dwarfs, M dwarf sample from SDSS and spectroscopically confirmed quasars from DES. It is important to note that all of them have spectroscopic confirmation.

Each calibration sample has been matched to the target sample. In all cases, we again use a matching radius of $2''$ to DES coordinates.

Table 2. Information about the photometric passbands from DES Y3, VHS DR3 and AllWISE. Columns are the survey acronym, the filter name, the effective wavelength and the magnitude limit at 5σ in AB.

Survey	Filter	λ_c (μm)	$m_{5\sigma}$ (AB)
DES	i	0.775	23.75
DES	z	0.925	23.05
DES	Y	1.0	20.75
VHS	J	1.25	21.2
VHS	H	1.65	19.85
VHS	K_s	2.15	20.4
AllWISE	$W1$	3.4	19.80
AllWISE	$W2$	4.6	19.04

3.1 Gagné's sample of brown dwarfs

The Gagné compilation [8] contains a list of most of the spectroscopically confirmed BDs up to 2014, covering spectral types from late M to LT dwarfs. It consists of 1772 sources, covering most parts of the sky to distances less than 100 pc. The spectral classification in this sample is given by its optical classification anchored to the standard L dwarf scheme of Kirkpatrick et al. (1999) or by its near-infrared classification anchored to the scheme for T dwarfs from Burgasser et al. (2006b). Some of the brown dwarfs present in this sample have both classifications. In most cases, both estimations agree, but for a few of them ($\approx$ 10%), there is a discrepancy of more than one spectral types, which can be considered as due to peculiarities. In these cases, we adopted the optical classification. We tested the effect of using one or another value in the creation of the templates and found discrepancies of $\lesssim$ 3%.

From the initial list of 1772 BDs, we removed objects that are considered peculiar (in colour space) or that are part of a double system, categories given in the Gagné compilation and also sources with spectral type M, yielding a remaining list of 1629 BDs. From this list, 233 are present in the DES footprint, but when we match at $2''$ between the DES and Gagné sample, we only recover 150 of these. For the remaining 83 that are not matched within $2''$, we visually inspected the DES images to find their counterparts beyond the $2''$ radius, recovering in this process 58 additional LT types to the DES sample. Therefore, our sample totals 208 known LT dwarfs, while 25 are not found due to partial coverage of the footprint or due to high proper motions.

Repeating the same procedure but for VHS: in the entire VHS footprint (not only in the $DES \cap VHS$ region), but we find 163 LT dwarfs at $2''$ radius. Here we did not repeat the process of manually recovering missing objects. In the $DES \cap VHS$ region, we end with 104 confirmed LT dwarfs,

[8] https://jgagneastro.wordpress.com/list-of-ultracool-dwarfs/

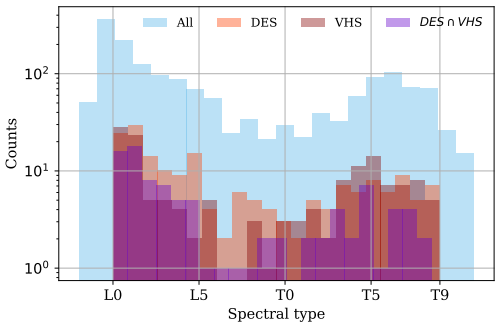

Figure 2. The distribution of known BDs in the Gagné sample for different overlaps. The original sample contains 1,629 BDs, 208 of which are found in the DES Y3 data, 163 in the VHS DR3 data and 104 in the $DES \cap VHS$ data, after removal of M types and young L types.

from 139 in the $DES \cap VHS$ common footprint. The missing sources are due to the same effects of partial coverage or high proper motions.

During our analysis, we found that BDs tagged as "young" in the Gagné sample were biasing the empirical colour templates used for classification (see details in Section 5.1). BDs are tagged as "young" in the Gagné sample whenever they are found as members of a Young Moving Group (YMG) or are otherwise suspected of having ages less than a few 100 $Myrs$. Young BDs are typically found to exhibit redder photometric colours in the near-infrared due to the effects of low-gravity and/or different cloud properties (e.g. Faherty et al. 2016). We, therefore, removed those from the calibration sample.

As a result, our final LT calibration sample contains 208 sources in the Y3 DES sample, 104 in the $DES \cap VHS$ region, 163 in VHS DR3 alone and 128 with $VHS \cap AllWISE$. These are the final samples we use to calibrate the empirical colour templates for BDs, depending on the colour to parameterize (For example, for $(J-H)$ we use the VHS sample with 163 sources, whereas for $(i-z)$ and $(z-Y)$, we use the DES sample with 208 sources). These templates will also feed the *GalmodBD* simulation for the LT population (Section 8).

In Fig. 2 we show the number of BDs as a function of the spectral type in the Gagné sample, matched to different photometric data. At this point, we assume that the colour templates we will obtain from these samples are representative of the whole brown dwarf population. Later, in section 4, we will compare the target sample to the calibration sample and confirm that this approximation is valid.

3.2 M dwarfs

The sample of M dwarfs comes from a spectroscopic catalogue of 70,841 visually inspected M dwarfs from the seventh data release of the SDSS (West et al. 2011), confined to the Stripe82 region. After matching with the target sample at a $2''$ radius, we end up with 3,849 spectroscopically confirmed M dwarfs with spectroscopic classification, from M0 to M9. We use this sample to create templates for our classification schema, with particular care for the transition from M9 to L0. These templates will also feed the *GalmodBD* simulation for the M population (Section 8).

3.3 Quasars

Quasars have been traditionally a source of contaminants in brown dwarf searches since they are point-like, and at high redshift, they can be very red, especially in infrared searches using WISE or 2MASS data, for instance. On the other hand, this degeneracy can be broken with the use of optical information, as shown in Reed et al. (2015) and Reed et al. (2017). We use two samples of confirmed quasars in DES, one from Tie et al. (2017) up to z=4 and the one from Reed et al. (2017) with $z > 6$. In principle, quasars follow a different colour locus (as seen in Reed et al. (2017)) but some contamination might remain after the colour cuts, and we will treat them as a source of extragalactic contamination in Section 6.1.

3.4 Colour templates

To define our colour selection, to classify BDs and to produce realistic colours in the simulation, we create colour templates as a function of the spectral type in $(i-z)_{AB}$, $(z-Y)_{AB}$, $(Y_{AB}-J_{Vega})$, $(J-H)_{Vega}$, $(H-K_s)_{Vega}$, $(K_s-W1)_{Vega}$ and $(W1-W2)_{Vega}$.

Since M dwarfs are much more abundant than BDs in our samples, we adopt different approaches to build the colour templates, depending on the available number of calibrating sources. For M and L0 dwarfs, where we have enough statistics, we take the mean value for each spectral type as the template value, selecting sources with $SNR > 5\sigma$ only. Beyond L0, since we do not have enough statistics for all spectral types, we follow a different approach: we fit the colour versus spectral type distribution locally in each spectral type using both first order and second order polynomials. For instance, for L7 we fit the colour distribution between L3 and T3, and with the given first and second order polynomials, we interpolate the result for L7. Finally, the colour value for the given spectral type is taken as the average of the two polynomial fits.

The empirical templates can be seen in Fig. 3. The template values are listed in Table 3. We found several degeneracies in colour space. For example, in $(H-K_s)$, one cannot distinguish spectral types between early-L and late-L/early-T because their colours are the same, or in $(W1-W2)$, where we cannot discriminate between mid-M stars and early-mid/L-dwarfs for the same reason. Since several colours exhibit degeneracies in their colour-spectral type relationships, it is important to have multiple colours to establish a good spectral type calibration and therefore the need for a combination of optical and infrared data.

In terms of the dispersion about the templates, it increases with spectral type, with some exceptions. For example, in $(W1-W2)$ the dispersion for M types is larger than for some LT types. In the T regime, in general, the dispersion due to variations in metallicity, surface gravity or cloud cover, among other effects, can be of the same order or bigger than the dispersion introduced by differences

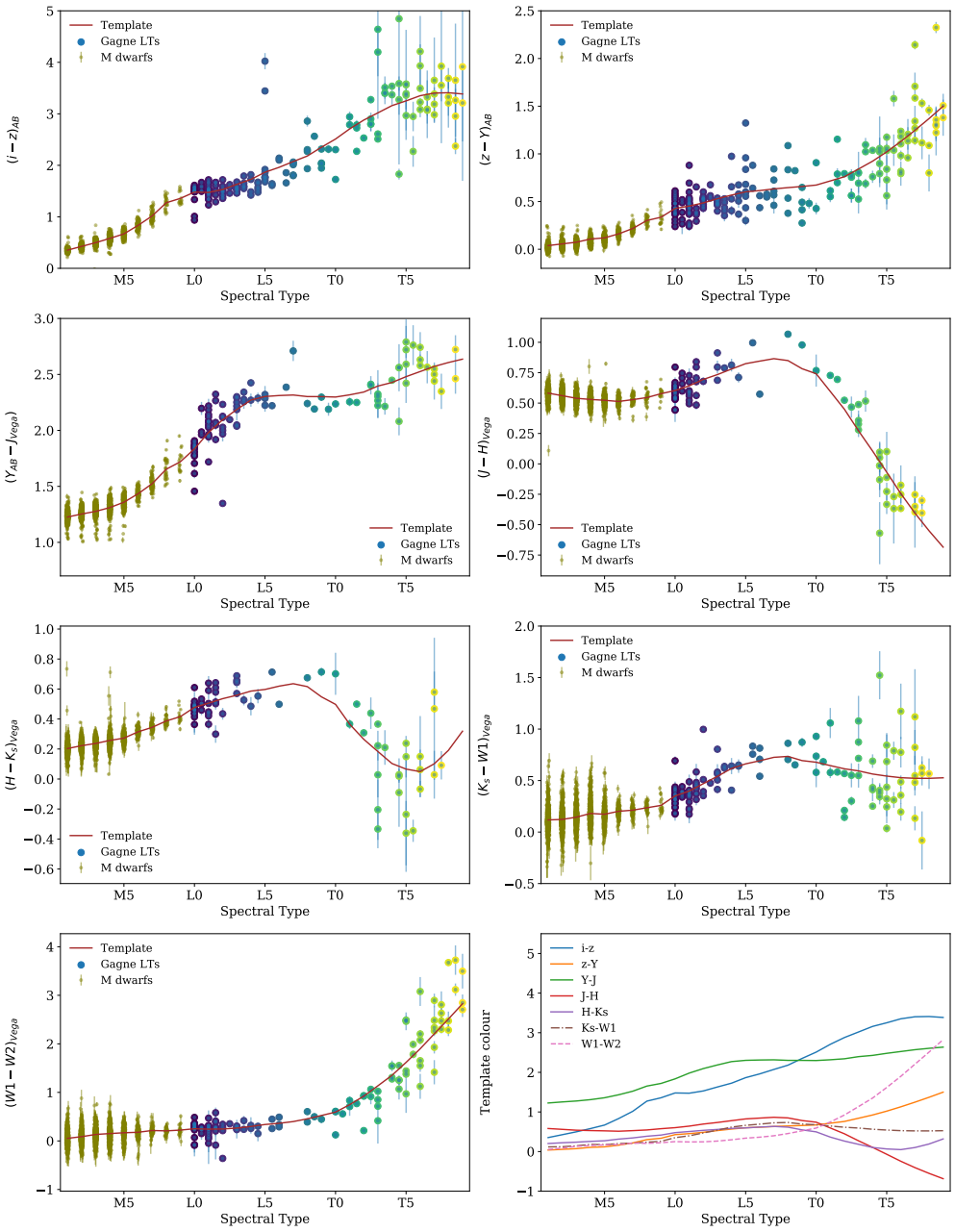

Figure 3. Colours as a function of the spectral type in the MLT spectral regime. M dwarfs are shown in olive, in blue, green and yellow are BDs with their colour given by their spectral type, as seen in Fig 4. These templates are used during the classification and to feed the *GalmodBD* simulations. In the last panel, we compare all the templates together. Since several colours exhibit degeneracies in their colour-spectral type relationships, it is essential to have multiple colours to establish a good spectral type calibration.

in signal-to-noise. Possible peculiar objects will be identified with high χ^2 when compared to the empirical templates.

In the last panel of Fig. 3, we compare all the templates together. From here, we find that $(i-z)$ colour has the largest variation through the ML range, demonstrating the importance of the optical filters to separate M dwarfs from LT dwarfs. $(W1-W2)$ is very sensitive to T types (as expected by design), and $(Y-J)$ is also important for the ML transition. The other bands will add little to the M/L transition, but they will help on L/T transition. Similar findings were already presented in Skrzypek et al. (2015).

4 MLT COLOUR SELECTION

In this section we explain the steps to select our initial list of LT candidates from the target sample. In Fig. 4, we show the colour-colour diagrams of known BDs, M dwarfs and quasars. Clearly, some of these colour-colour diagrams are more efficient to disentangle LT dwarfs from other point sources than others. Furthermore, at $z \sim 22$, we are still mostly complete in the i band, although not necessarily for late T types. Therefore we do not demand detection in i band, but we still impose a minimum $(i-z)$ colour as a selection criterion, very efficient to remove quasars from our sample, as attested by Fig. 4.

The nominal cut at $z_{AB} = 22$ is set to ensure that the combination $DES \cap VHS$ takes full advantage of both surveys, something that was not possible earlier due to the brighter magnitude limits imposed by SDSS. At $z_{AB} = 22$, we are limited at $J_{Vega} \sim 19.7$. This corresponds to $z_{AB} - J_{Vega} \sim 2.30$, which is the colour of an L0 according to the templates presented in Table 3. This is brighter by at least 0.7 magnitudes than the 5σ limit on VHS. In other words, we will be able to reach $z_{AB} = 22.7$ in upcoming DES updates and still remain complete in optical and VHS bands for the LT types. The magnitude limits on VHS bands are also deeper than its predecessors. For example, UKIDSS has a global depth limit of $J_{Vega} \sim 19.6$ (Warren et al. 2007), while VHS has $J_{Vega} \sim 20.3$.

We define the colour space where BDs are found to reside. We initially aim at high completeness in color space, at the expense of allowing for some contamination by M dwarfs and extragalactic sources. Purity is later improved at the classification stage (Section 5).

The entire selection process can be summarized in 7 stages as detailed below and listed in Table 4:

(i) Quality cuts on DES and matching to VHS (explained in Section 2). We end up with 42,046,583 sources after applying a matching within 2″ between the DES and the VHS, and selecting sources with `SEXTRACTOR_FLAGS_z,Y = 0` and `IMAFLAGS_ISO_i,z,Y = 0`.

(ii) Magnitude limit cut in $z < 22$ and signal-to-noise greater than 5σ in z, Y, J. We end up with 28,259,901 sources.

(iii) We first apply a cut in the optical bands $(i-z)$, removing most quasar contamination while maintaining those sources for which i band has no detection. We decided to apply a cut of $(i-z) > 1.2$. In comparison with previous surveys, as seen in Table 1, this is a more relaxed cut, initially focusing on high completeness in our sample at the expense of purity. This cut eliminates more than 99.8% of the catalogue, leaving us with a sample of 65,041 candidates.

(iv) We apply a second selection to the target sample in the space $(z-Y)$ vs. $(Y-J)$. From Fig. 4, we decided the cut to be: $(z-Y) > 0.15$, $(Y-J) > 1.6$ avoiding the $z > 6$ QSO colour locus. The surviving number of sources is 35,548. This cut is actually very similar to the cut proposed in Skrzypek et al. (2016). They imposed $Y - J > 0.8$ (Vega). Transforming our Y band to Vega, our equivalent cut would be $Y - J > 0.7$.

(v) Finally, we apply the footprint mask. In this process, we end up with 35,426 candidates. This is the sample that goes into classification. Extragalactic contamination is treated after running the classification.

(vi) Apply the *photo-type* method (Skrzypek et al. 2015) to estimate the spectral type in the MLT range for all the targets. We call this method *classif* (see Section 5). After removal of the M types, we ended with 12,797 LT types.

(vii) Removal of extragalactic contamination (see Section 6.1). We end up with the final sample of 11,745 LT types from which 11,545 are L types, and 200 are T types. There is also extragalactic contamination in the M regime, as explained in the next section.

5 SPECTRAL CLASSIFICATION

In this section we explain the method to assign spectral types to our candidate list and evaluate its uncertainties based on the calibration samples. We implement the same classification method presented in Skrzypek et al. (2015) and Skrzypek et al. (2016), based on a minimization of the χ^2 relative to the MLT empirical templates. Our method uses the templates created in Section 3.4. We refer to our classification code as *classif*.

As mentioned earlier, we impose a 5σ detection in z, Y, J. For the rest of the bands, we require a 3σ detection. If the magnitude error exceeds this limit, we consider the source as not observed in the given band. However, there is one exception, the $W1$ magnitude, which is cut at 5σ in the AllWISE catalogue.

Let a set of N_{bands} observed for the j-th candidate to be $\{m_{ji}$, i=1,$N_{bands}\}$ and their photometric uncertainties be $\{\sigma_{m_{ji}}$, i=1,$N_{bands}\}$. Let also a set of colour templates be $\{c_{i,k}$, i=1,N_{bands}, k=1,$N_{mod}\}$, which give the magnitude difference between band b and the reference band z. Hence $c_{z,k} = 0$ by construction. Let's consider the template intrinsic dispersion to be $\{\sigma_{c_{i,k}}$, i=1,N_{bands}, k=1,$N_{mod}\}$, which we fix for all bands and templates to $\sigma_c = 0.07$, as also done by Skrzypek et al. (2016). The total error for band b, for the j-th candidate will be $\sigma_{bj} = \sqrt{\sigma^2_{m_{jb}} + \sigma^2_c}$.

The first step in the classification process for the j-th candidate is, for each of the k-th spectral type (N_{mod}), calculate the inverse variance weighted estimate of the reference magnitude (in our case z) as:

$$\hat{m}_{j,z,k} = \frac{\sum_{b=1}^{N_{bands}} \frac{m_{jb} - c_{bk}}{\sigma^2_{bj}}}{\sum_{b=1}^{N_{bands}} \frac{1}{\sigma^2_{bj}}} \quad (1)$$

Table 3. Template values as a function of the spectral type in the MLT regime. These are the best-fit values shown in Fig. 3 and that are later used in the classification and to feed the *GalmodBD* simulation.

Spectral Type	Colour						
	$(i-z)_{AB}$	$(z-Y)_{AB}$	$(Y_{AB}-J_{Vega})$	$(J-H)_{Vega}$	$(H-K_s)_{Vega}$	$(K_s-W1)_{Vega}$	$(W1-W2)_{Vega}$
M1	0.35	0.04	1.23	0.58	0.20	0.12	0.05
M2	0.43	0.06	1.25	0.56	0.22	0.12	0.09
M3	0.50	0.07	1.28	0.54	0.24	0.14	0.13
M4	0.58	0.11	1.31	0.53	0.26	0.18	0.15
M5	0.67	0.12	1.36	0.52	0.27	0.17	0.17
M6	0.83	0.16	1.43	0.51	0.31	0.20	0.18
M7	1.02	0.22	1.52	0.53	0.34	0.21	0.21
M8	1.27	0.30	1.65	0.54	0.39	0.24	0.21
M9	1.36	0.34	1.72	0.58	0.42	0.26	0.22
L0	1.48	0.43	1.83	0.60	0.48	0.35	0.25
L1	1.47	0.45	1.98	0.64	0.51	0.40	0.24
L2	1.53	0.49	2.09	0.69	0.54	0.47	0.25
L3	1.63	0.53	2.19	0.73	0.56	0.54	0.26
L4	1.73	0.57	2.27	0.78	0.59	0.62	0.30
L5	1.87	0.60	2.30	0.82	0.60	0.66	0.34
L6	1.96	0.62	2.31	0.84	0.62	0.69	0.36
L7	2.07	0.63	2.32	0.87	0.64	0.72	0.40
L8	2.18	0.65	2.30	0.85	0.62	0.73	0.46
L9	2.35	0.66	2.30	0.78	0.55	0.69	0.52
T0	2.51	0.67	2.30	0.74	0.50	0.68	0.59
T1	2.71	0.72	2.32	0.60	0.36	0.64	0.75
T2	2.88	0.76	2.34	0.45	0.26	0.61	0.92
T3	3.02	0.84	2.40	0.27	0.18	0.59	1.13
T4	3.16	0.92	2.43	0.11	0.10	0.56	1.35
T5	3.25	1.02	2.48	-0.07	0.07	0.54	1.62
T6	3.35	1.13	2.53	-0.24	0.05	0.53	1.90
T7	3.40	1.25	2.57	-0.40	0.10	0.52	2.21
T8	3.41	1.37	2.61	-0.55	0.20	0.52	2.51
T9	3.39	1.50	2.64	-0.68	0.32	0.53	2.83

Table 4. Steps used in this paper to classify LT sources in $DES \cap VHS \cap WISE$. First, quality cuts are applied to the data to remove spurious targets. Next, a magnitude limit is imposed in the z band and finally, colour cuts are applied to select only the reddest objects. These are the sources that enter the classification. Finally, extragalactic contamination is removed.

Step	Description	Percentage Removed	Number Remaining
0	DES Y3 sample (DR1)		399,263,026

1	Matching 2 arcseconds to VHS
	`FLAGS_z,Y=0`
	`IMAFLAGS_ISO_i,z,Y=0`
		89.5%	42,046,583

2	$z < 22$ $SNR\_z, Y, J > 5\sigma$	33%	28,259,901
3	$(i-z)_{AB} > 1.2$	99.8%	65,041
4	$(z-Y)_{AB} > 0.15$ $Y_{AB} - J_{Vega} > 1.6$	45%	35,548
5	Footprint masking	0.3%	35,426
6	LT Classification	64%	12,797
7	Remove extragalactic contamination	8%	11,745

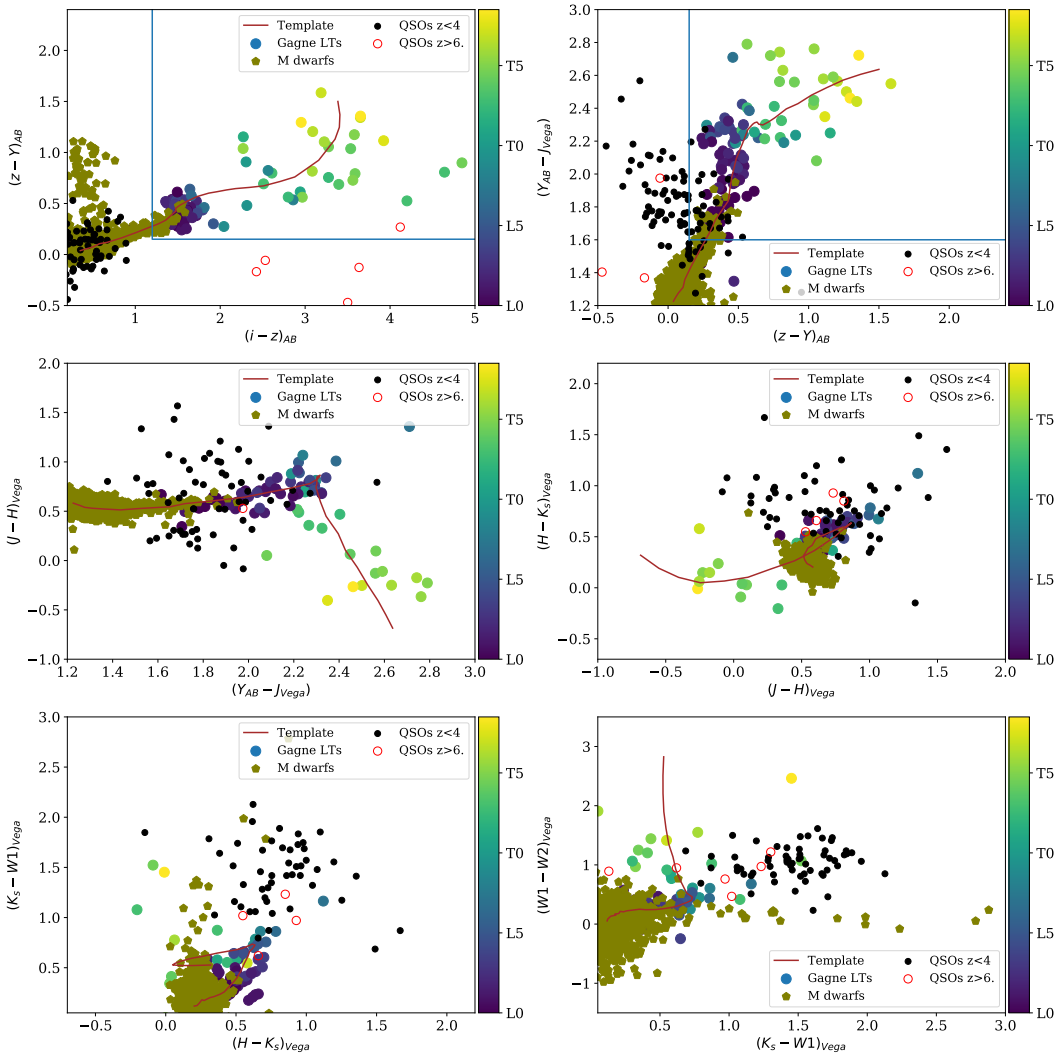

Figure 4. Colour-colour diagrams for spectroscopically confirmed BDs, M dwarfs and quasars that are found in the target sample. Each panel corresponds to a specific colour-colour space. In all panels, M dwarfs are shown as olive circles. Quasars as black circles for $z < 4$ and as empty red circles for $z > 6$, whereas LT dwarfs are shown as filled circles with their colour a function of the spectral type, as depicted in the colour bar on the right. The colour templates that were empirically derived (see Section 3.4) are shown by the brown line. The colour cuts applied to the sample before classification are depicted by the blue lines in the first two panels.

Next, the above value is used to calculate the χ^2 value for the k-th spectral type, for each j-th candidate:

$$\chi^2(\{m_j\},\{\sigma_{bj}\},\hat{m}_{z,k},k) = \sum_{b=1}^{N_{bands}} \left(\frac{m_{jb}-\hat{m}_{z,k}-c_{b,k}}{\sigma_{bj}}\right)^2 \qquad (2)$$

Finally, we assign the spectral type that gives the minimum χ^2 value.

5.1 Classification performance on known samples

In this section we apply *classif* to our list of known BDs and M dwarfs to assess how well the method works. We run the code on the Gagné list of 104 known BDs (including young BDs) and in the West list of known M dwarfs. Results are summarized in Fig. 5, where we show the photometric spectral type versus the spectroscopic classification, separately for M (left) and LT types (right). In these figures, the dia-

mond points are those where the difference between the true spectral type and the photometric estimation is greater or equal to 4 ($\Delta_t >= 4$). There are 8 sources with $\Delta_t >= 4$, from which 6 of them are young L types.

We estimate the accuracy of the method using:

$$\sigma_{classif} = \frac{\sum_{j=1}^{N_{candidates}} |\Delta t|}{N_{candidates}} \frac{\sqrt{2N_{candidates}}}{2} \quad (3)$$

Dividing in M types (from West sample), L and T types (Gagné sample), we get $\sigma_M = 0.69$ (for M with spectral type M7 or higher), $\sigma_L = 1.47$ and $\sigma_T = 1.12$ and a global $\sigma_{LT} = 1.37$. If we now estimate the errors but without the young L types, the metrics improve to $\sigma_L = 1.03$ and $\sigma_T = 1.12$ and a global $\sigma_{LT} = 1.06$, a precision compatible to what was found in Skrzypek et al. (2016). Nonetheless, it is obvious from Fig. 5 that it is much more appropriate to use a 3σ value for how well one establish a photometric spectral type for these low-mass objects, thereby implying that the best one can do in estimating photometric spectral types is ±2 for M types and ±3 for LT-dwarfs.

Another test we perform is to estimate the spectral types for those LT candidates in the overlapping sample with Skrzypek et al. (2016), consisting of 74 sources. We run *classif* on these 74 sources and compare both photometric estimators. In general, we find an excellent agreement with $\sigma_{classif,skrzypek} = 0.38$. In Fig. 6 we show the comparison between the two methods.

6 CLASSIFICATION OF THE TARGET SAMPLE

After confirming that our method reliably classifies MLT spectral types, we run *classif* on the target sample presented in Section 4, a sample of 35,426 candidates. A visual inspection of the candidates demonstrates that all are real sources. The main caveat in our methodology might be residual contamination by extragalactic sources. We next explain our star-galaxy separation method.

6.1 Extragalactic contamination

To remove possible extragalactic contamination, we run `Lephare` photo-z code on the whole candidate list using galaxy and quasar templates spanning various redshifts, spectral types and internal extinction coefficients (the `Lephare` configuration used is presented in Appendix A). For those candidates where the best-fit is $\chi^2_{lephare} < \chi^2_{classif}$, we assign them a galaxy or quasar class and are no longer considered MLT types. This method also has the potential to identify interesting extragalactic targets.

It is worth noting that running `Lephare` onto the Gagné sample, we can recover most known LT types. Only one brown dwarf in the Gagné sample is assigned a galaxy class, which is already known to be a very peculiar L7 type called *ULAS J222711-004547* (Marocco et al. 2014). It has a $\chi^2_{classif} > 630$, while the rest of the 103 BDs have a $\chi^2_{classif} < 130$. Also, the classification is robust concerning changes in the galaxy libraries used in the `Lephare` configuration: we tested various choices of galaxy templates, and the number of extragalactic contaminants remained constant within errors.

6.2 Results

After running *classif* and `Lephare` on the target sample, we obtain 32,608 sources classified as MLT types. From these, 20,863 are M types, 11,545 are L types and are 200 T types. Our catalogue also includes 2,818 candidates classified as galaxies or quasars. A preliminary discussion about the properties of the extragalactic sources is given in Appendix B. In Section 7 we show an example of the data published in electronic format and its explanation. It consists of a table with all the 11,745 candidates in the target sample with LT spectral type including the photometry used and the *classif* results.

Sources with a number of bands available for classification (`NBANDS`) less than 5 (3 or 4) are generally assigned to extragalactic spectral types; likewise those have the best-fit MLT template as M types. By visually inspecting the spectral energy distribution of sources with `NBANDS` < 5, compared to the best-fit templates of MLT types, galaxies and quasars, we conclude that the classification is ambiguous and should be taken with caution when `NBANDS` < 5. From the catalogue of 35,426 targets, 6% have `NBANDS` < 5. If we consider only those with spectral type L, the percentage goes down to 3.7% (469 targets), i.e., 3.7% of the L types have `NBANDS` < 5, from which 96% (449 targets) are assigned to a galaxy template instead of to an L type. This effect contributes to the uncertainty associated with the removal of extragalactic contamination.

At this point, we compare the colour distribution as a function of the spectral type for the target sample with respect to the empirical templates of Section 3.4. We assumed that the templates were representative of the LT population. In Fig. 7 we can see the comparison. Our modelling reproduces the target sample colour distribution. Only in the late T regime, we find some discrepancies. This effect is due to both the lack of statistics when we calculated the empirical templates in this regime, and to the intrinsic dispersion in colours in the T regime.

6.3 Photometric properties of the LT population

We analyse the properties of the 11,745 LT types found in the target sample. The distribution of spectral types can be found in Fig. 8 in logarithmic scale. In Fig. 9 we show the distribution of bands available for classification.

The $\chi^2_{classif}$ of the fits are generally very good, in agreement with the theoretical curve for the same degrees of freedom. In our model we have two free parameters, the brightness of the source and the spectral type, therefore the degrees of freedom are $N_{bands}-2$. The $\chi^2_{classif}$ distribution can be found in Fig. 10. The theoretical curve is a summation over the χ^2 curves for degrees of freedom $1, 2, 3, 4, 5$ (corresponding to $N_{bands} = 3, 4, 5, 6, 7, 8$ respectively, where each curve was multiplied by the percentage of total sources with each number of bands. The reduced χ^2 defined as $\frac{\chi^2}{(d.o.f)}$ is close to one, with a mean value of $\overline{\frac{\chi^2}{(d.o.f)}} = 1.3$ and a median value $med(\frac{\chi^2}{(d.o.f)}) = 0.95$.

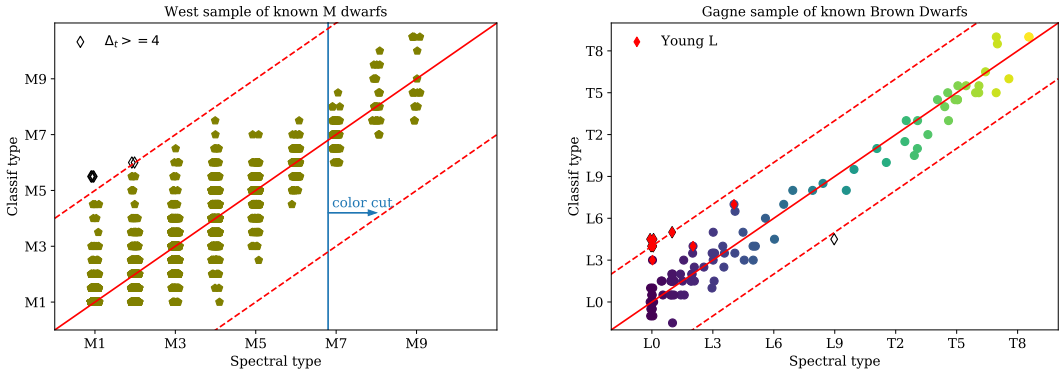

Figure 5. Classification performance for M dwarfs (left) and LT types (right). In both panels, sources with a misclassification higher or equal 4 are shown as diamond symbols. Red dashed lines indicate the limits where the difference between the spectroscopic and photometric classification is equal to 4. On the right panel, we also tag young L types, which were not used to build the templates but are shown here to illustrate their peculiar nature, with a classification that is always higher than 2. The classification have a mean uncertainty of $\sigma_M = 0.69$ (for M dwarfs passing the colour cuts) and $\sigma_L = 1.03$ and $\sigma_T = 1.12$ for the LT sample without the young L types. For visualization purposes we have applied small random shifts smaller than $\Delta_{template} \pm 0.1$ to the true spectral types (only in the x-axis).

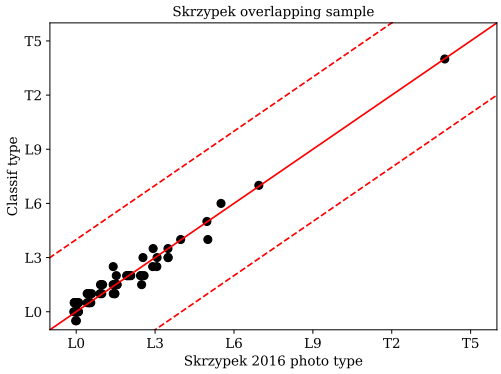

Figure 6. Comparison between the photometric classification of Skrzypek et al. (2016) and *classif* for 74 common LT candidates found in the footprint. We find an excellent agreement between both estimates with a mean dispersion of $\sigma_{classif} = 0.38$. For visualization purposes we have applied small random shifts smaller than $\Delta_{template} \pm 0.1$ to the Skrzypek et al. (2016) types (only in the x-axis).

In our analysis, we tag BDs as peculiar (in terms of colours) if their $\chi^2_{classif}$ is beyond 99.7% of the probability, which in a z-score analysis means having a $\chi^2_{classif} > 3\sigma$ off the median. In our case, we set the cut-off at 3.5σ instead to accommodate the natural dispersion of LT types. Since the $\chi^2_{classif}$ distribution is not normal we define σ based on the median absolute deviation (MAD) instead of the standard deviation, and since the distribution is non-symmetrical, we apply a double MAD strategy. Since T types have intrinsically more colour dispersion than L types, we treat them separately. Applying the double MAD algorithm to the $\chi^2_{classif}$ distribution of L and T types, for a cut-off $= 3.5\sigma$, we end up with 461 L types labeled as peculiar ($\approx 4\%$) and 6 T types tagged as peculiar ($\approx 3.5\%$). These limits are equivalent to say that L types are peculiar whenever their $\chi^2_{classif} > 20$. and that T types are peculiar whenever their $\chi^2_{classif} > 46.5$. Peculiar sources can be identified in the catalogue reading the `PECULIAR` column as explained in Section 7.

6.3.1 *Photometric distances*

We estimate photometric distances using the distance modulus:

$$d(Type)[i] = 10 * 10^{(m_z[i] - M_z(Type))/5} \quad (4)$$

Absolute magnitudes have been anchored to *M_W1* and *M_W2* from Dupuy & Liu (2012) as explained in Section 8.1. We compare two estimates for the distance: one where we use all available bands from the $i, z, Y, J, H, K_s, W1, W2$ set, and then we average over the bands to give a mean value, and the other where we use band z only. The distance distribution can be found in Fig. 11 for the averaged value. In Fig. 12 we show the difference between the averaged value and the z band estimate. In general, both definitions agree. In the published catalogue both estimates are given with names `DISTANCE_AVG` and `DISTANCE_Z`.

7 ELECTRONIC CATALOGUE

This is the largest photometric LT catalogue published to date, containing 11,745 sources. We also publish the M dwarf catalog in a separate table containing 20,863 sources. Table 5 shows a sample of the LT catalogue,

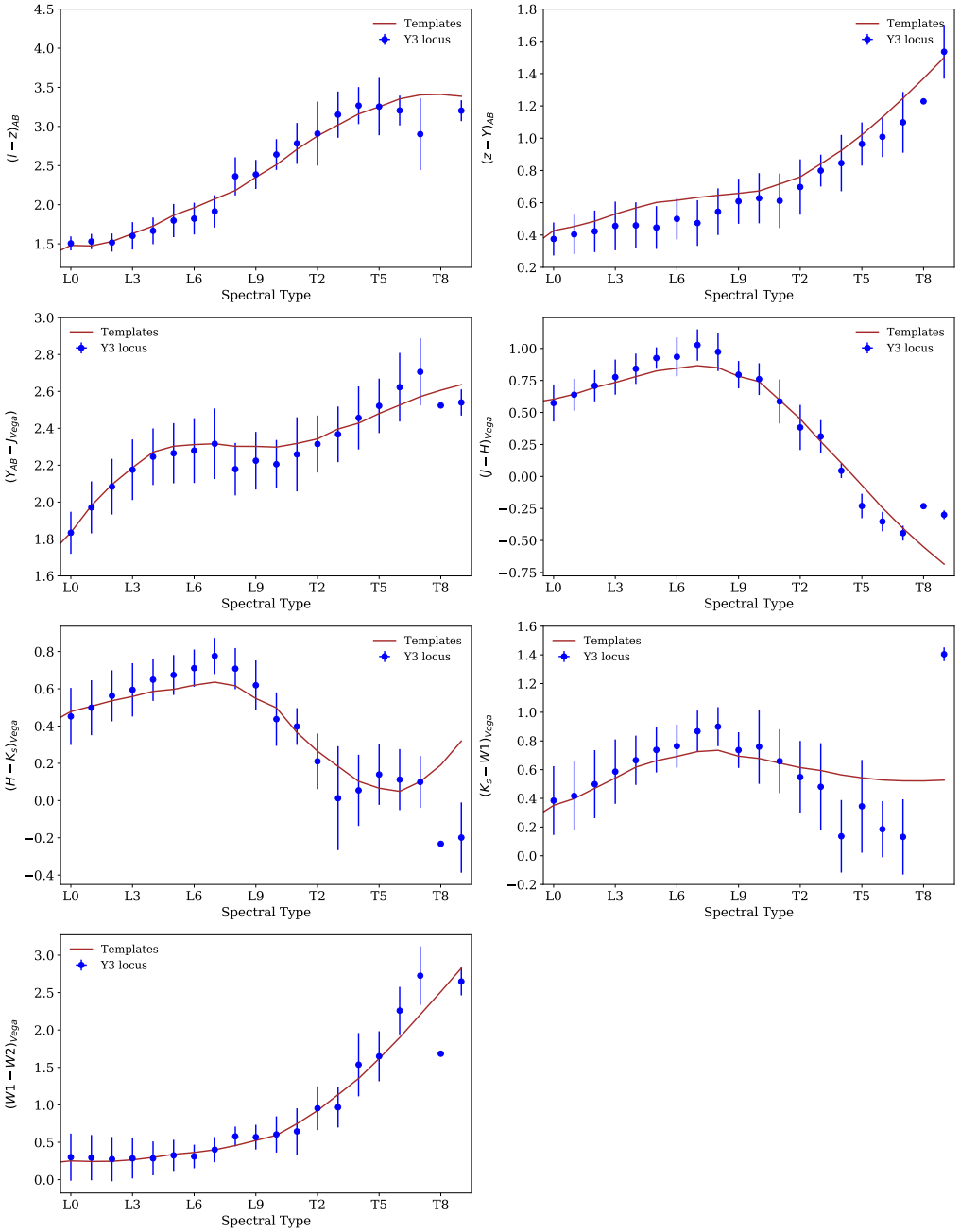

Figure 7. Comparison between the colour templates and the locus of the LT candidates. Blue points show the mean and standard deviation colour for candidates with the given spectral type. In brown, the empirical templates used. The agreement is good through all the spectral space, with deviations appearing in the late T type regime, where the calibration sample is very sparse, confirming the initial assumption that the calibration sample is representative of the whole LT population.

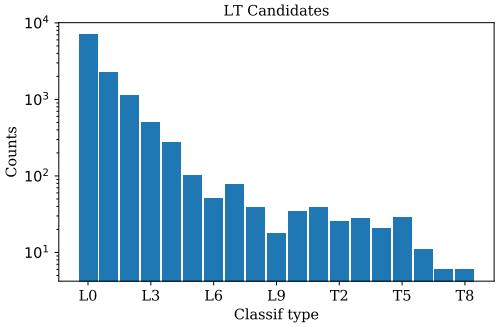

Figure 8. The distribution of spectral types for the LT candidates. We classify 20,863 sources as M dwarfs (from M7 to M9, not shown here), 11,545 as L types (from L0 to L9) and 200 as T types (from T0 to T9).

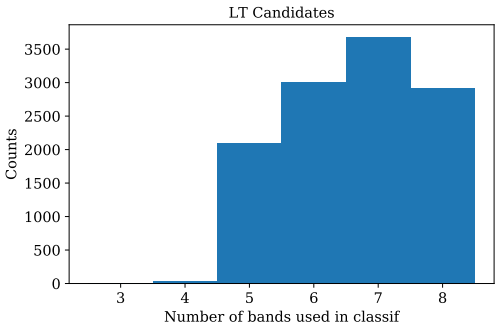

Figure 9. The number of bands (N_{bands}) used during the classification. This information is used to assign weights when we calculate the theoretical χ^2 distribution in Fig. 10.

which can be accessed at `https://des.ncsa.illinois.edu/releases/other/y3-mlt`. The number of LT types found in the target sample is subject to completeness and purity effects (see Section 12).

Spectral type is given by `SPT_PHOT` with the following convention: L types are assigned `SPT_PHOT` from 10 to 19, corresponding to L0 to L9, and from 20 to 29 for the T types, corresponding with T0 to T9. In the M dwarf catalogue, M types are assigned `SPT_PHOT` from 6 to 9. We also give the χ^2 of the classification and the number of bands used with columns `XI2_CLASSIF` and `NBANDS`. Distances are provided with 2 estimates, one based on band z only (`DISTANCE_Z`) and another based on the average of the distances calculated in all the available bands (`DISTANCE_AVG`). We also tag if the source is peculiar based on a z-score analysis of its χ^2, where `PECULIAR`=1 is peculiar and `PECULIAR`=0 is not. Distances and the peculiar tag are only present in the LT catalogue. The LT and the M Catalogues also include i, z, Y magnitudes from DES, J, H, K_s from VHS and $W1, W2$ from AllWISE as used in the classification. DES magnitudes are corrected

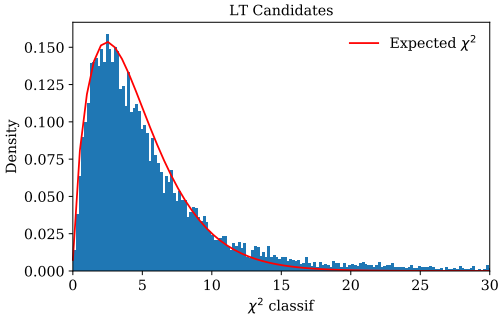

Figure 10. χ^2 distribution for the LT candidates, together with the theoretical expectation. In order to calculate this curve, we add, proportional to the numbers in Fig. 9, the degrees of freedom. Our distribution follows the expected curve, therefore our errors reflect the dispersion of the model. The reduced χ^2 defined as $\frac{\chi^2}{(d.o.f)}$ is close to one, with a mean value of $\overline{\frac{\chi^2}{(d.o.f)}}$ = 1.3 and a median value $med(\frac{\chi^2}{(d.o.f)})$ = 0.95.

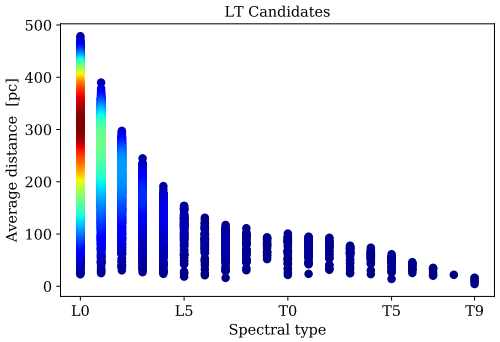

Figure 11. Distances as a function of spectral type. Distances have been calculated using the average value from the distance modulus obtained using all available bands. The colour scale represents the density. Most LT candidates are early L types at distances smaller than 500 parsecs.

with updated zeropoints different from those present in the public DR1 release (Dark Energy Survey Collaboration et al. 2018) and they will be published in the future.

We matched the M and LT catalogues with Gaia DR2 release (Gaia Collaboration et al. 2018), but the amount of matches was very low in the LT catalogue. Only 282 matches were found (2.4%). In the M catalogue, we found 1,141 matches (5.4%), but these spectral types are not the scope of this paper.

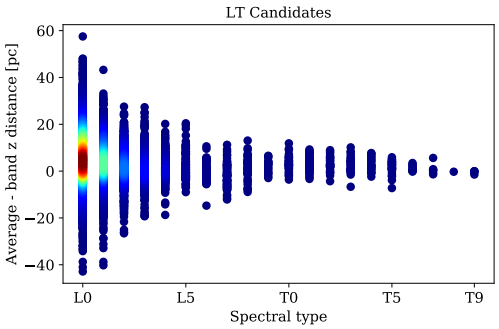

Figure 12. Difference between the two distance estimators. In one where we only use z band and another where the average value over all available bands is used. The colour scale represents the density.

Table 5. Example of the LT catalogue published, distances and peculiar flag are only present in the LT catalogue. SPT_PHOT is the spectral type, NBANDS the number of bands used in classification and XI2_CLASSIF the χ^2 for the best-fit in *classif*. DISTANCE_AVG is the average distance calculated from apparent magnitudes in all the available bands (in parsecs) and DISTANCE_Z the distance calculated from the apparent magnitude in DES z band (in parsecs). HPIX_512 is the *Healpix* pixel ID for $order = Nest$ and $nside = 512$ and PECULIAR is a category given if it has a $\chi^2 > 3.5\sigma$ median absolute deviations (1 = peculiar, 0 = no peculiar).

COADD_OBJECT_ID	RA	DEC	SPT_PHOT	NBANDS	XI2_CLASSIF	DISTANCE_AVG	DISTANCE_Z	HPIX_512	PECULIAR
293254901	16.568	-52.537	8	5	4.326	419.848	406.993	2240708	0
302513036	18.383	-51.732	10	5	5.944	277.501	270.822	2240815	0
232352550	23.216	-63.690	8	5	3.974	380.790	370.102	2142795	0
237139089	313.501	-60.505	8	5	1.837	582.501	555.256	2935140	0
204133552	322.767	-53.430	9	5	4.503	491.583	495.687	2939932	0
71547410	330.937	-57.231	10	7	3.993	308.368	306.911	2915933	0
185491825	315.506	-53.252	9	5	1.530	393.643	398.255	2945055	0
93231446	33.147	-51.827	8	7	0.971	262.541	259.220	2244895	0

Table 5 – *continued* DES magnitudes are in AB. i, z are PSF magnitudes from "SOF" while Y band is from "Sextractor". VHS magnitudes are in Vega and are aperture magnitudes at 2 arcseconds.

PSF_MAG_I	PSF_MAGERR_I	PSF_MAG_Z	PSF_MAGERR_Z	AUTO_MAG_Y	AUTO_MAGERR_Y	JAPERMAG3	JAPERMAG3ERR
21.971	0.029	20.735	0.016	20.580	0.088	18.937	0.039
22.571	0.041	20.937	0.022	20.394	0.068	18.722	0.037
21.738	0.028	20.529	0.014	20.292	0.088	18.588	0.050
22.800	0.055	21.410	0.040	21.156	0.159	19.466	0.086
22.893	0.051	21.603	0.031	21.389	0.172	19.693	0.108
22.736	0.043	21.209	0.027	20.882	0.088	18.803	0.055
22.488	0.033	21.128	0.018	20.768	0.089	18.949	0.055
21.069	0.013	19.756	0.007	19.467	0.029	17.857	0.031

Table 5 – *continued* VHS magnitudes are in Vega and are aperture magnitudes at 2 arcseconds. WISE magnitudes are in Vega and are magnitudes measured with profile-fitting photometry. For more details visit https://des.ncsa.illinois.edu/releases/other/y3-mlt.

HAPERMAG3	HAPERMAG3ERR	KSAPERMAG3	KSAPERMAG3ERR	W1MPRO	W1SIGMPRO	W2MPRO	W2SIGMPRO
-9999.	-9999.	17.921	0.105	-9999.	-9999.	-9999.	-9999.
-9999.	-9999.	17.773	0.108	-9999.	-9999.	-9999.	-9999.
-9999.	-9999.	17.937	0.156	-9999.	-9999.	-9999.	-9999.
-9999.	-9999.	18.868	0.329	-9999.	-9999.	-9999.	-9999.
-9999.	-9999.	18.266	0.178	-9999.	-9999.	-9999.	-9999.
18.309	0.078	17.860	0.106	17.604	0.175	17.292	-9999.
-9999.	-9999.	18.098	0.157	-9999.	-9999.	-9999.	-9999.
-9999.	-9999.	16.835	0.060	16.702	0.071	16.476	0.189

8 MODELING THE NUMBER COUNTS OF LT DWARFS

This section describes the effort to create robust expected number counts of LT dwarfs. The algorithm is called *GalmodBD*. It is a `Python` code that computes expected galactic counts of LT dwarfs, both as a function of magnitude, colour and direction on the sky, using the fundamental equation of stellar statistics. It was adapted from the code used by Santiago et al. (1996) and Kerber et al. (2001) to model HST star number counts, and by Santiago et al. (2010) for a preliminary forecast of DES star counts. In the current analysis, we kept the density laws for the different Galactic components, and simply replaced the specific luminosity functions of normal stars by the BD number densities as a function of the spectral type presented in Subsection 8.1.

GalmodBD also creates synthetic samples of LT dwarfs based on the expected number counts for a given footprint. Besides a model for the spatial distribution of BDs, *GalmodBD* uses empirically determined space densities of objects, plus absolute magnitudes and colours as a function of spectral type. The model is described in Subsection 8.1. The point generating process is described in Subsection 9. The validation tests are provided in Appendix C.

8.1 *GalmodBD*

For convenience, we will refer to the space density versus spectral type relation as the luminosity function (LF), which is somewhat of a misnomer, since luminosity does not scale uniquely with spectral type in the LT regime. We refer to the colours versus spectral type relations as C-T relation. The code requires several choices of structural parameters for the Galaxy, such as the density law and local normalisation of each Galactic component. Equally crucial are parameters that govern the region of the sky and magnitude and colour ranges where the expected counts will be computed.

These parameters are listed in different configuration files. Currently, only one choice of LF is available, taken from Table 8 of Marocco et al. (2015). More specifically, for types earlier than L4, we use Cruz et al. (2007) space density values; from L4 to T5 we use those of Marocco et al. (2015) themselves, and for later types than T5 we use Burningham et al. (2013).

For the C-T relations, we first build absolute magnitude vs. spectral type relations for AllWISE data. *M_W1*, and *M_W2* versus type relations are taken from Figures 25, 26 and Table 14 of Dupuy & Liu (2012). Once we anchor absolute magnitudes in these bands, we use the C-T relations found in Section 3 in Table 3, Fig. 3 to populate *M_i,M_z,M_Y,M_J,M_H,M_Ks*.

The expected number counts are computed by direct application of the fundamental equation of stellar statistics. In summary, given a choice of apparent magnitude range in some filter, and some direction in the sky (pointer), we go through distance steps and for each of them, find the range of LT spectral types whose absolute magnitudes fit into the chosen apparent magnitude range. We then compute the volume element in the selected direction and distance and multiply it by the appropriate LF value.

The final number count as a function of apparent magnitude is the sum of these contributions for all appropriate combinations of spectral types (through their associated absolute magnitudes) and distances. Because we also have colour versus type relations, we can also perform the same integral over distance and type range to compute number counts as a function of colour.

GalmodBD incorporates extinction and dereddened using the Schlegel et al. (1998, SFD98) dust maps, although it can also use (Burstein & Heiles 1982) maps. Conversion from A_V and E(B-V) to SDSS A_i, A_z and E(i-z) are based on An et al. (2008). Nonetheless, in this first application of the code, we have not included any reddening effect since our sample is concentrated in the solar neighborhood.

The code currently permits many choices of magnitudes and colours for number counts modeling, including colours in SDSS and DES in the optical, VHS and 2MASS in the near-infrared and AllWISE in the infrared.

In Appendix C we validate the *GalmodBD* simulation comparing its predictions with a prediction based on a single disk component analytical count.

9 SYNTHETIC CATALOGUES

Besides determining expected N(m) and N(col) for BDs within some magnitude range and over some chosen area on the sky, the code also generates synthetic samples based on these number counts. This is done for every chosen direction, distance and type (absolute magnitude) by randomly assigning an absolute magnitude within the range allowed by the spectral type bin, and then converting it to apparent magnitude. We use the same random variable to assign absolute magnitudes within each bin for all filters, in order to keep the synthetic objects along the stellar locus in colour-colour space.

For a complete description, we also need to assign random magnitude errors to mimic an observed sample, which will depend on the particular case. Therefore, error curves as a function of magnitude for each filter are required. In subsection 10.2 we detail this step for our sample. By default, *GalmodBD* accepts an exponential error distribution. In case of more sophisticated models, the error must be introduced afterward.

For synthetic dwarfs, the code outputs its Galactic component, spectral type, Galactic coordinates (l,b) of the centre of the pointer, distance and magnitudes in the set of filters, for example: i_{DES}, i_{SDSS}, z_{DES}, z_{SDSS}, Y_{DES}, J_{VHS}, J_{2MASS}, H_{VHS}, H_{2MASS}, $K_{s,VHS}$, $K_{s,2MASS}$, $W1$ and $W2$. Both the true and observed magnitudes, as well as their errors, are output, regardless of the chosen pair (mag, colour) used in the output expected model counts. This latter choice, coupled with the apparent magnitude range and the direction chosen, however, affects the total number of points generated.

In order to have a synthetic sample with coordinates, we randomly assign positions to the sources within the given pointer area (see Section 10.1).

These simple synthetic catalogues can be compared to a real catalogue of BD candidates by correcting the expected numbers for the visibility mask, that accounts for catalogue depth and detection variations, and for estimates of purity and completeness levels of the observed catalogue.

10 *GALMODBD* IN THE TARGET SAMPLE

In this section we detail the input information used to feed the *GalmodBD* simulation that reproduces the $DES \cap VHS \cap AllWISE$ data. Besides the empirical colour template relations, we need to define the footprint of the simulation and the photometric error model to produce realistic MLT catalogues.

10.1 Footprint and pointers definition

To create a sample that resembles the target sample, we create a grid of pointers following the DES tile distribution.

DES coadd data are divided into square (in spherical coordinates) regions of equal area, covering 0.534 deg^2 each, called tiles. We use this information to define our pointers covering the area occupied in Fig. 1. The pointers defined to run *GalmodBD* have the same coordinates as the centre of the DES tiles and the same area of 0.534 deg^2. Later, tiles are intersected with the VHS footprint in the DES area, covering the brown areas in the same figure. Eventually, we end with 5187 pointers of 0.534 deg^2, covering 2,374 deg^2.

After running the simulation in each pointer, we assign random positions within the area of the pointer to each object in the simulated catalogue. At this point we would need to consider the effect of incompleteness in the footprint, i.e., apply the footprint mask.

To study the effect the mask might have in the number of BDs recovered by our method, for each *GalmodBD* run, we create multiple synthetic position catalogues and pass the data through the footprint mask. Eventually, obtaining a statistic of the mean and standard deviation (std) of the number of MLT sources that we will lose. In our case we run 500 realizations for each *GalmodBD* model to calculate the effect on footprint completeness in Section 12.

10.2 Mimic DES photometric properties

Another ingredient in the *GalmodBD* simulation is the photometric errors that apply to the simulated data to create an observed synthetic sample.

To model the signal-to-noise distribution we start by selecting a random sample of the $DES \cap VHS \cap AllWISE$ data, limited to $z < 23$ and selecting point sources only using the extended classification from DES Y3 data. We next apply the following algorithm for each band:

First, we divide the sample in magnitude bins of width=0.1. For each bin, we estimate the probability density function of the magnitude error using a kernel density estimation (`KDE`).

With the `KDE` information for each thin magnitude bin, we can assign a magnitude error for a given magnitude with a dispersion that follows the `KDE`. Once an error is assigned to a source, we estimate apparent magnitudes assuming a Gaussian distribution centred in the true apparent magnitude and with a standard deviation equals to their magnitude error.

We extract the `KDE` for magnitude bins where we have more than 60 objects. In the extreme cases of very bright or very faint objects in the magnitude distribution, this requirement is not met. Therefore we expand the distribution along the bright end by repeating the `KDE` from the brightest bin with enough statistics. In the faint end, we fit the mean and sigma of the faintest 4 bins with enough statistics by a second-order polynomial and extrapolate this fit towards fainter magnitudes.

In Fig. 13 we summarize the error modeling for the bands of interest: i, z, Y and J. In the Figures, we compare the error distribution as a function of magnitude for the real data, individually for each band, with the simulated data. The median and dispersion agree very well for all bands.

11 *GALMODBD* RESULTS

In Table 6 we show the result of running *GalmodBD* for different galactic models varying the thin disk scale height at $h_{z,thin} = 250, 300, 350, 400, 450, 500, 550\ pc$ and the local thick-to-thin disk density normalisation $n_{sun,thick} = 5, 10, 15, 20\%$ defined as $n_{sun,thick} = \rho_{thick}(R_\odot)/\rho_{thin}(R_\odot)$. After some testing, it was clear the LT number counts were most sensitive to these two parameters. We ran the simulation for M dwarfs ranging M0 to M9 and BDs from L0 to T9 (even though the scale height of LT types does not need to be the same as for M types).

We run *GalmodBD* up to a true apparent magnitude limit of $z_{true} < 25$. Next, we assign errors and observed magnitudes as explained in Section 10.2. Later, we select MLT with $z_{obs} <= 22$ and $(SNR) > 5\sigma$ in z, Y, J to build our simulated MLT parent catalogues. Using these catalogues, we can study the completeness and purity of our sample (see Section 12).

In Table 6, the third column is the number of M types for a given model that pass the colour cuts defined in Section 4 and $z_{obs} < 22$ and $(SNR) > 5\sigma$ in z, Y, J. The fourth column is the number of LT types when $z_{obs} < 22$ and $(SNR) > 5\sigma$ in z, Y, J. We have not applied here the colour cut, since it is a source of incompleteness and we treat it together with other effects in Section 12.

12 PURITY AND COMPLETENESS

In this section we detail the various sources of error in the measurement of the number counts of LT dwarfs from the target sample. We will use a combination of both the calibration samples and the *GalmodBD* simulation. There are two issues to consider: one is to identify and quantify contamination and incompleteness effects on our sample, so we can correct the simulated numbers in order to compare them to the data. The other is assessing the uncertainty associated with these corrections and the expected fluctuations in the corrected number counts. The effects we consider are:

– Colour-colour incompleteness: how many LT we lose by applying the colour cut to select candidates.
– Loss of targets from the catalogue due to proper motions.
– Footprint effects: how many LT we lose due to masking effect.
– Loss of LTs due to misclassification.
– Contamination of targets due to unresolved binary systems in our magnitude-limited catalogue.
– Contamination by M dwarfs and extragalactic sources.

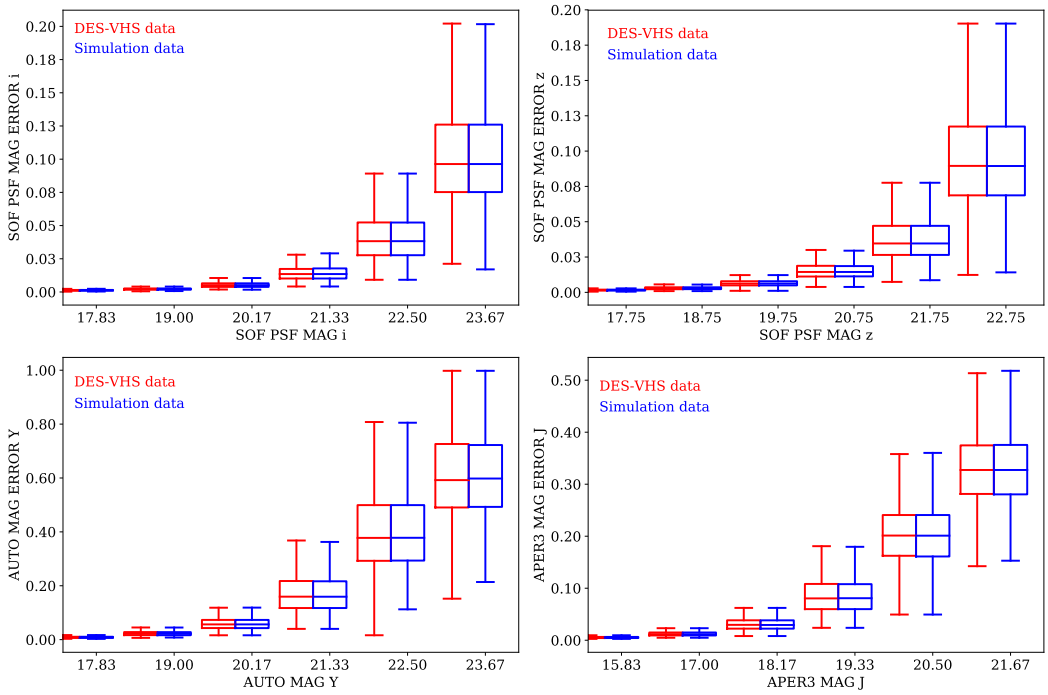

Figure 13. Box-plot comparing the magnitude uncertainties as a function of magnitude for DES i, z, Y and VHS J data, versus the modeled distribution in *GalmodBD* simulation. In red, the $DES \cap VHS$ distribution, in blue, the simulated distribution. The horizontal line within the box indicates the median, boundaries of the box indicate the 25th- and 75th-percentile, and the whiskers indicate the highest and lowest values of the distribution. The median and dispersion agree very well for all bands.

12.1 Incompleteness

To assess how many BDs we miss due to the colour-colour selection, we look at the number of LT types that do not enter our colour selection both in the Gagné sample as well as in the *GalmodBD* simulation. The colour range selected was chosen to minimize incompleteness. But peculiar early L dwarfs may eventually be found outside our colour range. In the Gagné sample, from the list of 104 known BDs (including young types), 2 are left outside the colour range (2%). In *GalmodBD*, we haven't modeled peculiar BDs and therefore, the incompleteness level should be low. Applying the colour cut to the *GalmodBD* outputs, as expected, led to a mean completeness of 98.8%. We define the colour-colour completeness correction to be the average of the two. The uncertainty associated with this correction should be low. Conservatively, we define the uncertainty to be of 1%, leading to $C_{colour} = 98.4 \pm 1.\%$.

In order to estimate the number of missing sources due to proper motions, we will assume that the mean proper motion of LT types decreases with distance. Considering a conservative 3-year difference in astrometry between DES and VHS, a $2''$ matching radius should be complete for distances > 50 pc. In fact, looking at the BDs that we recover visually beyond the $2''$ radius in Section 3.1 and that have distances in the Gagné sample, more than 95% of the missing BDs have a distance < 50 pc. So we can set this as an upper limit for this effect. Above 50 pc, we match at $2''$ almost all of the BDs presented in the calibration sample. Likewise, we do match some of the BDs below 50 pc, at least 20% of them.

In summary, matching the Gagné sample to DES within $2''$ we recover 20% of the BDs below 50 pc and 100% above that distance. This is a conservative limit, but it gives us a sense of the percentage loose by proper motions. Note that we have not considered here that we might miss some of the targets due to the incompleteness of the footprint so the 20% should be higher.

If we now look at the *GalmodBD* simulation, we predict the number of LT types with distances < 50 pc to be 2% of the whole sample. Considering an 80% completeness and an error in the determination comparable to the effect itself, it results in a proper motion completeness correction of $C_{pm} = 98.4 \pm 2\%$.

In terms of footprint incompleteness, we apply the algorithm presented in Section 10.1 to estimate the effect of the footprint mask: we produce 500 realizations of each *GalmodBD* model and estimate the mean and std of LT type number counts that survive the masking process. We

Table 6. Number of BDs as a function of MW structural parameters in *GalmodBD*. $h_{z,thin}$ is the thin disk scale height in parsecs, $n_{sun,thick}$ is the local thick-to-thin disk density normalisation in percentage. The third column is the number of M types after the magnitude limit cut, the signal-to-noise cut and the colour cut. The fourth column is the number of LT types applying only the magnitude limit cut and the signal-to-noise cut and the fifth column is the number of early L types defined as those with spectral types less than L4. This last column will be compared with the number of BDs detected in our sample to give a first estimate of the thin disk scale height for early L types.

$h_{z,thin}$ pc	$n_{sun,thick}$ %	M types [$snr > 5\sigma + z < 22$ + colour cut]	LT types [$snr > 5\sigma + z < 22$]	Early L types (L0, L1, L2, L3)
250	5	11,609	8,403	7,427
250	10	12,869	9,094	8,055
250	15	14,121	9,742	8,663
250	20	15,428	10,475	9,333
300	5	13,782	9,426	8,381
300	10	15,113	10,086	8,992
300	15	16,366	10,821	9,663
300	20	17,652	11,427	10,211
350	5	15,768	10,197	9,118
350	10	17,018	10,887	9,758
350	15	18,173	11,507	10,336
350	20	19,599	12,151	10,929
400	5	17,329	10,891	9,798
400	10	18,611	11,590	10,454
400	15	19,968	12,313	11,079
400	20	21,345	12,958	11,684
450	5	18,831	11,463	10,343
450	10	20,015	12,022	10,873
450	15	21,486	12,774	11,575
450	20	22,653	13,384	12,115
500	5	20,231	11,891	10,764
500	10	21,425	12,589	11,409
500	15	22,732	13,255	12,028
500	20	24,086	14,100	12,785
550	5	21,217	12,297	11,152
550	10	22,551	13,038	11,811
550	15	23,859	13,763	12,501
550	20	25,121	14,359	13,033

then average over all models to obtain a model-independent completeness correction of $C_{foot} = 93.6 \pm 3.5\%$.

Finally, there is the effect of misclassification of LT types as M types. We estimated the incompleteness of LT types due to misclassification as $C_{classif} = 85 \pm 1\%$. In the next subsection, we describe this correction along with the corresponding contamination effect, namely the misclassification of M dwarfs as LT types.

12.2 Contamination

Our LT dwarfs catalogue is limited to $z \leq 22$. Unresolved binary systems containing two LT dwarfs will have a higher flux than a single object and hence will make into the catalogue even though each member of the system individually would not. This boosts the total number of LTs in our sample. We estimate the effect of unresolved binarism systems as follows. According to Luhman (2012) (and references therein), the fraction of binaries decreases with the mass of the primary, while the mass ratio ($q = m1/m2$) tends to unity (equal-mass binaries). In our case, we are only interested in those binaries where the primary is an LT. Binary systems with the LT as secundary, will have a small mass ratio ($q << 1$), and therefore, they will be uncommon. Also, we cannot census this type of population since the light from the primary will dominate the light from secondary. Luhman (2012) quotes different estimates the fraction of binaries where the primary is an LT, f_{bin}. Observational data suggest $f_{bin} \simeq 7\%$, but may be prone to incompleteness, especially for close pairs. Theoretical models of brown dwarf formation predict f_{bin} in the 20% – 30% range (Maxted & Jeffries 2005; Basri & Reiners 2006). Nonetheless, a recent estimate by Fontanive et al. (2018) would confirm the empirical trend of Luhman (2012) and therefore we here adopt $f_{bin} = 0.07$. If we assume that $q \sim 1$ in all cases, we will obtain binary systems that have the same spectral type as the primary, but with a magnitude that is 0.75 times brighter (since the system flux is twice that of the primary). To estimate the contamination by binaries in the target sample, we follow the description of Burningham et al. (2010). Ac-

cording to equation 3 in that paper, the correction factor is:

$$P_{binary} = \frac{\gamma - 1}{\gamma + 1/f_{bin} - 1} \quad (5)$$

where $\gamma = 2\sqrt{2}$ for equal mass/luminosity binaries, and $f_{bin} = 0.07$. Finally, we get $P_{binary} = 111 \pm 1\%$.

There are two additional sources of contaminants applied here: one is the migration of M dwarfs that have been wrongly assigned as LT type after running *classif*, and the other is the contamination by extragalactic sources.

Ideally, in order to estimate the contamination by M dwarfs and the incompleteness of LT types due to the photometric classification, we should run *classif* on the output of *GalmodBD*. Unfortunately, our classification code is fed with the same templates used in the simulation and, therefore, the classification uncertainty we get by running *classif* in *GalmodBD* is unrealistically low. In order to estimate the number of M dwarfs that are classified as LT types and vice versa, we perturb the true spectral types for *GalmodBD* sources following a normal distribution with dispersion given in Section 5.1: $\sigma_M = 0.69$, $\sigma_L = 1.03$ and $\sigma_T = 1.12$ and mean value centred in the true spectral type.

Once we perturb the true spectral types to get a pseudo-photometric calibration in *GalmodBD*, we can estimate how many LTs will be classified as M, and vice versa. We estimate this number for all the *GalmodBD* realizations and find that $\sim 11\%$ of M dwarfs (after the colour cut) are given LT type. This corresponds to contamination by about 14-19% of the corresponding LT simulated sample. This means a mean LT purity level of $P_{class} = 83 \pm 2\%$. We also use the same procedure applied on the *GalmodBD* data to assess the number of LT types migrating to M type. This is an additional incompleteness of $C_{class} = 85 \pm 1\%$, to be added to those from the previous subsection.

The removal of extragalactic contaminants is another source of uncertainty. We saw in Section 6 that $\lesssim 10\%$ of the MLT sample have galaxy or quasar class. These are not modeled in *GalmodBD*, and therefore we do not need to apply a correction due to extragalactic contamination, although there will always be uncertainty associated with it. Based on tests with different `Lephare` SED libraries and the ambiguity in classification for sources with `NBANDS` < 5, we estimate a standard deviation associated with the removal of extragalactic sources of $\sigma_{SG} \sim 5.\%$.

12.3 Completeness and purity summary

Summarizing all these effects, we estimate the completeness and contamination up to $z < 22$ at 5σ as:

– Completeness due to the colour-colour cut of $C_{colour} = 98.4 \pm 1.\%$.
– Completeness due to proper motions of $C_{pm} = 98.4 \pm 2\%$.
– Completeness due to masking of $C_{foot} = 93.6 \pm 3.5\%$.
– Completeness due to LT misclassified as M types of $C_{class} = 85 \pm 1\%$.
– Contamination due to unresolved binary systems measured as the fraction $f_{bin} = 7\%$ of sources: $K_{bin} = 11 \pm 1\%$.
– Contamination of the LT sample due to M types classified as LTs: $K_{class} = 17 \pm 2\%$.
– Uncertainty in the extragalactic contamination removal algorithm introduces an additional systematic error of $\sigma_{extra} = 5.\%$.

Combining all these effects, we define a correction factor:

$$CP_{LT} = \frac{C_{colour} * C_{pm} * C_{foot} * C_{class}}{(1 - K_{bin}) * (1 - K_{class})} \quad (6)$$

that multiplies the LT sample. This correction factor accounts for the effect of incompleteness and purity, and applies to our definition with $z < 22$ and 5σ in z, Y, J. Different magnitude limits would lead to different corrections. In this case, the final correction factor is $C_{LT} = 1.05$. This factor is applied to the number of detected LT $N(LT)_{obs} = 11,745$ to get an estimate of the total number of LT in the footprint up to $z < 22$ with at least a 5σ detection in z, Y, J as $N(LT)_{true} = N(LT)_{obs} * C_{LT}$. At first approximation, the uncertainty in the number of LT types is the square root of the sum of the squares of the individual errors listed above:

$$\sigma_{LT} = \sqrt{\sigma_{col}^2 + \sigma_{pm}^2 + \sigma_{bin}^2 + \sigma_{foot}^2 + \sigma_{cl,C}^2 + \sigma_{cl,P}^2 + \sigma_{ex}^2} \quad (7)$$

with $\sigma_{LT} \sim 7\%$. Finally, the number of LT's to compare against the different SFH scenarios is in round numbers $N(LT) \sim 12,300 \pm 900$. If we only select the early L types (L0, L1, L2 and L3) for which we want to estimate the thin disk scale height, the number to compare with becomes $N(L_{0,1,2,3}) \sim 11,500 \pm 800$.

13 THE THIN DISK SCALE HEIGHT

Jurić et al. (2008) estimate the thin disk scale height and the local thick-to-thin disk density normalisation of SDSS M dwarfs up to a distance of 2 kpc. They found $h_{z,thin} = 300\ pc$ and $n_{sun,thick} = 12\%$.

As a first application of the brown dwarf catalogue and *GalmodBD*, we compare the number of observed LT types with different realizations of *GalmodBD* to shed light on the thin disk scale height of the LT population. Since T types are less than 2% of the sample and go only up to 100 pc, in practice, we are estimating the scale height of the early L types. A previous attempt to measure the thin disk scale height of L types can be found in Ryan et al. (2005), where they estimate a value of $h_{z,thin} = 350 \pm 50$ using only 28 LT types and on a very simplistic Galactic model. Since our model is more detailed and we have a much higher statistic, we believe that our results will be more reliable. More recently, Sorahana et al. (2018) have used data from the first data release from the Hyper Suprime Camera (HSC, Miyazaki et al. 2018; Aihara et al. 2018) to estimate the vertical thin disk scale height of early L types with an estimate between 320 pc and 520 pc at 90% confidence.

Comparing the value of $N(LT) \sim 12000 \pm 900$ with the grid of *GalmodBD* (Table 6), we do find a higher scale height than that of M dwarfs, as Ryan et al. (2005) found, of the order of $h_{z,thin} \sim 450pc$. Nonetheless, there is a degeneracy between the thin disk scale height and $n_{sun,thick}$ and therefore we cannot yet rule out a models with $h_{z,thin} = 300\ pc$:

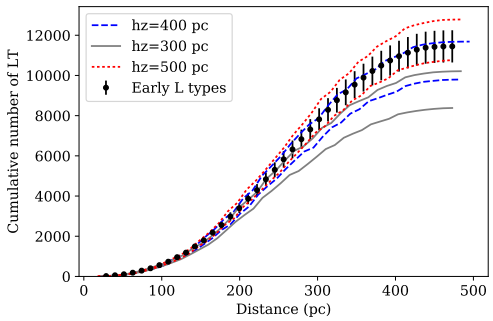

Figure 14. Comparison of the number counts of early L types (L0, L1, L2 and L3) with three models of the thin disk scale height. In Grey we show models with a scale height similar to that for M dwarfs (Jurić et al. 2008) with $h_z = 300\ pc$, in dashed blue, models with $h_z = 400\ pc$ and in red, models with $h_z = 500\ pc$. For each model we show two estimates, one where $n_{sun,thick} = 5\%$ (lower limit) and another where $n_{sun,thick} = 20\%$ (upper limit).

considering the error in the number counts $\sigma_{LT} \sim 900$, there are models of $h_{z,thin} = 300\ pc$ which predicts a number of LT types within 1σ of our measurement. In Fig. 14 we compare the number counts to various models taken from *GalmodBD*. In Grey we show two models for $h_{z,thin} = 300\ pc$, one with $n_{sun,thick} = 5\%$ (lower limit) and another with $n_{sun,thick} = 20\%$ (upper limit). In dashed blue we show models for $h_{z,thin} = 400\ pc$, for same values of $n_{sun,thick}$ and in red points we show models for $h_{z,thin} = 500\ pc$.

In order to constraint the thin disk scale height, we will perform a Markov chain Monte Carlo analysis which will marginalize over $n_{sun,thick}$. This will be the scope of a future analysis. We will wait until the full coverage of DES and VHS have been achieved, covering $\sim 5000 deg^2$. Here we will apply the same methodology presented here, for magnitudes $z < 22.7$, increasing both the area and the distance of the surveyed sample.

14 CONCLUSION

In this paper, we apply a photometric brown dwarf classification scheme based on Skrzypek et al. (2015) to $DES \cap VHS \cap AllWISE$ data using 8 bands covering a wavelength range between 0.7 μm and 4.6 μm. Since several degeneracies are found in colour space between spectral types M,L and T, the use of multiple bands are required for a good spectral type calibration.

In comparison with Skrzypek et al. (2015), we can go to greater distances in the L regime due to the deeper DES and VHS samples, in contrast with the $SDSS \cap UKIDSS$ design. This way, we classify 11,745 BDs in the spectral regime from L0 to T9 in $\approx 2,400\ deg^2$, with a similar spectral resolution of 1 spectral type. We make this catalogue public in electronic format. It can be downloaded from `https://des.ncsa.illinois.edu/releases/other/y3-mlt`. This is the largest LT sample ever published. We further estimate the purity and completeness of the sample. We estimate the sample to be $\sim 77\%$ complete and $\sim 74\%$ pure at $z_{AB} < 22$. Finally, we can calculate the total number of LTs in the $DES \cap VHS$ footprint to be $\sim 12,300 \pm 900$.

During the classification, we identify 2,818 possible extragalactic sources that we removed from the catalogue, containing 57 quasars at high redshift. The removal of extragalactic sources increases the uncertainty in the determination of the number of LT types.

In parallel, we have presented the *GalmodBD* simulation, a simulation that computes LT number counts as a function of SFH parameters. In our analysis, we found that the thin disk scale height and the thin-to-thick disk normalisation were the parameters that most affect the number counts. Nonetheless, more free parameters are available in the simulation. When comparing the simulation output with the number of LT expected in the footprint, we put constraints on the thin disk scale height for early L-types, finding a value that is in agreement with recent measurements, like the one found in Sorahana et al. (2018) with $h_z \sim 400\ pc$.

Having these two ingredients, a robust simulation of number counts, and a methodology to select BDs in $DES \cap VHS \cap AllWISE$ will allow us to do a precise measurement of the thin disk scale height of the L population, putting brown dwarf science in its Galactic context. This will be the scope of future analyses.

ACKNOWLEDGMENTS

Funding for the DES Projects has been provided by the U.S. Department of Energy, the U.S. National Science Foundation, the Ministry of Science and Education of Spain, the Science and Technology Facilities Council of the United Kingdom, the Higher Education Funding Council for England, the National Center for Supercomputing Applications at the University of Illinois at Urbana-Champaign, the Kavli Institute of Cosmological Physics at the University of Chicago, the Center for Cosmology and Astro-Particle Physics at the Ohio State University, the Mitchell Institute for Fundamental Physics and Astronomy at Texas A&M University, Financiadora de Estudos e Projetos, Fundação Carlos Chagas Filho de Amparo à Pesquisa do Estado do Rio de Janeiro, Conselho Nacional de Desenvolvimento Científico e Tecnológico and the Ministério da Ciência, Tecnologia e Inovação, the Deutsche Forschungsgemeinschaft and the Collaborating Institutions in the Dark Energy Survey.

The Collaborating Institutions are Argonne National Laboratory, the University of California at Santa Cruz, the University of Cambridge, Centro de Investigaciones Energéticas, Medioambientales y Tecnológicas-Madrid, the University of Chicago, University College London, the DES-Brazil Consortium, the University of Edinburgh, the Eidgenössische Technische Hochschule (ETH) Zürich, Fermi National Accelerator Laboratory, the University of Illinois at Urbana-Champaign, the Institut de Ciències de l'Espai (IEEC/CSIC), the Institut de Física d'Altes Energies, Lawrence Berkeley National Laboratory, the Ludwig-Maximilians Universität München and the associated Excellence Cluster Universe, the University of Michigan, the National Optical Astronomy Observatory, the University of Nottingham, The Ohio State University, the University of

Pennsylvania, the University of Portsmouth, SLAC National Accelerator Laboratory, Stanford University, the University of Sussex, Texas A&M University, and the OzDES Membership Consortium.

Based in part on observations at Cerro Tololo Inter-American Observatory, National Optical Astronomy Observatory, which is operated by the Association of Universities for Research in Astronomy (AURA) under a cooperative agreement with the National Science Foundation.

The DES data management system is supported by the National Science Foundation under Grant Numbers AST-1138766 and AST-1536171. The DES participants from Spanish institutions are partially supported by MINECO under grants AYA2015-71825, ESP2015-66861, FPA2015-68048, SEV-2016-0588, SEV-2016-0597, and MDM-2015-0509, some of which include ERDF funds from the European Union. IFAE is partially funded by the CERCA program of the Generalitat de Catalunya. Research leading to these results has received funding from the European Research Council under the European Union's Seventh Framework Program (FP7/2007-2013) including ERC grant agreements 240672, 291329, and 306478. We acknowledge support from the Australian Research Council Centre of Excellence for All-sky Astrophysics (CAASTRO), through project number CE110001020, and the Brazilian Instituto Nacional de Ciência e Tecnologia (INCT) e-Universe (CNPq grant 465376/2014-2).

This manuscript has been authored by Fermi Research Alliance, LLC under Contract No. DE-AC02-07CH11359 with the U.S. Department of Energy, Office of Science, Office of High Energy Physics. The United States Government retains and the publisher, by accepting the article for publication, acknowledges that the United States Government retains a non-exclusive, paid-up, irrevocable, world-wide license to publish or reproduce the published form of this manuscript, or allow others to do so, for United States Government purposes.

This publication makes use of data products from the Wide-field Infrared Survey Explorer, which is a joint project of the University of California, Los Angeles, and the Jet Propulsion Laboratory/California Institute of Technology, and NEOWISE, which is a project of the Jet Propulsion Laboratory/California Institute of Technology. WISE and NEOWISE are funded by the National Aeronautics and Space Administration.

The analysis presented here is based on observations obtained as part of the VISTA Hemisphere Survey, ESO Programme, 179.A-2010 (PI: McMahon).

This paper has gone through internal review by the DES collaboration.

ACR acknowledges financial support provided by the PAPDRJ CAPES/FAPERJ Fellowship and by "Unidad de Excelencia María de Maeztu de CIEMAT - Física de Partículas (Proyecto MDM)".

The authors would like to thank Jacqueline Faherty and Joe Filippazzo for their help on the early stages of this project.

REFERENCES

Abell P. A., et al., 2009
Aihara H., et al., 2018, Publication of the Astronomical Society of Japan, 70
Albert L., Artigau É., Delorme P., Reylé C., Forveille T., Delfosse X., Willott C. J., 2011, Aj, 141, 203
An D., et al., 2008, The Astrophysical Journal Supplement Series, 179, 326
Arnouts S., Cristiani S., Moscardini L., Matarrese S., Lucchin F., Fontana A., Giallongo E., 1999, MNRAS, 310, 540
Arnouts S., et al., 2007, A&A, 476, 137
Banerji M., et al., 2015, MNRAS, 446, 2523
Basri G., Reiners A., 2006, AJ, 132, 663
Bertin E., Arnouts S., 1996, A&AS, 117, 393
Bochanski J. J., Munn J. A., Hawley S. L., West A. A., Covey K. R., Schneider D. P., 2007, AJ, 134, 2418
Bruzual G., Charlot S., 2003, MNRAS, 344, 1000
Burgasser A. J., 2007, ApJ, 659, 655
Burgasser A. J., et al., 2003, ApJ, 592, 1186
Burgasser A. J., Kirkpatrick J. D., Cruz K. L., Reid I. N., Leggett S. K., Liebert J., Burrows A., Brown M. E., 2006a, ApJSupplement, 166, 585
Burgasser A. J., Geballe T. R., Leggett S. K., Kirkpatrick J. D., Golimowski D. A., 2006b, ApJ, 637, 1067
Burke D. L., et al., 2018, AJ, 155, 41
Burningham B., 2018, preprint, (arXiv:1805.05661)
Burningham B., et al., 2010, MNRAS, 406, 1885
Burningham B., et al., 2013, Monthly Notices of the Royal Astronomical Society, 433, 457
Burstein D., Heiles C., 1982, Aj, 87, 1165
Chiu K., Fan X., Leggett S. K., Golimowski D. A., Zheng W., Geballe T. R., Schneider D. P., Brinkmann J., 2006, Aj, 131, 2722
Coleman G. D., Wu C.-C., Weedman D. W., 1980, ApJS, 43, 393
Cross N. J. G., et al., 2012, A&A, 548, A119
Cruz K. L., et al., 2007, Aj, 133, 439
Dalton G. B., et al., 2006, in Society of Photo-Optical Instrumentation Engineers (SPIE) Conference Series. p. 62690X, doi:10.1117/12.670018
Dark Energy Survey Collaboration et al., 2016, MNRAS, 460, 1270
Dark Energy Survey Collaboration et al., 2018, ApJS, 239, 18
Day-Jones A. C., Marocco F., Pinfield D. J., Zhang Z. H., Burningham B., Deacon N., Ruiz M. T., et al. 2013, MNRAS, 430, 1171
Drlica-Wagner A., et al., 2018, The Astrophysical Journal Supplement Series, 235, 33
Dupuy T. J., Liu M. C., 2012, Apjs, 201, 19
Faherty J. K., Burgasser A. J., Cruz K. L., Shara M. M., Walter F. M., Gelino C. R., 2009, Aj, 137, 1
Faherty J. K., et al., 2012, ApJ, 752, 56
Faherty J. K., et al., 2016, ApJS, 225, 10
Folkes S. L., Pinfield D. J., Kendall T. R., Jones H. R. A., 2007, MNRAS, 378, 901
Fontanive C., Biller B., Bonavita M., Allers K., 2018, MNRAS, 479, 2702
Gagné J., et al., 2017, ApJS, 228, 18
Gaia Collaboration et al., 2018, A&A, 616, A1
Ilbert O., et al., 2006, A&A, 457, 841
Jurić M., Ivezić Ž., Brooks A., Lupton R. H., Schlegel D., Finkbeiner D., et al. 2008, ApJ, 673, 864
Kerber L. O., Javiel S. C., Santiago B. X., 2001, A&A, 365, 424
Kinney A. L., Calzetti D., Bohlin R. C., McQuade K., Storchi-Bergmann T., Schmitt H. R., 1996, ApJ, 467, 38
Kirkpatrick J. D., et al., 1999, ApJ, 519, 802
Kirkpatrick J. D., et al., 2011, ApJs, 197, 19
Lawrence A., et al., 2007, Monthly Notices of the Royal Astronomical Society, 379, 1599
Leggett S. K., Morley C. V., Marley M. S., Saumon D., Fortney J. J., Visscher C., 2013, ApJ, 763, 130

Leggett S. K., Morley C. V., Marley M. S., Saumon D., 2015, ApJ, 799, 37
Liu M. C., et al., 2013, ApJ, 777, L20
Lodieu N., et al., 2012, AaP, 548, A53
Looper D. L., et al., 2008, ApJ, 686, 528
Luhman K. L., 2012, Araa, 50, 65
Mainzer A., et al., 2011, ApJ, 731, 53
Marocco F., et al., 2014, MNRAS, 439, 372
Marocco F., et al., 2015, Monthly Notices of the Royal Astronomical Society, 449, 3651
Marocco F., et al., 2017, MNRAS, 470, 4885
Maxted P. F. L., Jeffries R. D., 2005, MNRAS, 362, L45
McMahon R. G., Banerji M., Gonzalez E., Koposov S. E., Bejar V. J., Lodieu N., Rebolo R., VHS Collaboration 2013, The Messenger, 154, 35
Miyazaki S., et al., 2018, PASJ, 70, S1
Morganson E., et al., 2018, PASP, 130, 074501
Pinfield D. J., Jones H. R. A., Lucas P. W., Kendall T. R., Folkes S. L., Day-Jones A. C., Chappelle R. J., Steele I. A., 2006, MNRAS, 368, 1281
Prevot M. L., Lequeux J., Maurice E., Prevot L., Rocca-Volmerange B., 1984, A&A, 132, 389
Reed S. L., et al., 2015, MNRAS, 454, 3952
Reed S. L., et al., 2017, MNRAS, 468, 4702
Ryan Jr. R. E., Hathi N. P., Cohen S. H., Windhorst R. A., 2005, ApJLetters, 631, L159
Santiago B. X., Gilmore G., Elson R. A. W., 1996, MNRAS, 281, 871
Santiago B., Yanny B., Yanny 2010, in Bruzual G. R., Charlot S., eds, IAU Symposium Vol. 262, Stellar Populations - Planning for the Next Decade. pp 265–269, doi:10.1017/S1743921310002899
Schlafly E. F., Finkbeiner D. P., 2011, ApJ, 737, 103
Schlegel D. J., Finkbeiner D. P., Davis M., 1998, Apj, 500, 525
Schmidt S. J., West A. A., Hawley S. L., Pineda J. S., 2010, Aj, 139, 1808
Skemer A. J., et al., 2016, ApJ, 826, L17
Skrzypek N., Warren S. J., Faherty J. K., Mortlock D. J., Burgasser A. J., Hewett P. C., 2015, A&A, 574, A78
Skrzypek N., Warren S. J., Faherty J. K., 2016, A&A, 589, A49
Smith L., Lucas P. W., Burningham B., Jones H. R. A., Smart R. L., Andrei A. H., Catalán S., Pinfield D. J., 2014, MNRAS, 437, 3603
Sorahana S., Nakajima T., Matsuoka Y., 2018, preprint, (arXiv:1811.07496)
Tie S. S., et al., 2017, Aj, 153, 107
Warren S. J., et al., 2007, ArXiv Astrophysics e-prints,
West A. A., Morgan D. P., Bochanski J. J., Andersen J. M., et al. 2011, aj, 141, 97
Wright E. L., et al., 2010, AJ, 140, 1868
Zhang Z. H., Homeier D., Pinfield D. J., Lodieu N., Jones H. R. A., Allard F., Pavlenko Y. V., 2017, MNRAS, 468, 261

15 AFFILIATIONS

[1] Centro de Investigaciones Energéticas, Medioambientales y Tecnológicas (CIEMAT), Madrid, Spain
[2] Laboratório Interinstitucional de e-Astronomia - LIneA, Rua Gal. José Cristino 77, Rio de Janeiro, RJ - 20921-400, Brazil
[3] Observatório Nacional, Rua Gal. José Cristino 77, Rio de Janeiro, RJ - 20921-400, Brazil
[4] Instituto de Física, UFRGS, Caixa Postal 15051, Porto Alegre, RS - 91501-970, Brazil
[5] Center for Astrophysics Research, University of Hertfordshire, Hatfield AL10 9AB, UK
[6] Harvard-Smithsonian Center for Astrophysics, Cambridge, MA 02138, USA
[7] Black Hole Initiative at Harvard University, 20 Garden Street, Cambridge, MA 02138, USA
[8] George P. and Cynthia Woods Mitchell Institute for Fundamental Physics and Astronomy, and Department of Physics and Astronomy, Texas A&M University, College Station, TX 77843, USA
[9] Institute of Astronomy, University of Cambridge, Madingley Road, Cambridge CB3 0HA, UK
[10] Kavli Institute for Cosmology, University of Cambridge, Madingley Road, Cambridge CB3 0HA, UK
[11] Physics Department, 2320 Chamberlin Hall, University of Wisconsin-Madison, 1150 University Avenue Madison, WI 53706-1390
[12] LSST, 933 North Cherry Avenue, Tucson, AZ 85721, USA
[13] Fermi National Accelerator Laboratory, P. O. Box 500, Batavia, IL 60510, USA
[14] Cerro Tololo Inter-American Observatory, National Optical Astronomy Observatory, Casilla 603, La Serena, Chile
[15] Instituto de Fisica Teorica UAM/CSIC, Universidad Autonoma de Madrid, 28049 Madrid, Spain
[16] Department of Physics and Astronomy, University of Pennsylvania, Philadelphia, PA 19104, USA
[17] Department of Physics & Astronomy, University College London, Gower Street, London, WC1E 6BT, UK
[18] Kavli Institute for Particle Astrophysics & Cosmology, P. O. Box 2450, Stanford University, Stanford, CA 94305, USA
[19] SLAC National Accelerator Laboratory, Menlo Park, CA 94025, USA
[20] Department of Astronomy, University of Illinois at Urbana-Champaign, 1002 W. Green Street, Urbana, IL 61801, USA
[21] National Center for Supercomputing Applications, 1205 West Clark St., Urbana, IL 61801, USA
[22] Institut de Física d'Altes Energies (IFAE), The Barcelona Institute of Science and Technology, Campus UAB, 08193 Bellaterra (Barcelona) Spain
[23] Kavli Institute for Cosmological Physics, University of Chicago, Chicago, IL 60637, USA
[24] Institut d'Estudis Espacials de Catalunya (IEEC), 08034 Barcelona, Spain
[25] Institute of Space Sciences (ICE, CSIC), Campus UAB, Carrer de Can Magrans, s/n, 08193 Barcelona, Spain
[26] Santa Cruz Institute for Particle Physics, Santa Cruz, CA 95064, USA
[27] Institució Catalana de Recerca i Estudis Avançats, E-08010 Barcelona, Spain
[28] Department of Astrophysical Sciences, Princeton University, Peyton Hall, Princeton, NJ 08544, USA
[29] School of Physics and Astronomy, University of Southampton, Southampton, SO17 1BJ, UK
[30] Instituto de Física Gleb Wataghin, Universidade Estadual de Campinas, 13083-859, Campinas, SP, Brazil
[31] Computer Science and Mathematics Division, Oak Ridge National Laboratory, Oak Ridge, TN 37831
[32] Department of Physics, University of Michigan, Ann Arbor, MI 48109, USA
[33] Argonne National Laboratory, 9700 South Cass Avenue, Lemont, IL 60439, USA

APPENDIX A: LEPHARE CONFIGURATION

In this section we detail the `Lephare` configuration we used to separate extragalactic sources from the main MLT catalogue. We run separately `Lephare` for galaxy and quasar templates.

We used `AVEROIN` galaxy template library, containing 62 different templates including starburst, spiral, elliptical and irregular galaxies from Coleman et al. (1980), Kinney et al. (1996), and Bruzual & Charlot (2003) and tuned in the mid-infrared (from 3.6 to 4.5 microns) based on VVDS-CFHTLS-SWIRE photometry and VVDS spectra. They were used for the first in Arnouts et al. (2007). We allow for internal extinction following the extinction law by Prevot et al. (1984) up to a E(B-V) = 0.3. In Table A1 we summarize the configuration parameters we used in `Lephare`.

For quasars, we use the default quasar template list from `Lephare` and we refer to their documentation for details about the templates used. In Table A2 we summarize the configuration used for the quasar run.

We further need the filter passbands for i, z, Y (DES), J, H, K_s (VHS) and $W1, W2$ (WISE). The DES passbands are the most updated versions of the calibrated transmission curves as shown in Burke et al. (2018), for the VHS passbands, we use the curves given at `ESO` instrument description page[9] while for the WISE filters we used the curves given at the WISE documentation page[10].

Finally, we add an error of 0.07 in quadrature to each magnitude error as we did for the main *classif* run and transform magnitudes to AB previous to run `Lephare`.

APPENDIX B: GALAXY CONTAMINATION IN THE MLT CATALOGUE

In this section we describe the extragalactic population found in the colour space defined in Section 4 after running `Lephare`. From the list of 2818 targets, 2,761 are galaxies, and 57 are quasars. Next, we show the properties of the galaxy population.

To avoid biases in our conclusions due to a wrong classification as explained in Section 6.1, we analyse only sources with `NBANDS` > 5. From the list of 2,761 extragalactic sources, 514 targets meet this requirement. In this sample, we identify two phenotypes of galaxies that mimic the LT colours: elliptical galaxies at redshifts $1. < z < 2.$ and another phenotype of spirals and irregulars with $5. < z < 6.$. In Fig. B1 we show the best-fit galaxy template versus the redshift. In colour scale, the best-fit MLT type is presented. In Fig. B2 we show the number of extragalactic sources as a function of galaxy spectral type. The contamination happens only in the ML regime.

APPENDIX C: VALIDATION

As a simple validation test, the expected number counts output from *GalmodBD* for a field with unit solid angle, in the case of a uniform BD LF of $n_0\ pc^{-3}$, and towards the Galactic poles may be compared to the trivial analytical solution for this particular case, which comes from direct integration of the fundamental equation of stellar statistics for a single disk exponential model:

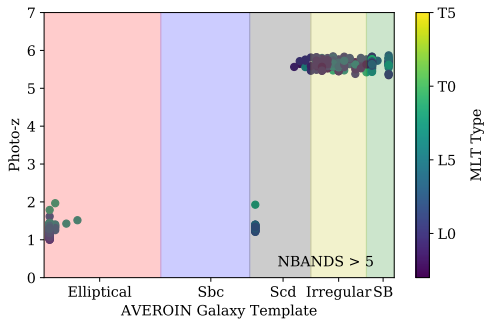

Figure B1. Best galaxy templates versus redshift for extragalactic targets with $NBANDS > 5$. The colour scale is given by the colour bar and represent the best-fit MLT type.

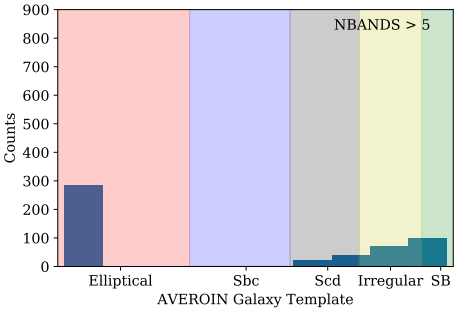

Figure B2. Best galaxy template distribution for extragalactic targets with $NBANDS > 5$.

$$N(m) = n_0[h_z\ f_1(d_1, d_2) + 2\ h_z^2\ f_2(d_1, d_2) + 2\ h_z^3\ f_3(d_1, d_2)] \quad \text{(C1)}$$

In the expression above, if $m, m + dm$ is some chosen bin in apparent magnitude, $N(m)dm$ will be the number of objects in the given bin. h_z is the model exponential scale height for the disk, and

$$f_1(d_1, d_2) = d_1^2\ exp(-d_1/h_z) - d_2^2\ exp(-d_2/h_z) \quad \text{(C2)}$$

$$f_2(d_1, d_2) = d_1\ exp(-d_1/h_z) - d_2\ exp(-d_2/h_z) \quad \text{(C3)}$$

$$f_3(d_1, d_2) = exp(-d_1/h_z) - exp(-d_2/h_z) \quad \text{(C4)}$$

[9] http://www.eso.org/sci/facilities/paranal/instruments/vircam/inst.html
[10] http://www.astro.ucla.edu/~wright/WISE/passbands.html

Table A1. Lephare configuration used when fitting the data to galaxy templates.

NAME	VALUE	EXPLANATION
GAL_SED	AVEROIN_MOD.list	List of 62 galaxy templates
GAL_FSCALE	1.	Arbitrary Flux Scale
FILTER_LIST	$i, z, Y, J, H, K_s, W1, W2$	List of paths to ascii files with passbands
TRANS_TYPE	0	Transmission type (0 = Energy, 1 = Nb of photons)
FILTER_CALIB	0	Filter calibration (0 = fnu=ctt)
MAGTYPE	AB	Magnitude type (AB or VEGA)
Z_STEP	0.04, 6., 0.1	dz, zmax, dzsup
COSMOLOGY	70, 0.3, 0.7	H0, Ω_M, Ω_Λ
EXTINC_LAW	SMC_prevot.dat	Extinction law
EB_V	0., 0.05, 0.1, 0.15, 0.2, 0.3	Allowed E(B-V) values
MOD_EXTINC	38, 62	Templates for which to apply extinction law
EM_LINES	NO	Allow emission lines
CAT_MAG	AB	Input Magnitude (AB or VEGA)
ERR_SCALE	0.07	Errors per band added in quadrature
Z_INTERP	YES	Redshift interpolation

Table A2. Lephare configuration used to fit the data to quasar templates.

NAME	VALUE	EXPLANATION
GAL_SED	QSO_MOD.list	List of 28 quasar templates
GAL_FSCALE	1.	Arbitrary Flux Scale
FILTER_LIST	$i, z, Y, J, H, K_s, W1, W2$	List of paths to ascii files with passbands
TRANS_TYPE	0	Transmission type (0 = Energy, 1 = Nb of photons)
FILTER_CALIB	0	Filter calibration (0 = fnu=ctt)
MAGTYPE	AB	Magnitude type (AB or VEGA)
Z_STEP	0.04, 9., 0.1	dz, zmax, dzsup
COSMOLOGY	70, 0.3, 0.7	H0, Ω_M, Ω_Λ
EB_V	None	Allowed E(B-V) values
CAT_MAG	AB	Input Magnitude (AB or VEGA)
ERR_SCALE	0.07	Errors per band added in quadrature
Z_INTERP	YES	Redshift interpolation

where

$$d_1 = 10^{(0.2(m-M_{ft}+5))}\ pc \quad \text{(C5)}$$

$$d_2 = 10^{(0.2(m-M_{br}+5))}\ pc \quad \text{(C6)}$$

are, respectively, the minimum and maximum distances out to which any BD can be observed with the apparent magnitude m. This minimum (maximum) distance inevitably corresponds to the least (most) luminous BD spectral type in some filter, whose absolute magnitude is M_{ft} (M_{br}).

Another simple validation test, again for the same special case as before, but this time involving all spectral types, is provided by the cumulative counts within some magnitude range $[m_{br}, m_{ft}]$, $N(\leq m)$:

$$N(\leq m) = \sum_{k}^{Nmod} n_0[h_z\ f_1(k,d_1,d_2) + 2\ h_z^2\ f_2(k,d_1,d_2) + 2\ h_z^3\ f_3(k,d_1,d_2)] \quad \text{(C7)}$$

where in the expression above, the sum is over all $Nmod$ BD spectral types, and the functions f_1, f_2, and f_3 are as given before. The minimum and maximum distances are now given by

$$d_1 = 10^{(0.2(m_{br}-M_k+5))}\ pc \quad \text{(C8)}$$

$$d_2 = 10^{(0.2(m_{ft}-M_k+5))}\ pc \quad \text{(C9)}$$

therefore corresponding to the minimum and maximum distances over which the k-th model contributes to the counts.

Completely analogous analytic expressions apply to the situation in which we model the number counts for $(l, b) = (180, 0)$ deg. In this case, all one needs to do is to replace the model disk scale height $h_{z,thin}$ by the scale length h_R.

In Fig. C1, we show the comparison of *GalmodBD* predictions with the analytical counts, based on a single disk component over a 1 sq. deg. field, and using n_0=4 10^{-4} $pc^{-3}mag^{-1}$, for the following cases: 1 - Galactic pole (left panel, using h_z = 150 pc); 2-(l, b) = $(180, 0,)$deg (right panel, with h_R = 2500 pc). The points are from *GalmodBD* and the lines are from the analytic expressions provided above. Open (filled) symbols are differential (cumulative) counts as a function of z band magnitude. *GalmodBD* clearly reproduces the expected counts.

This paper has been typeset from a TEX/LATEX file prepared by the author.

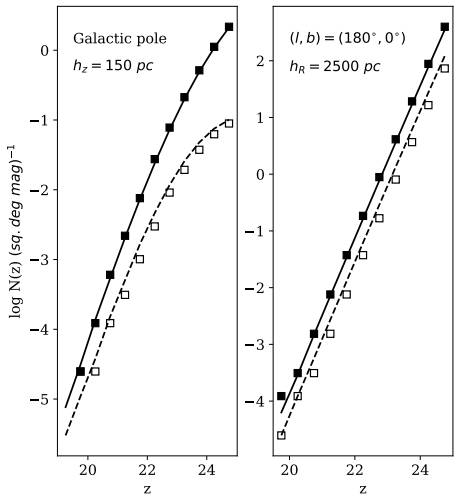

Figure C1. Left panel: Star counts as a function of z_{AB} towards the Galactic Pole using a single disk model with scale height $h_{z,thin}$ = 150 pc. Points come from *GalmodBD*: the open symbols are differential counts and the filled symbols are cumulative counts. The associated curves are the analytic formulae given by equations C1 and C7, respectively. Right panel: Same as in the previous panel, but now star counts towards the Galactic anti-centre, for a model with a single disk with horizontal scale length h_R = 2.5 kpc.

Chapter 3

Benchmark L and T dwarfs

In this section we describe candidate benchmark systems, specifically the wide binary systems made up of L or T dwarf candidates orbiting main sequence stars. Also, we present systems made up by two brown dwarfs. We also find in our search 2 multiple system candidates: a triple and a quadruple. The vast majority of the systems have $\lesssim 10000$ AU projected separation. The benchmark systems are useful to improve brown dwarf evolutionary models since their chemical composition and age constraints may be taken from the primary star if we assumed that the pair formed together, at the same time and in the same molecular cloud.

Our approach was to use our sample of L and T candidates selected from DES data (Carnero Rosell et al., 2019) and then search for possible companions. We used a common distance criterion, without any proper motion information. For Gaia DR2 and DES stars, we estimated distances using the `StarHorse` code and for the brown dwarfs, the distances were based on empirical templates ranging from L0 to T9. In order to assess the false positives, we compute chance alignment probabilities. We discarded pairs with probability $> 5\%$. From Gaia DR2 we found 65 pairs, from DES we found 123. And we identified 9 systems involving two brown dwarfs. This is the largest catalog containing candidate benchmark brown dwarfs to date. The vast majority of our brown dwarfs pair members are of early L type, in tune with the total sample of L and T candidates. Also, we determine that the typical binary fraction over all spectral types is $2 - 4\%$.

The rest of this chapter is presented as paper that is currently at internal review by DES members.

MNRAS **000**, 000–000 (2018) Preprint 1 July 2019 Compiled using MNRAS LATEX style file v3.0

L and T dwarfs wide binaries from the Dark Energy Survey DR1 and Gaia DR2 data

M. Dal Ponte[1,2]★, B. Santiago[1,2], A. Carnero Rosell[2,3], B. Burningham[4], DES MW Working group, Builders, +others
[1]*Universidade Federal do Rio Grande do Sul (UFGRS)*
[2]*Laboratório Interinstitucional de e-Astronomia (LIneA)*
[3]*Centro de Investigaciones Energéticas, Medioambientales y Tecnológicas (Ciemat)*
[4]*University of Hertfordshire*

Accepted XXX. Received YYY; in original form ZZZ

ABSTRACT
We present 188 candidate wide binary systems composed by L or T dwarfs orbiting main sequence stars, 9 double brown dwarf systems and 2 multiple systems candidate (triple and quadruple) with $\lesssim$ 10000 AU projected separation. Using a sample of 11,745 brown dwarfs candidates selected from DES data, we search for possible main sequence companions in Gaia DR2 and Dark Energy Survey data. We also search for systems made up by two brown dwarfs. The benchmark binary systems are very useful to improve brown dwarf evolutionary models since their chemical composition and ages may be taken from the primary star. We use a common distance criterion with no proper motion information. For the Gaia DR2 stars we estimate distances based on their parallaxes and photometry, using the `StarHorse` code, while for DES stars, the `StarHorse` distances were purely photometric for the majority of cases, with a small fraction having parallax measurement from Gaia DR2. L and T dwarfs distances are based on empirical templates ranging from L0 to T9. We also compute chance alignment probabilities in order to assess the physical nature of each pair. We found 70 possible pairs with Gaia DR2 primaries, 65 of them with chance alignment probabilities $< 5\%$. For DES primaries, these numbers are 132 and 123, respectively. Only 9 candidate systems composed by two brown dwarfs were identified. We cross-correlate our wide binary candidates with previous objects from the literature, either with common distances and proper motions or confirmed spectroscopically, having found 1 object in common. The vast majority of our L or T pair members are of early L type, as expected in comparison to our sample of L and T candidates. Also, we determine that the typical wide binary fraction over the L and T spectral types is $2-4\%$.

Key words: Brown Dwarfs, Benchmarks, Dark Energy Survey

1 INTRODUCTION

L,T and Y dwarfs, also called brown dwarfs (BDs), are presumed to be common objects in the Milky Way. Due their very low masses ($< 0.075 M_{\odot}$) and temperatures ($T_{\rm eff} < 2300K$), and hence luminosities, rank them among the most difficult sources to detect.

Their census has greatly improved since the appearance of infrared surveys, such the Two-Micron All-Sky Survey (2MASS; Skrutskie et al. 2006), the Deep Near Infrared Survey of the Southern Sky (DENIS; Epchtein et al. 1997), the UKIRT Infrared Deep Sky Survey (UKIDSS; Lawrence et al. 2007), the Wide-field Infrared Survey Explorer (WISE; Wright et al. 2010) and the VISTA Hemisphere Survey (VHS; McMahon et al. 2013). Among the optical surveys that unveiled substantial numbers of such as cool sources are the Sloan Digital Sky Survey (SDSS; York et al. 2000), and, more recently, the Dark Energy Survey (DES; Abbott et al. 2018). However, samples of known brown dwarfs are still restricted to distances of a few hundred parsecs from the Solar position.

On the theoretical side, many uncertainties about the interior, atmosphere and evolution of L and T dwarfs still remains. Models of brown dwarf structure often lack consistent boundary conditions between the interior and the atmosphere. Uncertainties also remains in terms of opacities, the equation of state and the importance of cloud condensation in the atmospheres. As in the case of stars, brown dwarf formation and evolution models should benefit from knowledge of chemical composition, masses and ages of a sizeable sample of such objects. Binary systems are ideal to study star formation, to benchmark stellar evolutionary models and to calibrate empirical relations that determine fundamental parameters. In this

★ E-mail: marina.ponte@ufrgs.br

scenario, large statistical samples could constrain the behavior and intrinsic variations of star formation and stellar properties of L and T dwarf population.

In terms of binary statistics, there is evidence that the binary frequency decreases as a function of spectral type. For solar-types stars, Raghavan et al. (2010) found that ~ 25% have a companion with separation wider than 100 AU, ~ 11 % wider than 1000 AU and Tokovinin & Lépine (2012) estimate 4.4 % wider than 2000 AU. However, searches for M,L or T dwarfs in wide binary systems remains incomplete. Recently Dhital et al. (2011) and Dhital et al. (2015) presented the Sloan Low-mass Wide Pairs of Kinematically Equivalent Stars (SLoWPoKES), a catalog containing common proper motion and common distance wide candidate pairs. For the mid-K and mid-M type dwarfs presented in both catalogs, the wide binary frequency was ~ 1.1%. However, the binary fraction for L and T dwarfs in wide systems is still uncertain.

Using DES+VHS+WISE data we were recently able to select and perform spectral classification using only photometry on a sample of ~ 11,000 brown dwarfs candidates (Carnero Rosell et al. 2019). Using this sample of L and T dwarfs we estimated the thin disk scale height of L dwarfs, which agreed with a recent measurements found by Sorahana et al. (2018). A more detailed description of the data, color cuts, spectral classification and modeling of the spatial distribution of L and T dwarfs is presented in Carnero Rosell et al. (2019).

In this paper we present the study of benchmark systems, specifically wide binary systems which contain L or a T dwarf orbiting main sequence (MS) stars. These systems are useful to improve brown dwarfs evolutionary models since their chemical composition and age constraints may be taken from the primary star, assuming that the pair formed at the same time, of the same material and evolved in the same environment. In Section 3 we describe our sample of brown dwarfs candidates selected from DES+VHS+WISE data. In Section 4 we discuss the photometric distance measurement for the L and T candidates and the spectro-photometric distance for the primary stars selected in the Gaia DR2 and DES data. In Section 5 we present the details about the candidate binaries and also we address the estimation of change alignment probability.

2 THE DATA

In this section we describe the data used to select L and T dwarf candidates and primaries stars used in our search for wide binary companions.

2.1 DES, VHS and WISE data

DES is a (~5,000deg^2) optical survey in the $grizY$ bands that uses the Dark Energy Camera (DECam; Flaugher et al. 2015). DECam is a wide-field (3 deg^2) imager at the prime focus of the Blanco 4m telescope in Cerro Tololo Inter-American Observatory (CTIO).

The DES footprint was selected to obtain a overlap with the South Pole Telescope survey (Carlstrom et al. 2011) and Stripe 82 from SDSS (Abazajian et al. 2009). The Galactic plane was avoided to minimize stellar foregrounds and extinction from interstellar dust in order to maintain the DES cosmological goals. Even though the main drive for DES is cosmological, the stellar data have been extensively used by the collaboration to identify new star clusters, streams and satellite galaxies in the MW Halo and beyond (Bechtol et al. 2015; Drlica-Wagner et al. 2015; Luque et al. 2017).

The first public data release of the Dark Energy Survey, DES DR1 (DR1; Abbott et al. 2018) is composed of 345 distinct nights spread over the first 3 years of DES operations, from 2013 August 15 to 2016 February 12. DR1 uses exposure times of 90s for $griz$ bands and 45s for Y band, yielding a typical single-epoch point-spread function (PSF) depth at signal-to-noise ratio (S/N) = 10 of g = 23.57, r = 23.34, i = 22.78, z = 22.10, and Y = 20.69 (AB system) (Morganson et al. 2018). The median air mass of DR1 survey-quality exposures was 1.22, with >99% of exposures taken at air mass <1.4. Meanwhile, the median delivered seeing (FWHM) was g = 1.12, r = 0.96, i = 0.88, z = 0.84, and Y = 0.90 arcseconds. The DES DR1 co-add source extraction process detected and cataloged 399,263,026 distinct objects. The star/galaxy separation scheme follows the `SExtractor SPREAD_MODEL`, which compares the fit of a local PSF model to a slightly extended exponencial disk model (Desai et al. 2012).

DES DR1 has many flags in order to avoid corrupted values due to image artifacts or reduction problems. the case of searches for L and T dwarfs and MS stars in the DES data, we demanded that `FLAGS_z,Y` = 0 (ensures no reduction problems in the z and Y bands) and `ISO_MAGFLAGS_i,z,Y` = 0 (ensures the object has not been affected by spurious events in the images in i,z,Y bands). In the case of LT dwarfs search, we also imposed a magnitude limit cut of $z < 22$ with a detection of 5σ at least in the z and Y magnitudes to ensure a high completeness in the i band. For the MS stars case, we imposed a magnitude limit cut of $i < 24$. The DES DR1 is a already a public release, but in our investigation we used `SOF_PSF_MAG_i,z` photometry, which is not been published yet. The SOF photometry is based on a different reduction using the `ngmix` code [1], with has better PSF and shape modeling. Even though we used nonpublic photometry, the `COADD_ID` are the same as those in the public release.

The VHS is a infrared survey imaging 18,000 deg^2 in the southern hemisphere which uses the 4m VISTA telescope at ESO Cerro Paranal Observatory, in Chile, with the VIRCAM camera (Dalton et al. 2006). The VHS has a full overlap with DES in two wavebands, J and K_s, with depth J = 20.3, K_s = 18.6 and partial coverage in H band, with depth H = 18.5 (Vega system) at 5σ for point sources. The VHS Data Release 3 has 42,046,641 sources in the region that overlaps the DES.

We also used the AllWISE data, which is a full sky infrared survey observing in the wavelength range 3.4, 4.6, 12, and 22 μm in $W1$, $W2$, $W3$ and $W4$ bands. The AllWISE is a combination of the WISE mission and NEOWISE (Mainzer et al. 2011). The AllWISE Catalog is >95% complete for sources with $W1 < 17.1$ and $W2 <$ 15.7 mag (Vega system). The AllWISE catalog has 58,764,954 sources in the region overlaping DES.

In order to match the three catalogs, we first matched DES to VHS using a positional matching radius of 2 arcseconds, and then we repeated the same procedure with the AllWISE catalog using the DES+VHS catalog. After matching the DES+VHS+WISE data, we removed every source that did not pass the DES quality cuts as explained before. The resulting catalog has 27,249,118 sources in 2374 deg^2 footprint and was used for the L and T dwarf search (Section 3) and also to search for primary star candidates (Section 5.2).

[1] https://github.com/esheldon/ngmix

2.2 Gaia

The Gaia astrometric mission was launched in December 2013 and placed 1.5 million km from the Earth. It is measuring positions, parallaxes, proper motions and photometry for over one billion sources to $G \simeq 20.7$, and obtaining physical parameters and radial velocities for millions of brighter stars. Its recent Data Release 2 (Gaia DR2; Gaia Collaboration et al. 2018), has covered the initial 22 months of data taking (from a predicted total of 5 years), with positions and photometry for 1.7×10^9 sources, full astrometric solution for 1.3×10^9, $T_{\rm eff}$, extinction, stellar radii and luminosities for $\simeq 10^8$ stars, and radial velocities for 7×10^7 of them. In this paper, Gaia DR2 was used to select primary star candidates to our sample of LT dwarfs. Particularly important for this purpose are the parallaxes, whose precision varies from < 0.1 mas for $G \leq 17$ to $\simeq 0.7$ mas for $G = 20$. They allow us to better discern dwarfs (whose distances will overlap those of the LT dwarfs from DES+VHS+WISE) from much more distant giants of similar colours, $T_{\rm eff}$ and chemistry. The distance estimated for primaries and secondaries are described in Section 4.2 and Section 4.1, respectively. The Gaia DR2 sample was cross-matched to the APASS (Henden & Munari 2014) and 2MASS catalogues, so as to increase the amount of photometric information available for each star. This is very important in the derivation of the distances, as explained in Section 4.2.

3 SAMPLE OF L AND T CANDIDATES

In Carnero Rosell et al. (2019) our initial goal was to search for L and T candidates in the DES+VHS+WISE data using a color-color cut criteria. We adopt $i_{AB} - z_{AB} > 1.2$, $z_{AB} - Y_{AB} > 0.15$ and $Y_{AB} - J_{Vega} > 1.6$ to perform the selection of the candidates. We used this initial sample of M,L and T dwarfs to run our spectral classification code, which uses only photometry, to estimate the spectral type. The spectral classification code was implemented using the same method as presented in Skrzypek et al. (2015) and Skrzypek et al. (2016), based on a minimization of the χ^2 relative to MLT empirical templates. We ended up with 11,745 L and T dwarfs candidates. More details about the selection method and the spectral classification can be found in Carnero Rosell et al. (2019).

4 DISTANCE MEASUREMENT

In this section we describe our method to measure distances for the L and T candidates, selected from DES+VHS+WISE sample, and for the possible primaries stars which were selected using DES+VHS+WISE and Gaia DR2 data.

4.1 L and T dwarfs candidates

Using our L and T sample described in Section 3, we use the spectral type from each candidate and our empirical model grid described in Carnero Rosell et al. (2019) to find the absolute magnitude and then obtain the distance modulus for each L and T dwarf. The empirical model grid lists absolute magnitudes in $izYJHKW1W2$ for dwarfs ranging from M1 to T9. We computed one distance modulus for each filter with available apparent magnitude. The resulting distance to each L and T was then taken to be the mean value among the available filters and we used the dispersion around the mean as the distance uncertainty. We did not apply any correction for extinction, since this is expected to be small out to the distances to ours candidates, which is smaller than 500 pc.

4.2 Primary stars

We use the Gaia DR2 (Gaia Collaboration et al. 2018) and the DES DR1+VHS+WISE to search for stars located close to our L or T dwarfs. The Gaia data was cut in $G < 18$ and the DES+VHS+WISE in $z < 22$. Every star in the Gaia DR2 sample has a distance measured by the `StarHorse` code (Queiroz et al. 2018).

`StarHorse` uses a Bayesian approach to determine masses, ages, distances and extinctions for field stars through the comparison of their observed spectroscopic, photometric and astrometric parameters with those from stellar evolution models. The models used were materialized by the `PARSEC` set of isochrones (Bressan et al. 2012). The code assumes spatial priors for each structural component of the Galaxy (thin and thick disks, bulge and halo). The priors also assume Gaussian metallicity and age distribution functions for each of them. The same prior on the Initial Mass Function (IMF) was assumed as the Chabrier IMF (Chabrier 2003) for all components. Gaussian likelihood functions were generated using the available observed parameter set and their associated uncertainties. In the case of Gaia DR2, this set included optical and near infrared (NIR) magnitudes and parallaxes. The code then computes the posterior distribution function over distance, marginalized for all other parameters. We take the median of this marginalized posterior as the best distance estimate, while the percentile positions are taken as the uncertainty.

For DES+VHS+WISE stars, `StarHorse` was applied only for those objects close enough to the L or T candidates to be considered as a potential primary star in a wide binary system, as will be discussed in the next section. In this case, we use optical and NIR photometry and parallaxes from Gaia when available.

5 THE SEARCH AND THE BENCHMARK CANDIDATES

We paired L and T candidates to potential primary stars using a search radius that corresponds to 10000 AU as the distance of the primary to the secondary. We choose this physical separation for wide binary systems, following Marocco et al. (2017). We perform this search for three sets of primaries: i) from the Gaia DR2 catalog, with distances based on `StarHorse` ; ii) from DES+VHS+WISE catalog, with photometric distances based on `StarHorse` ; iii) from the L and T candidates themselves. We describe in detail the way this pairing was done for each set, and also discuss the way chance alignment probabilities were computed in each case.

5.1 Primary stars from Gaia DR2

For the Gaia DR2 stars, we considered the individual `StarHorse` distances to each star and the photometric distances for the L and T candidates. We define a search radius equal to a distance of 10000 AU for the Gaia stars. Using this individual search radius for each Gaia star, we search for possible L or T companions within this radius. In order to refine our analysis, we also demand that the distance of the primary and the secondary is within 2σ of each other. Using this common distance criteria, we ended up with 70 candidate pairs as shown in Figure 1. The main characteristics of the candidates binary pairs are presented in Table 1, shown entirely in the Appendix.

For each possible pairs, we first estimate the chance alignment probability following an similar procedure used by Smart et al. (2017). The chance alignment probability is the probability that we find a physically unrelated object with the same common distance

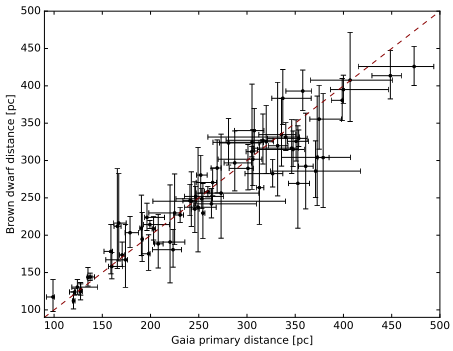

Figure 1. The common-distance pair candidates identified using the brown dwarf sample and Gaia DR2 stars. The horizontal axis represents the primary distance given by StarHorse and the vertical axis shows the secondary photometric distance. The error bars correspond to an uncertainty of 2σ. The uncertainties in the photometric distances of the brown dwarf sample are usually much larger than those of the Gaia stars, which are based on measured parallaxes.

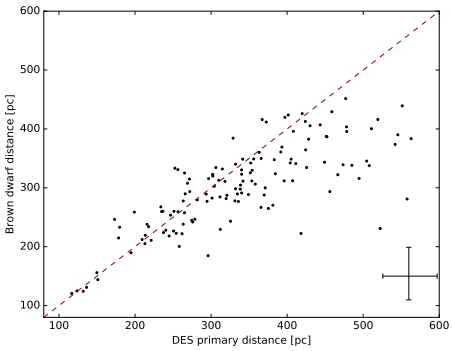

Figure 2. The common-distance pair candidates identified using the brown dwarf sample and DES stars. The horizontal axis represents the primary photometric distance given by StarHorse and the vertical axis shows the brown dwarf photometric distance. In this case, we suppress the error bars for each pair due to the number of sources showing only an average error.

within our uncertainties. For Gaia, we also considered a second approach using simulated data instead of Gaia catalog itself. We aim to compare this to different approaches, since for the sample that we will present in Section 5.2 and Section 5.3 we will rely only on simulations.

For each L or T with a matched Gaia primary candidate, we selected stars within a area of 2 deg^2, using the Gaia catalog itself. We then randomly selected half of the stars within this area and demanded that the distances of brown dwarf and the random star were again within 2σ of each other. We did not include the primary candidate in this random sampling. We calculate the fraction N/M of such common distance stars, where N is the number of stars which have the common distance with the L or T candidate and M is the total number of randomly selected stars. This is the chance alignment probability for a single pair event. We thus multiply the result by the total number of stars within the search radius to obtain the total chance alignment probability for the given L or T candidate. We did not include the Gaia primary candidate in this multiplying factor. In most cases, it was the only object within the search radius, which explains why most of the probabilities are zero. We considered as chance alignments contamination every pair that has a probability larger than 5%. Chance alignment are computed for each candidate system and can be found in Table 1.

We also considered a second approach to obtain the chance alignment contamination. We simulate stars within a 2 deg^2 from the L or T candidate using `Trilegal` (Girardi et al. 2005). The `Trilegal` simulated stars have a distance modulus without any uncertainty. In order to mimic an uncertainty in their distances, we use the uncertainty computed by `StarHorse` for the Gaia DR2 star whose distance is closest to that of the simulated `Trilegal` star. We thus assume that the uncertainty in distance for the simulated stars follows the same distribution as computed by `StarHorse` for real stars. The procedure to compute the chance alignment probability is then similar to that based on the actual distribution of Gaia DR2 stars around the brown dwarf candidates. We compute the fraction of simulated stars that lie within the common distance range at 2σ and then obtain the probability over all stars within the search radius by making an area normalization.

5.2 Primary stars from DES DR1

We search for primary stars using DES+VHS+WISE data. In this case, the search radius corresponds to 10000 AU at the lower distance limit for the L or T dwarf. We adopt this threshold because we do not have the distances for the entire DES catalog. In this case, a possible large uncertainty in the brown dwarfs distances, due to their photometric nature, will result in a larger search radius and could lead to the inclusion of false positives companions.

As mentioned in the previous section, in this case `StarHorse` distances were based on photometric measurements, with additional constraint from parallaxes for a small number of DES stars. We thus look for pairs within the search radius of each L or T candidate which also have a distance match within 2σ. This is the same procedure as in the case of the brighter Gaia DR2 primaries. But as we do not have distances for all stars within 2 deg^2 of the L or T candidate, we cannot use the DES+VHS+WISE catalog itself to estimate the chance alignment probability as we did previously. We are thus forced to rely exclusively on `Trilegal` simulations.

The procedure is the same as described in Section 5.1. We assign distance uncertainties to the simulated stars using the closest DES+VHS+WISE star and then require that the distances of the L or T candidate and the simulated star lie within 2σ of each other. Then we obtain the probability over all stars within the search radius. Also, for DES stars, we randomly selected 10000 stars to obtain the probability since all the simulated areas have more than $\sim$ 20000 stars.

We found a total of 132 possible pairs involving a DES+VHS+WISE primary and an L or T as a secondary, as shown the Figure 2. The characteristics are presented in Table 2, shown entirely in the Appendix.

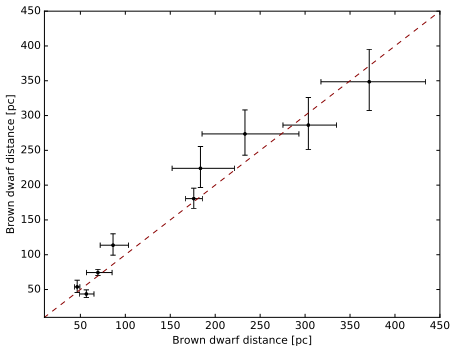

Figure 3. The common-distance for the brown dwarfs binary candidates identified. The horizontal and vertical axis show the brown dwarf photometric distance and the error bars correspond to an uncertainty of 2σ.

5.3 Wide binaries involving two brown dwarfs

We also used the L and T candidates sample to search for binaries among themselves. Again, we compute a search radius for each L or T dwarf and check if another brown dwarf appears inside this individual radius. We were able to identify 9 possible pairs as shown in Figure 3. The information about these possible binary pairs are presented in Table 1.

To obtain the chance alignment probability we used the `GalmodBD` simulation code presented in Carnero Rosell et al. (2019), which computes expected Galactic counts of L and T dwarfs as a function of magnitude, colour and direction on the sky. `GalmodBD` also creates synthetic samples of brown dwarfs based on the expected number counts for a given footprint, using empirically determined space densities of objects, absolute magnitudes and colours as a function of spectral type. For the current purpose, we computed the expected number of L and T dwarfs in a given direction and within the volume bracketed by the common range of distances and by the area within the angular separation of each possible pair. In all cases, the probability of chance alignment is < 0.2 %, as shown in Table 1.

6 DISCUSSION

In our search for binary pairs, we end up finding a possible triple system, as shown in Figure 5. This candidate triple system were identified among the brown dwarf sample along with a DES star. The characteristics of this system are also described in Table 2.

For our pair candidates, we inspected the images to verify how they look like. Figure 4 shows a sample of images of selected benchmark candidates. All of the images were taken from the DES Science Portal related to the DR1 public release images [2].

Figure 6 shows the projected separation versus the distance of our candidate sample. Our brown dwarf sample is limited to ~ 480 pc and despite our previous projected separation limit of 10000 AU, we end up having some pairs with a value larger than that limit. The reason is due to the way we obtain our search radius. We compute a search value that corresponds to 10000 AU projected separation at the lower limit of each star's distance. We decided to use the lower distance to increase the radius search and this option in many cases translates into a larger projected separation compared to our initial limit. However, the vast majority of our pair candidates concentrates at a distance range of 200-400 pc and projected separation < 10000 AU.

The figure also shows a lower limit in projected separation which is related to angular resolution of the DES and Gaia images, especially the former, from which the brown dwarf sample is drawn. Pairs whose angular separation is of the order or lower than the DES seeing limit will be harder to resolve. At a distance of 480 pc a 1.3 arcsec resolution limit will translate into a minimum separation of $\simeq 620$ AU, which is roughly what Figure 6 shows as a lower limit.

The left panel of Figure 7 shows the frequency distribution of L and T spectral types both in our total sample and for our candidates of wide binary systems. In both samples, the L0 dwarfs dominate. Even in a deep survey such DES, we are still bound to detect mainly L types at ~ 500 pc and this selection bias against later types clearly appears in the distributions. The right panel shows the fraction of wide binaries (within the projected separation limits discussed earlier) as a function of spectral type. We observe that the typical binary fraction is 2-4% over most of the spectral types.

In Table 3 we present the known pairs already published in the literature that were spectroscopically confirmed and has a brown dwarfs as a secondary. In Table 4 we present the common distance and/or common proper motion pairs identified so far. Using this information, we performed a search between our pair candidates and the known companions, but neither of the 197 pairs were identified among them. The main reason is because the majority of the know binaries with spectroscopic confirmation are unresolved binary pairs with a small projected separation and we are not able to resolve them.

We also perform a search using the catalog presented in Dhital et al. (2011) and Dhital et al. (2015), which contains low mass stars wide binaries identified using common distance and/or common proper motion. In this case, we were able to identify 1 common object. In Dhital et al. (2015) this particular system is presented as an M1+M1 binary pair, but we identified an L0 as a pair of the components, and also a DES star who has the same distance as this system. This leads us to the possibility of a quadruple system as illustrate the Figure 8. The objects that constitute this multiple system are described in Table 2.

7 SUMMARY AND CONCLUSIONS

Using the Gaia DR2 and DES+VHS+WISE data along with our sample of L and T candidates from Carnero Rosell et al. (2019), we identified 197 new wide binary candidates. The projected separation spreads from $600 \lesssim d_p \lesssim 10000$ AU projected separations. Our candidates were selected based on common distance criteria and with a chance alignment probability criteria of $< 5\%$. These binary and multiple system candidates involving substellar sources are crucial as benchmarks to evolutionary models below the hydrogen burning limit since properties such as metallicity and age, as well as masses, may be obtained for the primaries. The upper limit in projected distance results from our search strategy, in which we avoided larger separations that are more likely to be affected by contaminants. The lower limit in separation stems from the typical resolution of the DES images on which the brown dwarfs sample is based.

We found 65 pairs with a primary from Gaia DR2 catalogue

[2] `https://des.ncsa.illinois.edu/releases/dr1/dr1-access`

Table 1. The common-distance pair candidates identified among the brown dwarfs sample. In this case, A and B represents a different brown dwarf.

Spectral Type		Distance		Separation		Probability
A	B	A	B	["]	[AU]	[%]
L7	L2	69.5	74.3	131.5	9141.8	0.000
T5	T6	56.6	43.5	112.0	6345.8	0.007
L0	L0	303.6	286.2	25.6	7777.4	0.115
L2	L0	233.1	273.6	29.4	6859.0	0.170
L0	L0	371.3	348.5	29.5	10961.6	0.025
L4	L5	86.3	113.6	4.0	352.2	0.066
L0	L5	46.4	53.7	226.4	10514.6	0.224
L0	L0	176.1	180.6	59.1	10411.8	0.020
L1	L1	183.5	224.1	37.2	6832.9	0.045

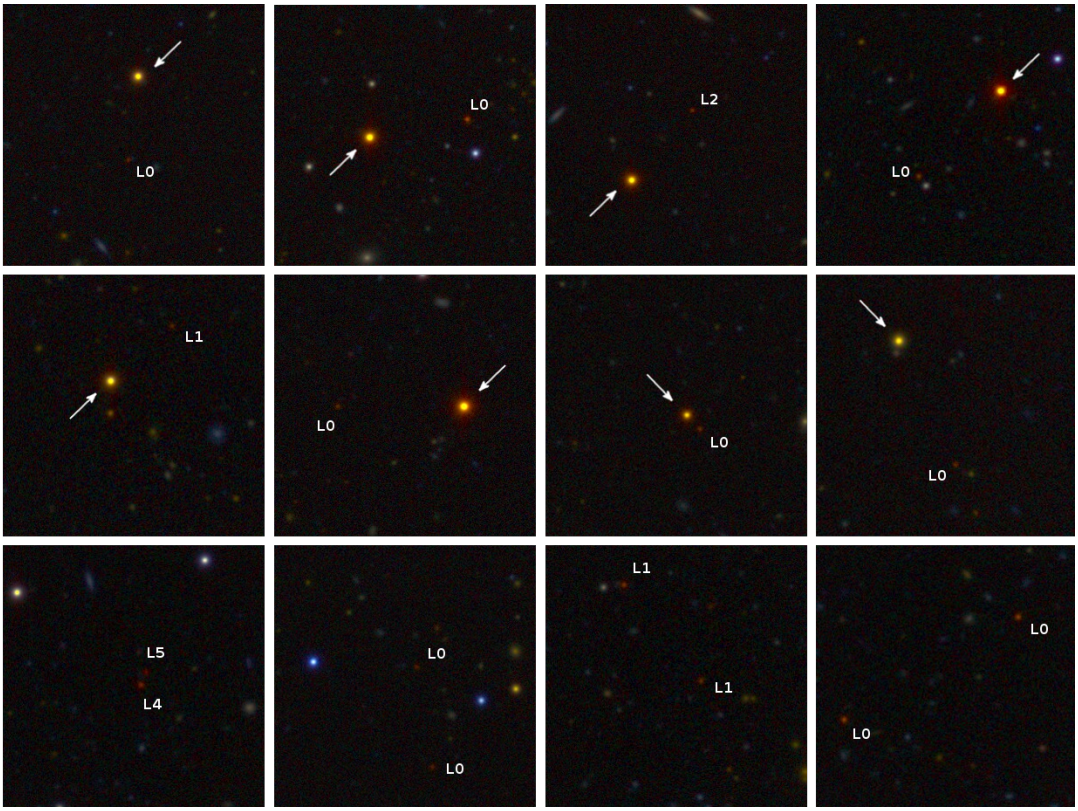

Figure 4. Images of selected benchmark candidates systems. The first row, we present the primary star from Gaia catalog and the L dwarfs as the secondary. The second row, the primary is from DES data and again, the L dwarfs as the secondary. In the last row we present some of the binary pairs composed by two brown dwarfs. The primary star is identified by an arrow and the brown dwarf by the spectral type.

limited to $G < 18$, for which distances are estimated from the `StarHorse` code using constraints from their measured parallaxes. Moreover, 123 of the primaries are in the DES+VHS+WISE sample. These latter tend to be fainter and their `StarHorse` distances are based mostly on photometry, although some have Gaia DR2 parallax information as well. In addition, we found 9 systems composed by two brown dwarfs. One of the L0+L0 pairs seems to be a triple system for which we separately matched each L0 secondary to a DES star. Another multiple candidate was found to contain a L0 dwarf associated to a DES star and to an Gaia DR2 M1+M1 double found by Dhital et al. (2015), therefore making up a poten-

Table 2. The common-distance multiple systems found in our search. In the first row we present the information of the quadruple system, where A refers to the Gaia DR2 star, B to DES star and C to the L0 dwarf. In the second row we present the information of the triple system, where A refers to DES star and B and C to the L0 dwarfs.

Distance			Spectral Type		Probability
A	B	C			[%]
345.5	345.2	285.7	L0		0.000
266.7	285.9	278.7	L0	L0	1.069

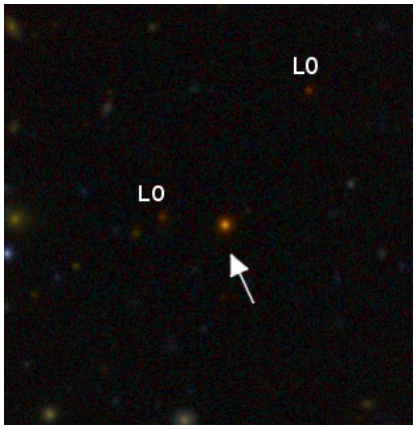

Figure 5. Image of the possible triple candidate system. The arrow indicates the DES star and two brown dwarfs are identified by the spectral type.

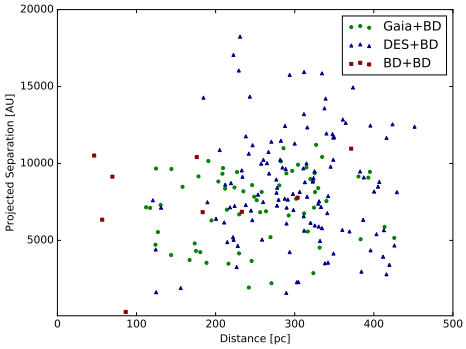

Figure 6. Projected pair separation in AU plotted against distance for all candidates. The colors and different symbols represent the three different samples presented previously, as indicated in the upper right corner. The zone of avoidance at small projected separations is caused by spatial resolution limits, while the paucity of pairs with separations larger than 10000 AU is due to the search method.

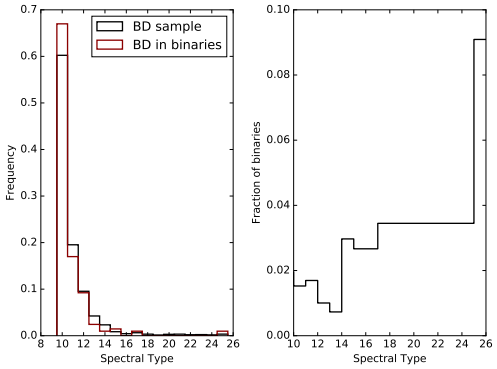

Figure 7. The left panel shows the total frequency distribution of L and T dwarfs (black line) and of brown dwarfs in candidate wide binary systems (red line), both as a function of spectral type. The right panel shows the observed fraction of wide binaries (in the separation range as shown in Figure 6) as a function of spectral type. Spectral type L0-T9 are represented by 10-29.

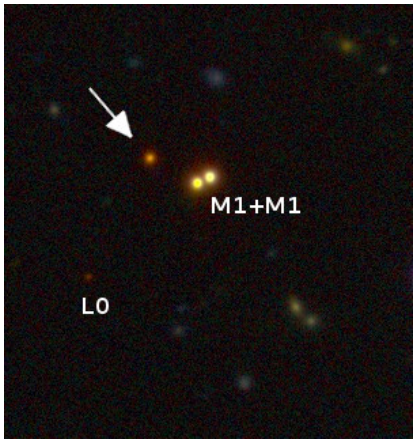

Figure 8. Image of the binary pair identify by Dhital et al. (2015) along with a common distance L0 and a DES star.

tial quadruple system. We found in total 199 independent multiple system candidates.

About 67% of our brown dwarfs found in binary or multiple systems are of the L0 type. Still they make up only $\simeq 2\%$ of the total sample of L0 by Carnero Rosell et al. (2019). The typical binary fraction over all spectral types ranges from $2-4\%$ in the projected separation range covered by this work.

ACKNOWLEDGMENTS

Funding for the DES Projects has been provided by the U.S. Department of Energy, the U.S. National Science Foundation, the Ministry of Science and Education of Spain, the Science and Technology Facilities Council of the United Kingdom, the Higher Education Funding Council for England, the National Center for Supercomputing Applications at the University of Illinois at Urbana-Champaign, the Kavli Institute of Cosmological Physics at the University of Chicago, the Center for Cosmology and Astro-Particle Physics at the Ohio State University, the Mitchell Institute for Fundamental Physics and Astronomy at Texas A&M University, Financiadora de Estudos e Projetos, Fundação Carlos Chagas Filho de Amparo à Pesquisa do Estado do Rio de Janeiro, Conselho Nacional de Desenvolvimento Científico e Tecnológico and the Ministério da Ciência, Tecnologia e Inovação, the Deutsche Forschungsgemeinschaft and the Collaborating Institutions in the Dark Energy Survey.

The Collaborating Institutions are Argonne National Laboratory, the University of California at Santa Cruz, the University of Cambridge, Centro de Investigaciones Energéticas, Medioambientales y Tecnológicas-Madrid, the University of Chicago, University College London, the DES-Brazil Consortium, the University of Edinburgh, the Eidgenössische Technische Hochschule (ETH) Zürich, Fermi National Accelerator Laboratory, the University of Illinois at Urbana-Champaign, the Institut de Ciències de l'Espai (IEEC/CSIC), the Institut de Física d'Altes Energies, Lawrence Berkeley National Laboratory, the Ludwig-Maximilians Universität München and the associated Excellence Cluster Universe, the University of Michigan, the National Optical Astronomy Observatory, the University of Nottingham, The Ohio State University, the University of Pennsylvania, the University of Portsmouth, SLAC National Accelerator Laboratory, Stanford University, the University of Sussex, Texas A&M University, and the OzDES Membership Consortium.

Based in part on observations at Cerro Tololo Inter-American Observatory, National Optical Astronomy Observatory, which is operated by the Association of Universities for Research in Astronomy (AURA) under a cooperative agreement with the National Science Foundation.

The DES data management system is supported by the National Science Foundation under Grant Numbers AST-1138766 and AST-1536171. The DES participants from Spanish institutions are partially supported by MINECO under grants AYA2015-71825, ESP2015-66861, FPA2015-68048, SEV-2016-0588, SEV-2016-0597, and MDM-2015-0509, some of which include ERDF funds from the European Union. IFAE is partially funded by the CERCA program of the Generalitat de Catalunya. Research leading to these results has received funding from the European Research Council under the European Union's Seventh Framework Program (FP7/2007-2013) including ERC grant agreements 240672, 291329, and 306478. We acknowledge support from the Australian Research Council Centre of Excellence for All-sky Astrophysics (CAASTRO), through project number CE110001020, and the Brazilian Instituto Nacional de Ciência e Tecnologia (INCT) e-Universe (CNPq grant 465376/2014-2).

This manuscript has been authored by Fermi Research Alliance, LLC under Contract No. DE-AC02-07CH11359 with the U.S. Department of Energy, Office of Science, Office of High Energy Physics. The United States Government retains and the publisher, by accepting the article for publication, acknowledges that the United States Government retains a non-exclusive, paid-up, irrevocable, world-wide license to publish or reproduce the published form of this manuscript, or allow others to do so, for United States Government purposes.

This publication makes use of data products from the Wide-field Infrared Survey Explorer, which is a joint project of the University of California, Los Angeles, and the Jet Propulsion Laboratory/California Institute of Technology, and NEOWISE, which is a project of the Jet Propulsion Laboratory/California Institute of Technology. WISE and NEOWISE are funded by the National Aeronautics and Space Administration.

The analysis presented here is based on observations obtained as part of the VISTA Hemisphere Survey, ESO Programme, 179.A-2010 (PI: McMahon).

This paper has gone through internal review by the DES collaboration.

ACR acknowledges financial support provided by the PAPDRJ CAPES/FAPERJ Fellowship and by "Unidad de Excelencia María de Maeztu de CIEMAT - Física de Partículas (Proyecto MDM)".

REFERENCES

Abazajian K. N., et al., 2009, ApJS, 182, 543
Abbott T. M. C., et al., 2018, ApJS, 239, 18
Anderson E., Francis C., 2012, Astronomy Letters, 38, 331
Bailey V., et al., 2014, ApJ, 780, L4
Bechtol K., et al., 2015, ApJ, 807, 50
Billères M., Delfosse X., Beuzit J.-L., Forveille T., Marchal L., Martín E. L., 2005, A&A, 440, L55
Bouy H., Brandner W., Martín E. L., Delfosse X., Allard F., Basri G., 2003, AJ, 126, 1526
Bowler B. P., Liu M. C., Cushing M. C., 2009, ApJ, 706, 1114
Bowler B. P., Liu M. C., Shkolnik E. L., Tamura M., 2012, ApJ, 756, 69
Bressan A., Marigo P., Girardi L., Salasnich B., Dal Cero C., Rubele S., Nanni A., 2012, MNRAS, 427, 127
Burgasser A. J., et al., 2000, ApJ, 531, L57
Burgasser A. J., Reid I. N., Leggett S. K., Kirkpatrick J. D., Liebert J., Burrows A., 2005, ApJ, 634, L177
Burningham B., et al., 2009, MNRAS, 395, 1237
Burningham B., et al., 2010, MNRAS, 404, 1952
Burningham B., et al., 2013, Monthly Notices of the Royal Astronomical Society, 433, 457
Caballero J. A., 2007, ApJ, 667, 520
Carlstrom J. E., et al., 2011, PASP, 123, 568
Carnero Rosell A., et al., 2019, arXiv e-prints, p. arXiv:1903.10806
Casagrande L., Schönrich R., Asplund M., Cassisi S., Ramírez I., Meléndez J., Bensby T., Feltzing S., 2011, A&A, 530, A138
Chabrier G., 2003, Publications of the Astronomical Society of the Pacific, 115, 763
Chauvin G., et al., 2005, A&A, 438, L29
Close L. M., Siegler N., Freed M., Biller B., 2003, ApJ, 587, 407
Crepp J. R., Gonzales E. J., Bechter E. B., Montet B. T., Johnson J. A., Piskorz D., Howard A. W., Isaacson H., 2016, ApJ, 831, 136
Currie T., Burrows A., Daemgen S., 2014, ApJ, 787, 104
Dalton G. B., et al., 2006, in Society of Photo-Optical Instrumentation Engineers (SPIE) Conference Series. p. 62690X, doi:10.1117/12.670018
Day-Jones A. C., et al., 2011, MNRAS, 410, 705

De Rosa R. J., et al., 2015, ApJ, 814, L3
Deacon N. R., et al., 2012a, ApJ, 755, 94
Deacon N. R., et al., 2012b, ApJ, 757, 100
Deacon N. R., et al., 2014, ApJ, 792, 119
Desai S., et al., 2012, ApJ, 757, 83
Dhital S., Burgasser A. J., Looper D. L., Stassun K. G., 2011, AJ, 141, 7
Dhital S., West A. A., Stassun K. G., Schluns K. J., Massey A. P., 2015, AJ, 150, 57
Drlica-Wagner A., et al., 2015, ApJ, 813, 109
Dupuy T. J., Liu M. C., 2012, Apjs, 201, 19
Epchtein N., et al., 1997, The Messenger, 87, 27
Faherty J. K., Burgasser A. J., West A. A., Bochanski J. J., Cruz K. L., Shara M. M., Walter F. M., 2010, AJ, 139, 176
Flaugher B., et al., 2015, AJ, 150, 150
Forveille T., et al., 2004, A&A, 427, L1
Gaia Collaboration Brown A. G. A., Vallenari A., Prusti T., de Bruijne J. H. J., Babusiaux C., Bailer-Jones C. A. L., 2018, preprint, (arXiv:1804.09365)
Gálvez-Ortiz M. C., Solano E., Lodieu N., Aberasturi M., 2017, MNRAS, 466, 2983
Gauza B., Béjar V. J. S., Pérez-Garrido A., Rosa Zapatero Osorio M., Lodieu N., Rebolo R., Pallé E., Nowak G., 2015, ApJ, 804, 96
Girardi L., Groenewegen M. A. T., Hatziminaoglou E., da Costa L., 2005, A&A, 436, 895
Gizis J. E., Monet D. G., Reid I. N., Kirkpatrick J. D., Burgasser A. J., 2000, MNRAS, 311, 385
Gizis J. E., Kirkpatrick J. D., Wilson J. C., 2001, AJ, 121, 2185
Goldman B., Marsat S., Henning T., Clemens C., Greiner J., 2010, MNRAS, 405, 1140
Golimowski D. A., et al., 2004, AJ, 128, 1733
Gomes J. I., et al., 2013, MNRAS, 431, 2745
Henden A., Munari U., 2014, Contributions of the Astronomical Observatory Skalnate Pleso, 43, 518
Kirkpatrick J. D., Allard F., Bida T., Zuckerman B., Becklin E. E., Chabrier G., Baraffe I., 1999, ApJ, 519, 834
Kirkpatrick J. D., et al., 2000, AJ, 120, 447
Kirkpatrick J. D., et al., 2011, The Astrophysical Journal Supplement Series, 197, 19
Kraus A. L., Ireland M. J., Cieza L. A., Hinkley S., Dupuy T. J., Bowler B. P., Liu M. C., 2014, ApJ, 781, 20
Lafrenière D., et al., 2007, ApJ, 670, 1367
Lafrenière D., Jayawardhana R., van Kerkwijk M. H., 2008, ApJ, 689, L153
Lagrange A. M., et al., 2010, Science, 329, 57
Lawrence A., et al., 2007, Monthly Notices of the Royal Astronomical Society, 379, 1599
Loutrel N. P., Luhman K. L., Lowrance P. J., Bochanski J. J., 2011, ApJ, 739, 81
Lowrance P. J., Becklin E. E., Schneider G., NICMOS IDT/EONS Team STIS/8176 Team 2000, in American Astronomical Society Meeting Abstracts. p. 52.03
Luhman K. L., et al., 2007, ApJ, 654, 570
Luhman K. L., Burgasser A. J., Bochanski J. J., 2011, ApJ, 730, L9
Luhman K. L., et al., 2012, ApJ, 760, 152
Luque E., et al., 2017, MNRAS, 468, 97
Mace G. N., et al., 2013, ApJ, 777, 36
Mainzer A., et al., 2011, ApJ, 731, 53
Marocco F., et al., 2017, MNRAS, 470, 4885
Marois C., Macintosh B., Barman T., Zuckerman B., Song I., Patience J., Lafrenière D., Doyon R., 2008, Science, 322, 1348
Martin E. L., Brandner W., Basri G., 1999, Science, 283, 1718
McCaughrean M. J., Close L. M., Scholz R. D., Lenzen R., Biller B., Brandner W., Hartung M., Lodieu N., 2004, A&A, 413, 1029
McMahon R. G., Banerji M., Gonzalez E., Koposov S. E., Bejar V. J., Lodieu N., Rebolo R., VHS Collaboration 2013, The Messenger, 154, 35
Metchev S. A., Hillenbrand L. A., 2004, ApJ, 617, 1330
Metchev S. A., Hillenbrand L. A., 2006, ApJ, 651, 1166
Morganson E., et al., 2018, PASP, 130, 074501
Mugrauer M., Seifahrt A., Neuhäuser R., Mazeh T., 2006, MNRAS, 373, L31
Mugrauer M., Neuhäuser R., Mazeh T., 2007, A&A, 469, 755
Murray D. N., et al., 2011, MNRAS, 414, 575
Mužić K., et al., 2012, AJ, 144, 180
Naud M.-E., et al., 2014, ApJ, 787, 5
Neuhäuser R., Guenther E. W., Wuchterl G., Mugrauer M., Bedalov A., Hauschildt P. H., 2005, A&A, 435, L13
Peretti S., et al., 2018, arXiv e-prints, p. arXiv:1805.05645
Phan-Bao N., et al., 2008, MNRAS, 383, 831
Pinfield D. J., et al., 2012, MNRAS, 422, 1922
Queiroz A. B. A., et al., 2018, MNRAS, 476, 2556
Radigan J., Lafrenière D., Jayawardhana R., Doyon R., 2008, ApJ, 689, 471
Raghavan D., et al., 2010, ApJS, 190, 1
Rebolo R., Zapatero Osorio M. R., Madruga S., Bejar V. J. S., Arribas S., Licandro J., 1998, Science, 282, 1309
Reid I. N., Walkowicz L. M., 2006, Publications of the Astronomical Society of the Pacific, 118, 671
Reylé C., et al., 2013, Memorie della Societa Astronomica Italiana, 84, 1050
Scholz R. D., 2010a, A&A, 510, L8
Scholz R. D., 2010b, A&A, 515, A92
Scholz R.-D., 2016, A&A, 587, A51
Scholz R. D., McCaughrean M. J., Lodieu N., Kuhlbrodt B., 2003, A&A, 398, L29
Seifahrt A., Guenther E., Neuhäuser R., 2005, A&A, 440, 967
Skrutskie M. F., et al., 2006, AJ, 131, 1163
Skrzypek N., Warren S. J., Faherty J. K., Mortlock D. J., Burgasser A. J., Hewett P. C., 2015, A&A, 574, A78
Skrzypek N., Warren S. J., Faherty J. K., 2016, A&A, 589, A49
Smart R. L., Marocco F., Caballero J. A., Jones H. R. A., Barrado D., Beamín J. C., Pinfield D. J., Sarro L. M., 2017, MNRAS, 469, 401
Smith L. C., et al., 2015, MNRAS, 454, 4476
Sorahana S., Nakajima T., Matsuoka Y., 2018, preprint, (arXiv:1811.07496)
Steele P. R., Burleigh M. R., Farihi J., Gänsicke B. T., Jameson R. F., Dobbie P. D., Barstow M. A., 2009, A&A, 500, 1207
Tokovinin A., Lépine S., 2012, AJ, 144, 102
Wilson J. C., Kirkpatrick J. D., Gizis J. E., Skrutskie M. F., Monet D. G., Houck J. R., 2001, AJ, 122, 1989
Wright E. L., et al., 2010, AJ, 140, 1868
York D. G., et al., 2000, AJ, 120, 1579
Zhang Z. H., et al., 2010, MNRAS, 404, 1817
Zuckerman B., Becklin E., 1988, International Astronomical Union Circular, 4652, 3
Zuckerman B., Song I., 2009, A&A, 493, 1149

Table 1: The common-distance pair candidates identified using the brown dwarfs sample and the Gaia DR2 data. The letter A represents the primary and B the secondary. The first probability refers to the approach which uses the Gaia catalog and the second for the simulated data as explained in Section 5.1. Here we show the both probabilities for comparison.

Distance		Spectral Type	Separation		Probability	
A	B	B	["]	[AU]	[%]	
346.3	316.5	L0	16.1	5576.6	0.000	1.291
245.9	235.0	L2	33.2	8187.7	0.000	1.234
448.6	413.5	L0	13.0	5874.4	0.000	1.091
197.9	175.1	L3	21.7	4313.5	4.800	1.736
203.1	208.5	L0	45.9	9331.4	1.546	1.609
191.3	194.7	L0	32.8	6293.4	0.000	2.269
120.1	112.0	L0	59.5	7150.0	0.501	1.028
305.1	324.3	L0	23.3	7128.6	0.000	4.566
127.4	124.5	L2	75.8	9669.2	0.000	0.763
312.8	263.6	L1	22.0	6889.7	0.000	1.390
399.9	395.0	L0	23.6	9453.3	0.000	1.005
406.9	407.6	L0	24.0	9786.5	14.411	2.027
170.5	173.5	L2	28.1	4798.6	0.000	0.603
159.8	158.1	L2	53.0	8481.9	0.000	1.388
273.1	256.3	L1	24.9	6827.2	0.000	2.931
224.9	229.8	L0	29.7	6691.2	0.000	2.037
331.7	319.8	L0	27.1	8991.6	0.000	3.341
306.0	301.7	L0	25.1	7707.8	0.000	2.028
378.9	303.9	L1	20.6	7820.2	13.920	2.190
319.9	325.1	L0	29.2	9369.5	0.000	1.251
287.3	296.8	L0	33.1	9515.3	0.000	1.397
360.8	292.3	L1	18.3	6619.8	0.000	1.573
371.0	285.8	L0	29.6	10988.9	0.000	0.921
326.5	282.4	L1	31.0	10131.3	0.000	0.955
190.5	209.3	L3	50.8	9699.3	0.000	2.785
263.1	241.9	L0	7.4	1936.4	0.000	0.848
335.7	334.6	L0	31.0	10424.	0.000	1.541
230.6	227.0	L0	40.9	9439.9	0.955	0.679
398.7	380.6	L0	22.9	9149.7	0.000	1.729
127.5	127.0	L4	43.4	5541.4	0.000	0.900
121.3	123.9	L2	38.8	4718.4	0.495	0.540
374.8	355.4	L0	24.0	9007.5	8.558	1.564
135.1	143.7	L0	29.9	4046.2	0.000	1.880
158.9	178.3	L2	57.6	9159.0	0.000	3.894
305.0	311.9	L0	22.1	6750.3	0.000	0.677
207.9	188.4	L0	17.0	3537.7	1.898	2.153
223.3	180.6	L0	18.9	4233.1	0.000	1.486
167.0	216.2	L0	20.8	3485.1	4.514	6.660
98.89	117.2	L7	71.8	7105.3	0.276	3.417
165.5	212.0	L0	50.4	8362.3	0.000	7.651
307.5	340.0	L0	24.5	7555.5	1.658	1.058
220.2	190.8	L0	46.1	10160.	2.615	3.643
264.3	270.5	L0	8.4	2213.9	0.000	1.228
301.0	289.4	L1	31.0	9355.5	0.000	1.498
337.1	383.3	L0	15.0	5074.1	0.000	3.130
240.8	246.2	L0	35.6	8594.9	0.000	0.888
246.7	251.9	L0	30.8	7611.7	1.374	0.921
280.8	323.5	L0	10.2	2872.2	0.000	2.366
249.2	237.4	L2	28.4	7098.9	5.508	3.248
137.3	144.1	L0	70.1	9639.9	0.533	1.067
269.0	289.9	L0	20.0	5407.9	5.049	2.843
252.0	280.5	L0	34.0	8572.9	0.000	1.421
350.9	325.7	L0	23.2	8143.6	0.000	1.202
199.3	214.2	L1	35.0	6993.5	0.260	0.978
259.4	258.2	L0	31.3	8145.3	0.000	0.444
254.2	229.6	L2	16.3	4154.3	0.000	1.356

Table 1 – continued from previous page

Distance		Spectral Type	Separation		Probability	
A	B	B	["]	[AU]	[%]	
242.2	245.4	L1	15.1	3660.1	0.000	1.598
353.5	329.6	L0	23.7	8396.3	0.000	0.963
347.7	314.8	L0	28.0	9738.7	0.000	0.727
352.7	269.3	L0	14.7	5207.9	0.000	2.121
124.1	130.4	L0	58.7	7299.0	0.375	1.903
253.1	248.7	L0	30.9	7839.6	0.000	0.662
372.7	304.2	L1	26.5	9915.6	0.000	2.989
340.2	331.4	L0	13.3	4527.9	0.000	1.152
316.5	327.0	L0	35.4	11209.	0.000	1.407
178.7	203.4	L0	49.3	8826.3	0.000	1.689
357.8	393.0	L0	25.3	9078.7	0.000	2.072
473.2	425.8	L0	10.9	5159.9	0.000	1.138
174.0	167.0	L3	21.4	3727.1	4.680	3.186
196.3	223.8	L1	43.0	8441.9	0.000	0.967

Table 2: The common-distance pair candidates identified using the brown dwarfs sample and the DES data. The letter A represents the primary and B the secondary. The primary with a measure parallax from Gaia are marked with an asterisk. In this case, we only have the probability measured with simulated data.

Distance		Spectral Type	Separation		Probability
A	B	B	["]	[AU]	[%]
393.1*	369.2	L0	14.1	5580.9	1.029
354.0	329.7	L1	20.8	7388.5	2.111
375.2*	264.9	L0	26.6	10017.5	1.234
404.0*	342.2	L1	19.4	7876.3	1.664
507.9	337.6	L0	26.7	13582.5	2.832
310.0*	312.8	L0	28.3	8782.0	1.400
194.6	189.6	L0	38.4	7480.2	1.767
349.1	288.6	L2	27.6	9637.1	2.004
256.3	330.8	L0	29.4	7540.8	0.927
271.9*	293.6	L0	15.5	4236.3	0.932
265.0*	257.6	L0	37.6	9985.5	1.665
304.2*	302.6	L0	7.50	2281.8	1.291
199.0	258.7	L1	25.3	5052.2	1.804
209.3	212.1	L0	41.1	8623.1	0.933
519.3*	416.0	L0	22.4	11653.1	1.150
258.2	200.5	L2	24.8	6406.9	3.549
261.8*	221.9	L0	19.8	5208.4	1.464
358.1*	306.2	L0	22.7	8145.1	2.063
332.1*	340.1	L0	35.9	11947.5	3.407
456.1*	293.6	L0	34.5	15750.8	1.440
428.2*	382.6	L0	22.1	9478.8	1.025
353.6*	311.6	L1	37.3	13204.7	3.019
338.6*	304.6	L1	6.75	2286.5	1.876
405.2*	348.7	L0	25.2	10242.9	1.921
274.5*	244.7	L0	25.2	6937.6	1.785
418.2	222.5	L0	40.7	17055.5	1.219
352.1*	342.0	L0	10.0	3551.6	1.248
320.8*	287.3	L0	24.0	7711.3	2.822
371.1*	299.9	L1	30.4	11292.9	3.688
411.3*	341.1	L0	16.4	6768.4	2.386
173.1	246.3	L2	36.4	6315.2	3.267
363.2*	360.1	L0	15.6	5675.3	0.838
522.3	230.8	L3	34.9	18240.6	3.097
452.4*	386.5	L0	14.0	6336.2	2.011
296.0	184.6	L1	48.2	14276.5	0.852
256.5*	259.2	L1	55.1	14150.9	7.084
301.3	282.5	L0	38.0	11479.2	1.914
252.4	333.2	L0	28.4	7174.5	4.984
233.9*	267.5	L0	39.9	9344.5	2.457
473.5	339.0	L0	30.0	14214.9	0.985
372.5*	411.6	L0	10.5	3937.0	1.031
401.4	423.6	L0	31.2	12544.7	4.612
265.1	325.1	L0	35.7	9489.9	2.541
338.3*	297.8	L1	23.6	8017.0	2.418
356.0*	349.0	L0	11.6	4144.8	1.252
213.4*	219.4	L2	40.8	8720.8	1.461
131.9*	124.2	L3	33.4	4407.6	1.866
458.8*	429.1	L0	17.7	8132.4	2.529
419.8	426.0	L0	11.1	4668.6	0.893
278.7	246.7	L0	40.1	11183.3	2.197
319.7*	281.6	L1	32.0	10242.5	2.074
334.5*	289.6	L1	18.2	6096.0	2.298
430.1*	405.3	L0	19.7	8493.2	0.937
213.0	205.1	L0	51.0	10872.1	1.184
221.1	210.8	L0	27.8	6164.3	1.334
302.2	319.9	L1	20.3	6143.3	2.335

Table 2 – continued from previous page

Distance		Spectral Type	Separation		Probability
	B	B	["]	[AU]	[%]
476.9*	451.5	L0	25.9	12388.4	2.703
302.0*	322.7	L1	29.2	8820.5	1.203
312.0	229.3	L1	51.3	16040.6	3.230
367.1*	415.9	L0	7.60	2793.2	1.168
557.6	281.0	L0	44.1	24611.5	5.234
365.8*	349.9	L0	31.9	11699.5	2.772
179.7*	233.0	L1	53.1	9548.4	4.232
332.1*	298.3	L0	20.9	6971.5	1.357
391.7*	360.8	L0	32.8	12852.8	2.439
443.4*	406.9	L0	19.8	8796.2	1.044
215.6	238.0	L0	33.8	7297.7	1.345
328.8	384.3	L0	9.02	2967.3	0.770
340.1*	330.3	L0	17.3	5901.3	2.159
510.7*	400.3	L0	16.0	8173.0	4.913
341.5*	348.6	L0	34.2	11681.9	3.957
306.2*	334.4	L0	18.9	5794.3	1.279
383.0	347.8	L0	31.0	11904.5	2.951
294.6*	277.0	L0	27.4	8098.0	2.290
340.2*	323.0	L0	26.1	8913.1	1.537
396.9*	419.6	L0	8.59	3411.7	2.576
151.0*	143.9	L2	47.2	7135.8	3.944
551.3*	439.2	L0	5.76	3176.2	6.117
425.6*	334.4	L0	37.2	15857.2	8.824
396.0*	311.8	L1	40.2	15942.1	4.144
449.2*	343.5	L0	26.2	11774.7	5.375
281.8*	279.5	L1	27.1	7641.8	1.100
244.8*	218.1	L0	29.1	7146.3	2.801
236.7	260.3	L0	43.2	10236.6	2.585
318.2*	310.8	L0	30.4	9681.7	1.645
381.2*	270.4	L0	29.9	11415.3	4.613
331.3*	277.8	L0	25.4	8423.1	2.816
271.5*	314.9	L0	36.8	9997.1	4.793
478.0*	403.4	L0	11.3	5402.5	2.208
407.2*	311.9	L0	13.8	5632.0	1.101
541.9*	373.7	L0	27.5	14937.1	1.653
424.3*	364.4	L0	29.7	12638.8	1.481
251.1*	260.0	L0	29.8	7492.0	1.211
123.5	124.8	L2	13.2	1631.7	3.248
240.4	228.0	L2	19.3	4640.8	1.939
263.3	238.1	L1	44.6	11761.3	1.776
408.1*	395.9	L0	10.6	4352.8	1.214
365.6*	266.8	L2	29.3	10743.4	2.042
311.7*	284.5	L1	31.2	9735.7	0.664
116.8	120.6	L2	65.1	7608.7	2.009
351.5*	325.3	L0	16.9	5969.2	3.720
466.6*	322.1	L1	35.8	16713.7	5.284
314.7*	331.9	L0	15.7	4962.0	3.528
335.9*	276.7	L0	26.6	8955.2	4.007
178.3	214.7	L2	27.3	4886.8	2.614
217.8*	233.9	L0	41.9	9137.4	2.084
246.7	253.5	L0	32.3	7972.7	1.918
265.9*	289.7	L0	26.8	7128.9	2.236
237.4*	224.0	L0	30.4	7237.4	2.113
485.0	338.1	L0	7.23	3511.5	1.838
234.9	259.7	L2	47.0	11050.3	6.546
340.1*	291.2	L0	22.4	7651.4	3.092
478.4*	395.6	L0	26.0	12462.2	2.073
254.2*	222.7	L1	19.8	5037.6	2.979
149.8*	155.8	L0	12.6	1901.5	1.434

Table 2 – continued from previous page

Distance		Spectral Type	Separation		Probability
	B	B	["]	[AU]	[%]
563.0*	383.5	L0	28.7	16190.5	4.821
545.5*	390.0	L0	30.3	16569.9	8.411
494.6*	315.8	L0	24.9	12341.2	3.360
296.7*	315.6	L0	26.4	7836.7	1.669
325.5	243.2	L2	44.0	14342.8	2.715
341.9*	311.3	L1	19.1	6565.0	1.659
384.4	323.8	L0	23.5	9051.1	3.003
263.4*	277.6	L1	27.5	7259.7	2.475
423.9*	412.6	L0	13.3	5661.6	0.973
275.7*	241.9	L0	38.5	10637.9	2.006
504.5*	345.4	L1	19.4	9791.4	3.295
293.5*	289.3	L0	5.38	1581.1	0.914
250.6*	226.5	L1	13.0	3266.1	1.573
451.5*	387.2	L0	20.1	9091.2	1.472
268.9	307.7	L1	22.3	6007.1	7.398
369.8	287.7	L1	33.6	12432.4	1.169
136.2	130.9	L5	52.3	7126.7	1.753

Table 3: Known objects that are spectroscopically confirmed companions. Based on Table 12 from Deacon et al. (2014).

Object	Separation		Spectral Type	Spectral Type	Companion Mass	Age	References
	[AU]	["]	Companion	Primary	$M_{\odot}$	[Gyr]	
HD65216B	7.00	253	M7+L2	G5	0.09	3-6	1
G 239-25	2.80	30	L0	M3	-	2.1-7.2	2,3,4
DENIS 0551-4434B	2.20	220	L0	M8.5	0.06	0.1-10	5
Denis-PJ1347-7610B	16.80	418	L0	M0	-	0.2-1.4	6
HD89744B	63.00	2460	L0	F7	0.077-0.080	1.5-3	7
NLTT2274B	23.00	483	L0	M4	0.081-0.083	4.5-10.0	8
LP312-49B	15.40	801	L0	M4	-	-	9
SDSSJ130432.93+090713.7B	7.60	374	L0	M4.5	-	-	9
SDSSJ163814.32+321133.5B	46.00	2420	L0	M4	-	-	9
1RXSJ235133.3+312720B	2.40	120	L0	M2	0.026-0.038	0.05-0.15	10
2MASS 12593933+0651255	23.86	1110	L0	M8	0.21	0.5	11
2MASS 09411195+3315060	7.44	244	L0	M5	0.23	< 10	11
HIP 2397 B	117.1	3970	L0.5	K5	-	0.3-2.5	12
HD 253662 B	20.1	> 1	L0.5	G8IV	-	0.3	12
HIP 59933 B	38.10	2170	L1	F8	-	0.5	12
HIP 63506 B	132.8	5640	L1	M0	-	0.0017-0.025	12
HIP 6407 B	44.90	2570	L1+T3	G5	-	-	12
η TelB	4.20	190	L1	A0V	0.04	0.6-2	13
LP213-68Bb	14.00	230	L1	M6.5	0.068-0.090	~0.03	14,15
GJ1048B	11.90	250	L1	K2	0.055-0.075	0.5-0.8	16
ABPicB	5.50	275	L1	K2	0.01	-	17
G124-62Ba	44.00	1496	L1+L1	dM4.5e	0.054-0.082	<0.002	18
HD 16270	11.90	254	L1	K3.5	-	0.0015-0.003	2,16,4
GQLupB	0.70	103	L1	K7	0.010-0.020	< 10	19
ROX42Bb	1.80	140	L1	M1	0.006-0.014	0.1	20,21
LSPM J0241+2553 B	31.20	2153	L1	WD	-	0.2	12
HIP 112422 B	16.0	1040	L1.5	K2	-	0.3	12
LSPM J0632+5053 B	47.4	4499	L1.5	G2	-	0.3	12
PMI 13518+4157 B	21.6	613	L1.5	M2.5	-	0.3	12
NLTT 44368 B	90.2	7760	L1.5	M3	-	0.37-0.5	12
PM 122118-1005 B	204.5	8892	L1.5	M2	-	0.3	12
β Cir	217.3	6656	L1	A3V	0.056	0.2-10.0	22
NLTT 1011 B	58.5	3990	L2	K7	-	1.0-10.0	12
G255-24B	38.30	9710	L2	K8	-	0.06-0.3	23
2MASSJ05254550-7425263B	44.00	2000	L2	M3	0.06-0.075	0.5-12	24
G196-3B	16.20	300	L2	M2.5	0.015-0.04	0.013-0.015	25
Gl618.1B	35.00	1090	L2.5	M0	0.06-0.079	5.5-8	7
HD106906b	7.10	650	L2.5	F5	0.003-0.007	-	26
HD221356	452.00	11900	L3	F8	0.072	3.3-5.1	27
GD 165	4.00	140	L3	DA	~0.075	3.0-4.0	28,29
G63-33B	66.00	2010	L3	K0	0.079-0.081	2.2-6.1	8
G73-26B	73.00	2774	L3	M2	0.079-0.081	0.5-4.7	8,9
ηCancriB	164.00	15020	L3.5	K3III	0.063-0.082	0.3	9
HD 49197	0.950	44	L4	F5	-	0.3	2,30,31
NLTT 26746 B	18.0	661	L4	M4	-	0.05-12.4	12
PMI 13410+0542 B	9.4	484	L4	M1	-	1.6-5.3	12
GJ 564	2.64	48	L4+L4	F9	-	1.8-3.5	2,32
HD 2057	218	9465	L4+L4	F8	0.045-0.083	7.0-12.0	2,8,30
G171-58B	218.00	9200	L4	F8	0.077-0.078	2.6-8	8
G200-28B	570.00	25700	L4	G5	0.055-0.075	0.010-0.013	8
LHS5166B	8.43	160	L4	M4.5	0.009-0.016	1-10	18
1RXSJ1609-2105b	2.20	330	L4	M0	0.060.075	0.08-0.3	33
GJ1001B	18.60	180	L4.5	M4	0.02-0.05	1-5	29,34,35
Gl417Bab	90.00	2000	L4.5+L6	G0+G0	0.051-0.074	3.5-10.0	29,36
G203-50B	6.40	135	L5.0	M4.5	-	-	37
GJ499B	516.00	1360	L5	K5+M4	-	-	23
G259-20B	30.00	650	L5	M2.5	-	0.5	38
2M1207-39	0.90	46	L5	M8	-	0.3	39

Table 3 – continued from previous page

Object	Separation		Spectral Type	Spectral Type	Companion Mass	Age	References
	[AU]	["]	Companion	Primary	$M_\odot$	[Gyr]	
HD 196180	13.51	907	L5	A3V	-	0.3	40
NLTT 55219 B	9.7	432	L5.5	M2	-	0.1-0.2	12
NLTT 31450 B	12.30	487	L6	M4	0.019-0.025	0.25-0.8	12
LP261-75B	13.00	450	L6	M4.5	0.032-0.076	0.15-0.3	41
2MASSJ01303563-4445411B	3.28	130	L6	M9	0.0112	0.13-0.4	42
VHS 1256-1257	8.06	102	L7	M7.5	0.012-0.031	0.6-3.4	43
HD203030B	11.00	487	L7.5	G8	0.04-0.074	1-2.5	44
Gl337CD	43.00	880	L8+>=L8	G8+K1	0.045-0.075	-	7,45
Gl584C	194.00	3600	L8	G1	0.06	1.3-4.3	46
PHL 5038	0.94	55	L8	DA	0.045-0.072	2.3	47
HD46588B	79.20	1420	L9	F7	0.07	-	48
HD 4747	-	-	L9	-	0.005	-	49,50
HR 8799	1.70	68	L	A5	~0.009	~5	51
β Pic	0.30	8-15	L	A5	0.060-0.073	-	52
ϵ Indi Ba	402.00	1460	T1	K5	0.06-0.07-6.	0.1-0.5	53,54
2MASSJ111806.99-064007.8B	7.70	650	T2	M4.5	0.012-0.030	0.009-0.013	55
HNPegB	43.00	795	T2.5	G0	0.07-0.13	0.3-2.8	56
GUPscB	41.97	2000	T3.5	M3	0.018-0.058	4-10	57
HIP38939B	88.00	1630	T4.5	K4	0.064-0.075	3.5-10	58
LSPMJ1459+0851B	365.00	21500	T4.5	DA	0.068-0.081	1.5-4.9	59
LHS2803B	67.60	1400	T5	M4.5	-	>1.6	24,60
HD118865B	148.00	9200	T5	F5	-	-	61
HIP73786B	63.80	1230	T6	K5	-	0.5-3.0	62,63
LHS302B	265.00	4500	T6	M5	0.02-0.035	2-5	64
G204-39B	198.00	2685	T6.5	M3	0.03-0.07	0.7-4.7	8
Gl570D	258.00	1500	T7	K4+M1.5+M3	0.018-0.058	~10	65
HD3651B	43.00	480	T7.5	K0	0.03-0.04	2.3-14.4	56,66
SDSSJ1416+30B	9.00	45	T7.5	L6p	0.019-0.047	> 3.5	67,68,69
LHS2907B	156.00	2680	T8	G1	-	> 2	38,70
LHS6176B	52.00	1400	T8	M4	0.020-0.050	< 1.0	38,61
Wolf1130B	188.50	3000	T8	sd M1.5+DA	0.005-0.0014	4.0-8.0	71
Ross458C	102.00	1162	T8.5	M0.5+M7	0.014-0.038	3.5-6	72
ξ UMa E	510.00	4100	T8.5	F9+G0	0.02-0.032	1.2-2	61
Wolf940B	32.00	400	T8.5	M4	0.03-0.10		73
WD0806-661	130.00	2500	Y0	DQ			74

References: (1) Mugrauer et al. (2007); (2) Anderson & Francis (2012); (3) Forveille et al. (2004); (4) Dupuy & Liu (2012); (5) Billères et al. (2005); (6) Phan-Bao et al. (2008); (7) Wilson et al. (2001); (8) Faherty et al. (2010); (9) Zhang et al. (2010); (10) Bowler et al. (2012); (11) Gálvez-Ortiz et al. (2017); (12) Deacon et al. (2014); (13) Lowrance et al. (2000); (14) Gizis et al. (2000); (15) Close et al. (2003); (16) Gizis et al. (2001); (17) Chauvin et al. (2005); (18) Seifahrt et al. (2005); (19) Neuhäuser et al. (2005); (20) Kraus et al. (2014); (21) Currie et al. (2014); (22) Smith et al. (2015); (23) Gomes et al. (2013); (24) Mužić et al. (2012); (25) Rebolo et al. (1998); (26) Bailey et al. (2014); (27) Caballero (2007); (28) Zuckerman & Becklin (1988); (29) Kirkpatrick et al. (1999); (30) Casagrande et al. (2011); (31) Metchev & Hillenbrand (2004); (32) Lafrenière et al. (2007); (33) Lafrenière et al. (2008); (34) Golimowski et al. (2004); (35) Martin et al. (1999); (36) Bouy et al. (2003); (37) Radigan et al. (2008); (38) Luhman et al. (2012); (39) Zuckerman & Song (2009); (40) De Rosa et al. (2015); (41) Reid & Walkowicz (2006); (42) Dhital et al. (2011); (43) Gauza et al. (2015); (44) Metchev & Hillenbrand (2006); (45) Burgasser et al. (2005); (46) Kirkpatrick et al. (2000); (47) Steele et al. (2009); (48) Loutrel et al. (2011); (49) Crepp et al. (2016); (50) Peretti et al. (2018); (51) Marois et al. (2008); (52) Lagrange et al. (2010); (53) Scholz et al. (2003); (54) McCaughrean et al. (2004); (55) Reylé et al. (2013); (56) Luhman et al. (2007); (57) Naud et al. (2014); (58) Deacon et al. (2012a); (59) Day-Jones et al. (2011); (60) Deacon et al. (2012b); (61) Burningham et al. (2013); (62) Scholz (2010b); (63) Murray et al. (2011); (64) Kirkpatrick et al. (2011); (65) Burgasser et al. (2000); (66) Mugrauer et al. (2006); (67) Scholz (2010a) ; (68) Burningham et al. (2010); (69) Bowler et al. (2009); (70) Pinfield et al. (2012); (71) Mace et al. (2013); (72) Goldman et al. (2010); (73) Burningham et al. (2009); (74) Luhman et al. (2011).

Table 4. The common-distance and common-proper-motion pair candidates identified in the literature.

Object	Separation [kAU[	Distance [pc[	Sp. Type Companion	Sp. Type Primary	$\mu_\alpha \cos\delta$ [mas yr^-1]	μ_δ [mas yr^-1]	References
J0223-5815	400	49 ±10	L0	M5	134.0±10	5.0±19	1
J1214+3721	153	82 ±17	L0	-	-122.6 ±10.6	82.0 ±17	1
J0939+3412	156	62 ±10	L0	-	-107.1 ±10.4	-64.3 ±12.6	1
ULAS J0255+0532	29	140 ±26	L0	F5	28 ±30	40 ±30	2
ULAS J0900+2930	16	197 ±37	L0	M3.5	-13 ±10	-27.8 ±8.8	2
ULAS J1222+1407	6.7	70 ±13	L0	M4	-74 ±20	-34 ±20	2
J0626+0029	252	67 ±14	L0.5	-	84 ±15	-92 ±15	1
J1632+3505	2	37 ±8	L0.5	K0	91.6 ±9.7	-65.3 ±11.9	1
J2037-4216	270	51 ±10	L1	-	229 ±10	-391 ±10	1
ULAS J1217+1427	2.7	216 ±41	L1	F8V	-49 ±8.2	-19.7 ±8.5	2
ULAS J1330+0914	61	149 ±30	L2	G5	-83 ±37	10 ±37	2
HD 3861 B			L3.5	F8V	-121 ±14	-79 ±13	3
J0230-0225	145	33 ±8	L8	K1	-105 ±8	-62.8 ±8.2	1
J1244+1232	286	46 ±8	T4	-	-104.8 ±8.6	4.5 ±7.3	1
J0758+2225	157	27 ±6	T6.5	-	329 ±16.8	51.3 ±14.9	1
J1150+0949	211	60 ±27	T6.5	-	-107.6 ±17.1	-31.9 ±4.5	1
J0915+0531	178	33 ±6	T7	-	-95 ±5.5	-57.7 ±4.4	1

References (1) Smart et al. (2017); (2) Marocco et al. (2017); (3) Scholz (2016).

Chapter 4

Conclusions and Future Perspectives

In this work we have presented the basic properties of L and T dwarfs and the current models that try to describe their internal structure and their evolution. We have also argued about the importance of larger samples of brown dwarfs and of benchmark systems than those currently available as an important step towards improving their evolutionary model. Large sample of L and T dwarfs will also provide a more detailed description of the spatial distribution of these sources and reliable values of the main parameters of Galactic structure as traced by this population.

In Chapter 2 we presented the selection and spectral classification of a sample containing 11,745 L and T dwarfs candidates, most of them L dwarfs, located in the common footprint of DES, VHS and WISE surveys. We also made the first estimate of the scale height for the L dwarfs, and found $h_{z,thin} \sim 450$ pc.

In Chapter 3 we presented the search for benchmarks systems, made up of a L or T dwarfs orbiting a main sequence star in a wide binary pair. We also searched for systems constituted by two brown dwarfs. We found 197 new pair candidates and 2 multiple systems: one seems to be a quadruple and another is a triple. The vast majority of the binary candidates are made up of L dwarfs. We found a binary fraction of $\simeq 2-4\%$ over all spectral types (L0-T9). This is small compared to other observational estimates, but one has to keep in mind that in our case, we only select systems with wide separation (projected separations in the $600-10,000$ AU), whereas most estimates in the literature involve spectroscopic binaries of much smaller separations. Dhital et al. (2011) study common distance and proper motion wide binaries spanning the mid-K to mid-M spectral range and find a similar binary fraction to ours (1.1%).

Under the assumption that the two (or more) stars were formed from the same gas cloud, these wide separation binaries and multiples provide means of estimating the system metallicity and age based on the brighter, and easier to study, primary star. The small orbital velocities also imply that their physically bound systems may be more easily identified using common proper motions and radial velocities. It is worth mention that proper motion measurements are expected to be provided by the DES collaboration, based on the six year observation baseline of the survey.

For our benchmark systems, we proposed a spectroscopic follow up using both SOAR and Gemini. From SOAR we are interested in the Gaia DR2 primary star members of the most probable benchmark candidates. Our goals are to determine atmospheric parameters (effective temperature and surface gravity) and metallicity. Combining the spectroscopic parameters with Gaia DR2 parallaxes and available photometry, we will then improve on the estimated distance of the system and infer the primary mass and age using the `StarHorse` code. From Gemini we are interested on the most probable brown dwarfs candidates of our benchmark candidates, to confirm their nature (spectral type), to better constrain their distances and, therefore, their association to the primary.

We certainly plan to extend the same analyses to the Y5/Y6 DES data, which will be photometrically deeper, allowing fainter candidates to be probed, and also leading to more reliable photometry for the current ones. This in turn will lead to an increase in the number of L and T dwarfs and a better estimate of the scale height. Their spatial distribution and associated luminosity function may then be analyzed in separately for each spectral type, at least for the L dwarfs.

References

[1] ABAZAJIAN, K. N., ADELMAN-MCCARTHY, J. K., AGÜEROS, M. A., ALLAM, S. S., ALLENDE PRIETO, C., AN, D., ANDERSON, K. S. J., ANDERSON, S. F., ANNIS, J., BAHCALL, N. A., AL., ET . The Seventh Data Release of the Sloan Digital Sky Survey. **ApJS**, v. 182, p. 543–558, June 2009.

[2] ABBOTT, T. M. C., ABDALLA, F. B., ALLAM, S., AMARA, A., ANNIS, J., ASOREY, J., AVILA, S., BALLESTER, O., BANERJI, M., BARKHOUSE, W., BARUAH, L., BAUMER, M., BECHTOL, K., BECKER, M. R., BENOIT-LÉVY, A., BERNSTEIN, G. M., BERTIN, E., BLAZEK, J., BOCQUET, S., BROOKS, D., BROUT, D., BUCKLEY-GEER, E., BURKE, D. L., BUSTI, V., CAMPISANO, R., CARDIEL-SAS, L., CARNERO ROSELL, A., CARRASCO KIND, M., CARRETERO, J., CASTANDER, F. J., CAWTHON, R., CHANG, C., CHEN, X., CONSELICE, C., COSTA, G., CROCCE, M., CUNHA, C. E., DANDREA, C. B., DA COSTA, L. N., DAS, R., DAUES, G., DAVIS, T. M., DAVIS, C., DE VICENTE, J., DEPOY, D. L., DEROSE, J., DESAI, S., DIEHL, H. T., DIETRICH, J. P., DODELSON, S., DOEL, P., DRLICA-WAGNER, A., EIFLER, T. F., ELLIOTT, A. E., EVRARD, A. E., FARAHI, A., FAUSTI NETO, A., FERNANDEZ, E., FINLEY, D. A., FLAUGHER, B., FOLEY, R. J., FOSALBA, P., FRIEDEL, D. N., FRIEMAN, J., GARCíA-BELLIDO, J., GAZTANAGA, E., GERDES, D. W., GIANNANTONIO, T., GILL, M. S. S., GLAZEBROOK, K., GOLDSTEIN, D. A., GOWER, M., GRUEN, D., GRUENDL, R. A., GSCHWEND, J., GUPTA, R. R., GUTIERREZ, G., HAMILTON, S., HARTLEY, W. G., HINTON, S. R., HISLOP, J. M., HOLLOWOOD, D., HONSCHEID, K., HOYLE, B., HUTERER, D., JAIN, B., JAMES, D. J., JELTEMA, T., JOHNSON, M. W. G., JOHNSON, M. D., KACPRZAK, T., KENT, S., KHULLAR, G., KLEIN, M., KOVACS, A., KOZIOL, A. M. G., KRAUSE, E., KREMIN, A., KRON, R., KUEHN, K., KUHLMANN, S., KUROPATKIN, N., LAHAV, O., LASKER, J., LI, T. S., LI, R. T., LIDDLE, A. R., LIMA, M., LIN, H.,

LÓPEZ-REYES, P., MACCRANN, N., MAIA, M. A. G., MALONEY, J. D., MANERA, M., MARCH, M., MARRINER, J., MARSHALL, J. L., MARTINI, P., MCCLINTOCK, T., MCKAY, T., MCMAHON, R. G., MELCHIOR, P., MENANTEAU, F., MILLER, C. J., MIQUEL, R., MOHR, J. J., MORGANSON, E., MOULD, J., NEILSEN, E., NICHOL, R. C., NOGUEIRA, F., NORD, B., NUGENT, P., NUNES, L., OGANDO, R. L. C., OLD, L., PACE, A. B., PALMESE, A., PAZ-CHINCHÓN, F., PEIRIS, H. V., PERCIVAL, W. J., PETRAVICK, D., PLAZAS, A. A., POH, J., POND, C., PORREDON, A., PUJOL, A., REFREGIER, A., REIL, K., RICKER, P. M., ROLLINS, R. P., ROMER, A. K., ROODMAN, A., ROONEY, P., ROSS, A. J., RYKOFF, E. S., SAKO, M., SANCHEZ, M. L., SANCHEZ, E., SANTIAGO, B., SARO, A., SCARPINE, V., SCOLNIC, D., SERRANO, S., SEVILLA-NOARBE, I., SHELDON, E., SHIPP, N., SILVEIRA, M. L., SMITH, M., SMITH, R. C., SMITH, J. A., SOARES-SANTOS, M., SOBREIRA, F., SONG, J., STEBBINS, A., SUCHYTA, E., SULLIVAN, M., SWANSON, M. E. C., TARLE, G., THALER, J., THOMAS, D., THOMAS, R. C., TROXEL, M. A., TUCKER, D. L., VIKRAM, V., VIVAS, A. K., WALKER, A. R., WECHSLER, R. H., WELLER, J., WESTER, W., WOLF, R. C., WU, H., YANNY, B., ZENTENO, A., ZHANG, Y., ZUNTZ, J., DES COLLABORATION, , JUNEAU, S., FITZPATRICK, M., NIKUTTA, R., NIDEVER, D., OLSEN, K., SCOTT, A., DATA LAB, N. The Dark Energy Survey: Data Release 1. **ApJS**, v. 239, p. 18, December 2018.

[3] ALBERT, L., ARTIGAU, É., DELORME, P., REYLÉ, C., FORVEILLE, T., DELFOSSE, X., WILLOTT, C. J. 37 New T-type Brown Dwarfs in the Canada-France Brown Dwarfs Survey. **AJ**, v. 141, p. 203, June 2011.

[4] ALLARD, F., HAUSCHILDT, P. H. Model atmospheres for M (sub)dwarf stars. 1: The base model grid. **ApJ**, v. 445, p. 433–450, May 1995.

[5] BARAFFE, I., CHABRIER, G., ALLARD, F., HAUSCHILDT, P. H. New Evolutionary Tracks for Very Low Mass Stars. **ApJ**, v. 446, p. L35, June 1995.

[6] BARAFFE, I., CHABRIER, G., ALLARD, F., HAUSCHILDT, P. H. Evolutionary models for low-mass stars and brown dwarfs: Uncertainties and limits at very young ages. **A&A**, v. 382, p. 563–572, February 2002.

[7] BARAFFE, I., CHABRIER, G., BARMAN, T. S., ALLARD, F., HAUSCHILDT, P. H. Evolutionary models for cool brown dwarfs and extrasolar giant planets. The case of HD 209458. **A&A**, v. 402, p. 701–712, May 2003.

[8] BATE, M. R., BONNELL, I. A. The origin of the initial mass function and its dependence on the mean Jeans mass in molecular clouds. **MNRAS**, v. 356, p. 1201–1221, February 2005.

[9] BATE, M. R., OGILVIE, G. I., LUBOW, S. H., PRINGLE, J. E. The excitation, propagation and dissipation of waves in accretion discs: the non-linear axisymmetric case. **MNRAS**, v. 332, p. 575–600, May 2002.

[10] BILDSTEN, L., BROWN, E. F., MATZNER, C. D., USHOMIRSKY, G. Lithium Depletion in Fully Convective Pre-Main-Sequence Stars. **ApJ**, v. 482, p. 442–447, June 1997.

[11] BONNELL, I. A., CLARK, P., BATE, M. R. Gravitational fragmentation and the formation of brown dwarfs in stellar clusters. **MNRAS**, v. 389, p. 1556–1562, October 2008.

[12] BOSS, A. P. Formation of Planetary-Mass Objects by Protostellar Collapse and Fragmentation. **ApJ**, v. 551, p. L167–L170, April 2001.

[13] BRETT, J. M., SMITH, R. C. A model atmosphere investigation of the effects of irradiation on the secondary star in a dwarf nova. **MNRAS**, v. 264, p. 641, October 1993.

[14] BURGASSER, A. J. Binaries and the L Dwarf/T Dwarf Transition. **ApJ**, v. 659, p. 655–674, April 2007.

[15] BURGASSER, A. J., KIRKPATRICK, J. D., CRUZ, K. L., REID, I. N., LEGGETT, S. K., LIEBERT, J., BURROWS, A., BROWN, M. E. Hubble Space Telescope NICMOS Observations of T Dwarfs: Brown Dwarf Multiplicity and New Probes of the L/T Transition. **ApJS**, v. 166, p. 585–612, October 2006.

[16] BURNINGHAM, B., CARDOSO, C. V., SMITH, L., LEGGETT, S. K., SMART, R. L., MANN, A. W., DHITAL, S., LUCAS, P. W., TINNEY, C. G., PINFIELD, D. J., ZHANG, Z., MORLEY, C., SAUMON, D., ALLER, K., LITTLEFAIR, S. P., HOMEIER, D., LODIEU, N., DEACON, N., MARLEY,

M. S., VAN SPAANDONK, L., BAKER, D., ALLARD, F., ANDREI, A. H., CANTY, J., CLARKE, J., DAY-JONES, A. C., DUPUY, T., FORTNEY, J. J., GOMES, J., ISHII, M., JONES, H. R. A., LIU, M., MAGAZZÚ, A., MAROCCO, F., MURRAY, D. N., ROJAS-AYALA, B., TAMURA, M. 76 T dwarfs from the UKIDSS LAS: benchmarks, kinematics and an updated space density. **MNRAS**, v. 433, p. 457–497, July 2013.

[17] BURNINGHAM, B., PINFIELD, D. J., LUCAS, P. W., LEGGETT, S. K., DEACON, N. R., TAMURA, M., TINNEY, C. G., LODIEU, N., ZHANG, Z. H., HUELAMO, N., JONES, H. R. A., MURRAY, D. N., MORTLOCK, D. J., PATEL, M., BARRADO Y NAVASCUÉS, D., ZAPATERO OSORIO, M. R., ISHII, M., KUZUHARA, M., SMART, R. L. 47 new T dwarfs from the UKIDSS Large Area Survey. **MNRAS**, v. 406, p. 1885–1906, August 2010.

[18] BURROWS, A., HUBBARD, W. B., LUNINE, J. I. Theoretical models of very low mass stars and brown dwarfs. **ApJ**, v. 345, p. 939–958, October 1989.

[19] CARLSTROM, J. E., ADE, P. A. R., AIRD, K. A., BENSON, B. A., BLEEM, L. E., BUSETTI, S., CHANG, C. L., CHAUVIN, E., CHO, H.-M., CRAWFORD, T. M., CRITES, A. T., DOBBS, M. A., HALVERSON, N. W., HEIMSATH, S., HOLZAPFEL, W. L., HRUBES, J. D., JOY, M., KEISLER, R., LANTING, T. M., LEE, A. T., LEITCH, E. M., LEONG, J., LU, W., LUEKER, M., LUONG-VAN, D., MCMAHON, J. J., MEHL, J., MEYER, S. S., MOHR, J. J., MONTROY, T. E., PADIN, S., PLAGGE, T., PRYKE, C., RUHL, J. E., SCHAFFER, K. K., SCHWAN, D., SHIROKOFF, E., SPIELER, H. G., STANISZEWSKI, Z., STARK, A. A., TUCKER, C., VANDERLINDE, K., VIEIRA, J. D., WILLIAMSON, R. The 10 Meter South Pole Telescope. **PASP**, v. 123, p. 568, May 2011.

[20] CARNERO ROSELL, A., SANTIAGO, B., DAL PONTE, M., BURNINGHAM, B., DA COSTA, L. N., JAMES, D. J., MARSHALL, J. L., MCMAHON, R. G., BECHTOL, K., DE PARIS, L., LI, T., PIERES, A., ABBOTT, T. M. C., ANNIS, J., AVILA, S., BERNSTEIN, G. M., BROOKS, D., BURKE, D. L., CARRASCO-KIND, M., CARRETERO, J., DE VICENTE, J., DRLICA-WAGNER, A., FOSALBA, P., FRIEMAN, J., GARCIA-BELLIDO, J., GAZTANAGA, E., GRUENDL, R. A., GSCHWEND, J., GUTIERREZ, G., HOLLOWOOD, D. L., MAIA, M. A. G., MENANTEAU, F., MIQUEL, R., PLAZAS, A. A., ROODMAN, A., SANCHEZ, E., SCARPINE, V.,

SCHINDLER, R., SERRANO, S., SEVILLA-NOARBE, I., SMITH, M., SOBREIRA, F., SUCHYTA, E., SWANSON, M. E. C., TARLE, G., VIKRAM, V., WALKER, A. R. Brown dwarf census with the Dark Energy Survey year 3 data and the thin disk scale height of early L types. **arXiv e-prints**, p. arXiv:1903.10806, Mar 2019.

[21] CHABRIER, G. The Galactic Disk Mass Budget. II. Brown Dwarf Mass Function and Density. **ApJ**, v. 567, p. 304–313, March 2002.

[22] CHABRIER, G., BARAFFE, I. Theory of Low-Mass Stars and Substellar Objects. **ARA&A**, v. 38, p. 337–377, 2000.

[23] CHABRIER, G., BARAFFE, I., ALLARD, F., HAUSCHILDT, P. Evolutionary Models for Very Low-Mass Stars and Brown Dwarfs with Dusty Atmospheres. **ApJ**, v. 542, p. 464–472, October 2000.

[24] CHABRIER, G., BARAFFE, I., PLEZ, B. Mass-Luminosity Relationship and Lithium Depletion for Very Low Mass Stars. **ApJ**, v. 459, p. L91, March 1996.

[25] CHIU, K., FAN, X., LEGGETT, S. K., GOLIMOWSKI, D. A., ZHENG, W., GEBALLE, T. R., SCHNEIDER, D. P., BRINKMANN, J. Seventy-One New L and T Dwarfs from the Sloan Digital Sky Survey. **AJ**, v. 131, p. 2722–2736, June 2006.

[26] DANTONA, F., MAZZITELLI, I. Evolution of very low mass stars and brown dwarfs. I - The minimum main-sequence mass and luminosity. **ApJ**, v. 296, p. 502–513, September 1985.

[27] DAY-JONES, A. C., MAROCCO, F., PINFIELD, D. J., ZHANG, Z. H., BURNINGHAM, B., DEACON, N., RUIZ, M. T., GALLARDO, J., JONES, H. R. A., LUCAS, P. W. L., JENKINS, J. S., GOMES, J., FOLKES, S. L., CLARKE, J. R. A. The sub-stellar birth rate from UKIDSS. **MNRAS**, v. 430, p. 1171–1187, April 2013.

[28] DHITAL, S., WEST, A. A., STASSUN, K. G., SCHLUNS, K. J., MASSEY, A. P. SLoWPoKES-II: 100,000 Wide Binaries Identified in SDSS without Proper Motions. **AJ**, v. 150, p. 57, August 2015.

[29] DHITAL, SAURAV, BURGASSER, ADAM J., LOOPER, DAGNY L., STASSUN, KEIVAN G. Resolved Spectroscopy of M Dwarf/L Dwarf Binaries. IV. Discov-

ery of AN M9 + L6 Binary Separated by Over 100 AU. **AJ**, v. 141, p. 7, January 2011.

[30] DORMAN, B., NELSON, L. A., CHAU, W. Y. Theoretical models of low-mass stars and brown dwarfs. I - The lower main sequence. **ApJ**, v. 342, p. 1003–1018, July 1989.

[31] ELMEGREEN, B. G. On the Initial Conditions for Star Formation and the Initial Mass Function. **ApJ**, v. 731, p. 61, April 2011.

[32] EPCHTEIN, N., DE BATZ, B., CAPOANI, L., CHEVALLIER, L., COPET, E., FOUQUÉ, P., LACOMBE, P., LE BERTRE, T., PAU, S., ROUAN, D., RUPHY, S., SIMON, G., TIPHÈNE, D., BURTON, W. B., BERTIN, E., DEUL, E., HABING, H., BORSENBERGER, J., DENNEFELD, M., GUGLIELMO, F., LOUP, C., MAMON, G., NG, Y., OMONT, A., PROVOST, L., RENAULT, J. C., TANGUY, F., KIMESWENGER, S., KIENEL, C., GARZON, F., PERSI, P., FERRARI-TONIOLO, M., ROBIN, A., PATUREL, G., VAUGLIN, I., FORVEILLE, T., DELFOSSE, X., HRON, J., SCHULTHEIS, M., APPENZELLER, I., WAGNER, S., BALAZS, L., HOLL, A., LÉPINE, J., BOSCOLO, P., PICAZZIO, E., DUC, P. A., MENNESSIER, M. O. The deep near-infrared southern sky survey (DENIS). **The Messenger**, v. 87, p. 27–34, Mar 1997.

[33] FAHERTY, J. K., RIEDEL, A. R., CRUZ, K. L., GAGNE, J., FILIPPAZZO, J. C., LAMBRIDES, E., FICA, H., WEINBERGER, A., THORSTENSEN, J. R., TINNEY, C. G., BALDASSARE, V., LEMONIER, E., RICE, E. L. Population Properties of Brown Dwarf Analogs to Exoplanets. **ApJS**, v. 225, p. 10, July 2016.

[34] FLAUGHER, B., DIEHL, H. T., HONSCHEID, K., ABBOTT, T. M. C., ALVAREZ, O., ANGSTADT, R., ANNIS, J. T., ANTONIK, M., BALLESTER, O., BEAUFORE, L., BERNSTEIN, G. M., BERNSTEIN, R. A., BIGELOW, B., BONATI, M., BOPRIE, D., BROOKS, D., BUCKLEY-GEER, E. J., CAMPA, J., CARDIEL-SAS, L., CASTANDER, F. J., CASTILLA, J., CEASE, H., CELA-RUIZ, J. M., CHAPPA, S., CHI, E., COOPER, C., DA COSTA, L. N., DEDE, E., DERYLO, G., DEPOY, D. L., DE VICENTE, J., DOEL, P., DRLICA-WAGNER, A., EITING, J., ELLIOTT, A. E., EMES, J., ESTRADA, J., FAUSTI NETO, A., FINLEY, D. A., FLORES, R., FRIEMAN, J., GERDES, D., GLADDERS, M. D., GREGORY, B., GUTIERREZ, G. R., HAO, J., HOLLAND, S. E., HOLM, S., HUFFMAN, D., JACKSON, C.,

JAMES, D. J., JONAS, M., KARCHER, A., KARLINER, I., KENT, S., KESSLER, R., KOZLOVSKY, M., KRON, R. G., KUBIK, D., KUEHN, K., KUHLMANN, S., KUK, K., LAHAV, O., LATHROP, A., LEE, J., LEVI, M. E., LEWIS, P., LI, T. S., MANDRICHENKO, I., MARSHALL, J. L., MARTINEZ, G., MERRITT, K. W., MIQUEL, R., MUÑOZ, F., NEILSEN, E. H., NICHOL, R. C., NORD, B., OGANDO, R., OLSEN, J., PALAIO, N., PATTON, K., PEOPLES, J., PLAZAS, A. A., RAUCH, J., REIL, K., RHEAULT, J.-P., ROE, N. A., ROGERS, H., ROODMAN, A., SANCHEZ, E., SCARPINE, V., SCHINDLER, R. H., SCHMIDT, R., SCHMITT, R., SCHUBNELL, M., SCHULTZ, K., SCHURTER, P., SCOTT, L., SERRANO, S., SHAW, T. M., SMITH, R. C., SOARES-SANTOS, M., STEFANIK, A., STUERMER, W., SUCHYTA, E., SYPNIEWSKI, A., TARLE, G., THALER, J., TIGHE, R., TRAN, C., TUCKER, D., WALKER, A. R., WANG, G., WATSON, M., WEAVERDYCK, C., WESTER, W., WOODS, R., YANNY, B., DES COLLABORATION, . The Dark Energy Camera. **AJ**, v. 150, p. 150, November 2015.

[35] GELINO, C. R., KIRKPATRICK, J. D., CUSHING, M. C., EISENHARDT, P. R., GRIFFITH, R. L., MAINZER, A. K., MARSH, K. A., SKRUTSKIE, M. F., WRIGHT, E. L. WISE Brown Dwarf Binaries: The Discovery of a T5+T5 and a T8.5+T9 System. **AJ**, v. 142, p. 57, August 2011.

[36] GOODWIN, S. P., WHITWORTH, A. Brown dwarf formation by binary disruption. **A&A**, v. 466, p. 943–948, May 2007.

[37] GRETHER, D., LINEWEAVER, C. H. How Dry is the Brown Dwarf Desert? Quantifying the Relative Number of Planets, Brown Dwarfs, and Stellar Companions around Nearby Sun-like Stars. **ApJ**, v. 640, p. 1051–1062, April 2006.

[38] GROSSMAN, A. S., HAYS, D., GRABOSKE, H. C., JR. The theoretical low mass main sequence. **A&A**, v. 30, p. 95–103, January 1974.

[39] HUÉLAMO, N., IVANOV, V. D., KURTEV, R., GIRARD, J. H., BORISSOVA, J., MAWET, D., MUŽIĆ, K., CÁCERES, C., MELO, C. H. F., STERZIK, M. F., MINNITI, D. WISE J061213.85-303612.5: a new T-dwarf binary candidate. **A&A**, v. 578, p. A1, June 2015.

[40] JANSON, M., HORMUTH, F., BERGFORS, C., BRANDNER, W., HIPPLER, S., DAEMGEN, S., KUDRYAVTSEVA, N., SCHMALZL, E., SCHNUPP, C.,

HENNING, T. The AstraLux Large M-dwarf Multiplicity Survey. **ApJ**, v. 754, p. 44, July 2012.

[41] KIRKPATRICK, J. D., CUSHING, M. C., GELINO, C. R., GRIFFITH, R. L., SKRUTSKIE, M. F., MARSH, K. A., WRIGHT, E. L., MAINZER, A., EISENHARDT, P. R., MCLEAN, I. S., THOMPSON, M. A., BAUER, J. M., BENFORD, D. J., BRIDGE, C. R., LAKE, S. E., PETTY, S. M., STANFORD, S. A., TSAI, C.-W., BAILEY, V., BEICHMAN, C. A., BLOOM, J. S., BOCHANSKI, J. J., BURGASSER, A. J., CAPAK, P. L., CRUZ, K. L., HINZ, P. M., KARTALTEPE, J. S., KNOX, R. P., MANOHAR, S., MASTERS, D., MORALES-CALDERÓN, M., PRATO, L. A., RODIGAS, T. J., SALVATO, M., SCHURR, S. D., SCOVILLE, N. Z., SIMCOE, R. A., STAPELFELDT, K. R., STERN, D., STOCK, N. D., VACCA, W. D. The First Hundred Brown Dwarfs Discovered by the Wide-field Infrared Survey Explorer (WISE). **ApJS**, v. 197, p. 19, December 2011.

[42] KIRKPATRICK, J. D., REID, I. N., LIEBERT, J., CUTRI, R. M., NELSON, B., BEICHMAN, C. A., DAHN, C. C., MONET, D. G., GIZIS, J. E., SKRUTSKIE, M. F. Dwarfs Cooler than "M": The Definition of Spectral Type "L" Using Discoveries from the 2 Micron All-Sky Survey (2MASS). **ApJ**, v. 519, p. 802–833, July 1999.

[43] KRAUS, A. L., HILLENBRAND, L. A. Multiple Star Formation to the Bottom of the Initial Mass Function. **ApJ**, v. 757, p. 141, October 2012.

[44] KUMAR, S. S. The Structure of Stars of Very Low Mass. **ApJ**, v. 137, p. 1121, May 1963.

[45] LAWRENCE, A., WARREN, S.J., ALMAINI, O., EDGE, A.C., HAMBLY, N.C., JAMESON, R.F., LUCAS, P., CASALI, M., ADAMSON, A., DYE, S., EMERSON, J.P., FOUCAUD, S., HEWETT, P., HIRST, P., HODGKIN, S.T., IRWIN, M.J., LODIEU, N., MCMAHON, R.G., SIMPSON, C., SMAIL, I., MORTLOCK, D., FOLGER, M. The ukirt infrared deep sky survey (ukidss). **Monthly Notices of the Royal Astronomical Society**, v. 379, n. 4, p. 1599–1617, 2007.

[46] LODIEU, N., BURNINGHAM, B., DAY-JONES, A., SCHOLZ, R.-D., MAROCCO, F., KOPOSOV, S., BARRADO Y NAVASCUÉS, D., LUCAS, P. W., CRUZ, P., LILLO, J., JONES, H., PEREZ-GARRIDO, A., RUIZ, M. T.,

PINFIELD, D., REBOLO, R., BÉJAR, V. J. S., BOUDREAULT, S., EMERSON, J. P., BANERJI, M., GONZÁLEZ-SOLARES, E., HODGKIN, S. T., MCMAHON, R., CANTY, J., CONTRERAS, C. First T dwarfs in the VISTA Hemisphere Survey. **A&A**, v. 548, p. A53, December 2012.

[47] LODIEU, N., HAMBLY, N. C., JAMESON, R. F., HODGKIN, S. T., CARRARO, G., KENDALL, T. R. New brown dwarfs in Upper Sco using UKIDSS Galactic Cluster Survey science verification data. **MNRAS**, v. 374, p. 372–384, January 2007.

[48] LODIEU, N., ZAPATERO OSORIO, M. R., REBOLO, R., MARTíN, E. L., HAMBLY, N. C. A census of very-low-mass stars and brown dwarfs in the σ Orionis cluster. **A&A**, v. 505, p. 1115–1127, October 2009.

[49] LUHMAN, K. L. The Formation and Early Evolution of Low-Mass Stars and Brown Dwarfs. **ARA&A**, v. 50, p. 65–106, September 2012.

[50] LUNINE, J. I., HUBBARD, W. B., MARLEY, M. S. Evolution and infrared spectra of brown dwarfs. **ApJ**, v. 310, p. 238–260, November 1986.

[51] MCMAHON, R. G., BANERJI, M., GONZALEZ, E., KOPOSOV, S. E., BEJAR, V. J., LODIEU, N., REBOLO, R., VHS COLLABORATION, . First Scientific Results from the VISTA Hemisphere Survey (VHS). **The Messenger**, v. 154, p. 35–37, December 2013.

[52] METCHEV, S. A., HILLENBRAND, L. A. The Palomar/Keck Adaptive Optics Survey of Young Solar Analogs: Evidence for a Universal Companion Mass Function. **ApJS**, v. 181, p. 62–109, March 2009.

[53] MORAUX, E., BOUVIER, J., STAUFFER, J. R., CUILLANDRE, J.-C. Brown dwarfs in the Pleiades cluster: Clues to the substellar mass function. **A&A**, v. 400, p. 891–902, March 2003.

[54] NELSON, L. A., RAPPAPORT, S. A., JOSS, P. C. The evolution of very low mass stars. **ApJ**, v. 311, p. 226–240, December 1986.

[55] OPPENHEIMER, B. R., KULKARNI, S. R., MATTHEWS, K., NAKAJIMA, T. Infrared Spectrum of the Cool Brown Dwarf Gl 229B. **Science**, v. 270, p. 1478–1479, December 1995.

[56] PADOAN, P., NORDLUND, Å. The Stellar Initial Mass Function from Turbulent Fragmentation. **ApJ**, v. 576, p. 870–879, September 2002.

[57] RAGHAVAN, D., MCALISTER, H. A., HENRY, T. J., LATHAM, D. W., MARCY, G. W., MASON, B. D., GIES, D. R., WHITE, R. J., TEN BRUMMELAAR, T. A. A Survey of Stellar Families: Multiplicity of Solar-type Stars. **ApJS**, v. 190, p. 1–42, September 2010.

[58] REBOLO, R., MARTIN, E. L., MAGAZZU, A. Spectroscopy of a brown dwarf candidate in the Alpha Persei open cluster. **ApJ**, v. 389, p. L83–L86, April 1992.

[59] REBOLO, R., ZAPATERO OSORIO, M. R., MARTíN, E. L. Discovery of a brown dwarf in the Pleiades star cluster. **Nature**, v. 377, p. 129–131, September 1995.

[60] SALPETER, E. E. The Luminosity Function and Stellar Evolution. **ApJ**, v. 121, p. 161, January 1955.

[61] SAUMON, D., BERGERON, P., LUNINE, J. I., HUBBARD, W. B., BURROWS, A. Cool zero-metallicity stellar atmospheres. **ApJ**, v. 424, p. 333–344, March 1994.

[62] SAUMON, D., CHABRIER, G., VAN HORN, H. M. An Equation of State for Low-Mass Stars and Giant Planets. **ApJS**, v. 99, p. 713, August 1995.

[63] SAUMON, D., MARLEY, M. S. The Evolution of L and T Dwarfs in Color-Magnitude Diagrams. **ApJ**, v. 689, p. 1327–1344, December 2008.

[64] SCHMIDT, S. J., WEST, A. A., HAWLEY, S. L., PINEDA, J. S. Colors and Kinematics of L Dwarfs from the Sloan Digital Sky Survey. **AJ**, v. 139, p. 1808–1821, May 2010.

[65] SHU, F. H., ADAMS, F. C., LIZANO, S. Star formation in molecular clouds - Observation and theory. **ARA&A**, v. 25, p. 23–81, 1987.

[66] SKRUTSKIE, M. F., CUTRI, R. M., STIENING, R., WEINBERG, M. D., SCHNEIDER, S., CARPENTER, J. M., BEICHMAN, C., CAPPS, R., CHESTER, T., ELIAS, J., HUCHRA, J., LIEBERT, J., LONSDALE, C., MONET, D. G., PRICE, S., SEITZER, P., JARRETT, T., KIRKPATRICK, J. D., GIZIS, J. E., HOWARD, E., EVANS, T., FOWLER, J., FULLMER, L., HURT, R., LIGHT, R., KOPAN, E. L., MARSH, K. A., MCCALLON, H. L.,

TAM, R., VAN DYK, S., WHEELOCK, S. The Two Micron All Sky Survey (2MASS). **AJ**, v. 131, p. 1163–1183, Feb 2006.

[67] SKRZYPEK, N., WARREN, S. J., FAHERTY, J. K. **A&A**, v. 589, p. A49, May 2016.

[68] SKRZYPEK, N., WARREN, S. J., FAHERTY, J. K., MORTLOCK, D. J., BURGASSER, A. J., HEWETT, P. C. **A&A**, v. 574, p. A78, February 2015.

[69] SORAHANA, S., NAKAJIMA, T., MATSUOKA, Y. Evaluation of the Vertical Scale Height of L Dwarfs in the Galactic Thin Disk. **ApJ**, v. 870, p. 118, January 2019.

[70] STAMATELLOS, D., MAURY, A., WHITWORTH, A., ANDRÉ, P. The lower limits of disc fragmentation and the prospects for observing fragmenting discs. **MNRAS**, v. 413, p. 1787–1796, May 2011.

[71] STAUFFER, J. R., HAMILTON, D., PROBST, R. G. A CCD-based search for very low mass members of the Pleiades cluster. **AJ**, v. 108, p. 155–159, July 1994.

[72] TARTER, J. C. **The interaction of gas and galaxies within galaxy clusters**. 1975. Tese de Doutoramento – California Univ., Berkeley.

[73] TOKOVININ, A., LÉPINE, S. Wide Companions to Hipparcos Stars within 67 pc of the Sun. **AJ**, v. 144, p. 102, October 2012.

[74] VANDENBERG, D. A., HARTWICK, F. D. A., DAWSON, P., ALEXANDER, D. R. Studies of late-type dwarfs. V - Theoretical models for lower main-sequence stars. **ApJ**, v. 266, p. 747–754, March 1983.

[75] WHITWORTH, A. P., ZINNECKER, H. The formation of free-floating brown dwarves and planetary-mass objects by photo-erosion of prestellar cores. **A&A**, v. 427, p. 299–306, November 2004.

[76] WRIGHT, E. L., EISENHARDT, P. R. M., MAINZER, A. K., RESSLER, M. E., CUTRI, R. M., JARRETT, T., KIRKPATRICK, J. D., PADGETT, D., MCMILLAN, R. S., SKRUTSKIE, M., STANFORD, S. A., COHEN, M., WALKER, R. G., MATHER, J. C., LEISAWITZ, D., GAUTIER, T. N., III, MCLEAN, I., BENFORD, D., LONSDALE, C. J., BLAIN, A., MENDEZ, B., IRACE, W. R., DUVAL, V., LIU, F., ROYER, D., HEINRICHSEN, I.,

HOWARD, J., SHANNON, M., KENDALL, M., WALSH, A. L., LARSEN, M., CARDON, J. G., SCHICK, S., SCHWALM, M., ABID, M., FABINSKY, B., NAES, L., TSAI, C.-W. The Wide-field Infrared Survey Explorer (WISE): Mission Description and Initial On-orbit Performance. **AJ**, v. 140, p. 1868–1881, December 2010.

[77] YORK, DONALD G., ADELMAN, J., ANDERSON, JR., JOHN E., ANDERSON, SCOTT F., ANNIS, JAMES, BAHCALL, NETA A., BAKKEN, J. A., BARKHOUSER, ROBERT, BASTIAN, STEVEN, BERMAN, EILEEN, BOROSKI, WILLIAM N., BRACKER, STEVE, BRIEGEL, CHARLIE, BRIGGS, JOHN W., BRINKMANN, J., BRUNNER, ROBERT, BURLES, SCOTT, CAREY, LARRY, CARR, MICHAEL A., CASTANDER, FRANCISCO J., CHEN, BING, COLESTOCK, PATRICK L., CONNOLLY, A. J., CROCKER, J. H., CSABAI, ISTVÁN, CZARAPATA, PAUL C., DAVIS, JOHN ERIC, DOI, MAMORU, DOMBECK, TOM, EISENSTEIN, DANIEL, ELLMAN, NANCY, ELMS, BRIAN R., EVANS, MICHAEL L., FAN, XIAOHUI, FEDERWITZ, GLENN R., FISCELLI, LARRY, FRIEDMAN, SCOTT, FRIEMAN, JOSHUA A., FUKUGITA, MASATAKA, GILLESPIE, BRUCE, GUNN, JAMES E., GURBANI, VIJAY K., DE HAAS, ERNST, HALDEMAN, MERLE, HARRIS, FREDERICK H., HAYES, J., HECKMAN, TIMOTHY M., HENNESSY, G. S., HINDSLEY, ROBERT B., HOLM, SCOTT, HOLMGREN, DONALD J., HUANG, CHI-HAO, HULL, CHARLES, HUSBY, DON, ICHIKAWA, SHIN-ICHI, ICHIKAWA, TAKASHI, IVEZIĆ, ŽELJKO, KENT, STEPHEN, KIM, RITA S. J., KINNEY, E., KLAENE, MARK, KLEINMAN, A. N., KLEINMAN, S., KNAPP, G. R., KORIENEK, JOHN, KRON, RICHARD G., KUNSZT, PETER Z., LAMB, D. Q., LEE, B., LEGER, R. FRENCH, LIMMONGKOL, SIRILUK, LINDENMEYER, CARL, LONG, DANIEL C., LOOMIS, CRAIG, LOVEDAY, JON, LUCINIO, RICH, LUPTON, ROBERT H., MACKINNON, BRYAN, MANNERY, EDWARD J., MANTSCH, P. M., MARGON, BRUCE, MCGEHEE, PEREGRINE, MCKAY, TIMOTHY A., MEIKSIN, AVERY, MERELLI, ARONNE, MONET, DAVID G., MUNN, JEFFREY A., NARAYANAN, VIJAY K., NASH, THOMAS, NEILSEN, ERIC, NESWOLD, RICH, NEWBERG, HEIDI JO, NICHOL, R. C., NICINSKI, TOM, NONINO, MARIO, OKADA, NORIO, OKAMURA, SADANORI, OSTRIKER, JEREMIAH P., OWEN, RUSSELL, PAULS, A. GEORGE, PEOPLES, JOHN, PETERSON, R. L., PETRAVICK, DONALD, PIER, JEFFREY R., POPE, ADRIAN, PORDES, RUTH,

PROSAPIO, ANGELA, RECHENMACHER, RON, QUINN, THOMAS R., RICHARDS, GORDON T., RICHMOND, MICHAEL W., RIVETTA, CLAUDIO H., ROCKOSI, CONSTANCE M., RUTHMANSDORFER, KURT, SAND FORD, DALE, SCHLEGEL, DAVID J., SCHNEIDER, DONALD P., SEKIGUCHI, MAKI, SERGEY, GARY, SHIMASAKU, KAZUHIRO, SIEGMUND, WALTER A., SMEE, STEPHEN, SMITH, J. ALLYN, SNEDDEN, S., STONE, R., STOUGHTON, CHRIS, STRAUSS, MICHAEL A., STUBBS, CHRISTOPHER, SUBBARAO, MARK, SZALAY, ALEXANDER S., SZAPUDI, ISTVAN, SZOKOLY, GYULA P., THAKAR, ANIRUDDA R., TREMONTI, CHRISTY, TUCKER, DOUGLAS L., UOMOTO, ALAN, VANDEN BERK, DAN, VOGELEY, MICHAEL S., WADDELL, PATRICK, WANG, SHU-I., WATANABE, MASARU, WEINBERG, DAVID H., YANNY, BRIAN, YASUDA, NAOKI, SDSS COLLABORATION, . The Sloan Digital Sky Survey: Technical Summary. **AJ**, v. 120, p. 1579–1587, Sep 2000.